LIÈGE université Library

https://lib.uliege.be

https://matheo.uliege.be

Influence of ions presence on the selective recovery of graphite from black mass using flotation and sedimentation (en ce compris une introduction à la méthodologie de la recherche)

Auteur : Vincent, Ariane
Promoteur(s) : Gaydardzhiev, Stoyan
Faculté : Faculté des Sciences appliquées
Diplôme : Master : ingénieur civil en chimie et science des matériaux, à finalité spécialisée en Chemical Engineering
Année académique : 2025-2026
URI/URL : http://hdl.handle.net/2268.2/27249

Avertissement à l'attention des usagers :

Tous les documents placés en accès ouvert sur le site le site MatheO sont protégés par le droit d'auteur. Conformément aux principes énoncés par la "Budapest Open Access Initiative"(BOAI, 2002), l'utilisateur du site peut lire, télécharger, copier, transmettre, imprimer, chercher ou faire un lien vers le texte intégral de ces documents, les disséquer pour les indexer, s'en servir de données pour un logiciel, ou s'en servir à toute autre fin légale (ou prévue par la réglementation relative au droit d'auteur). Toute utilisation du document à des fins commerciales est strictement interdite.

Par ailleurs, l'utilisateur s'engage à respecter les droits moraux de l'auteur, principalement le droit à l'intégrité de l'oeuvre et le droit de paternité et ce dans toute utilisation que l'utilisateur entreprend. Ainsi, à titre d'exemple, lorsqu'il reproduira un document par extrait ou dans son intégralité, l'utilisateur citera de manière complète les sources telles que mentionnées ci-dessus. Toute utilisation non explicitement autorisée ci-avant (telle que par exemple, la modification du document ou son résumé) nécessite l'autorisation préalable et expresse des auteurs ou de leurs ayants droit.

UNIVERSITE DE LIEGE
FACULTE DES SCIENCES APPLIQUEES

Influence of ions presence on the selective recovery of graphite from black mass using flotation and sedimentation

VINCENT Ariane

Master thesis presented to obtain the degree of :
Chemical and Materials engineering

Academic supervisor:
GAYDARDZHIEV Stoyan
Industrial supervisor:
VANDERBRUGGEN Anna
Co-supervisors:
LAMBERT Fanny
RIVERA Walter

Academic year: **2025 - 2026**

'Education is the most powerful weapon which you can use to change the world."

— Nelson Mandela

Acknowledgements

I am deeply grateful to everyone who contributed to the completion of this master's thesis.

First, I would like to express my sincere thanks to my academic supervisor, Stoyan Gaydardzhiev, for his guidance, support, and expertise throughout this work.

I would also like to thank my co-supervisors, Fanny Lambert and Walter Rivera, for their valuable expertise, advice, and support.

My sincere thanks also go to my industrial supervisor, Anna Vanderbruggen, for her kindness, expertise, and continuous support throughout my internship. I am also grateful to Amélia Nieto for her kindness and valuable advice. More generally, I would like to thank the entire Steval team for their warm welcome, kindness, and willingness to answer all my questions.

I would like to extend my thanks to the technicians at Gemme, Sabrina and Sébastien Blasutig, for carrying out all the analyses required for this master's thesis. I am also grateful to Seydou Landouré and Michèle Batutiako for sharing their expertise, and to Maria Farcas for carrying out the preparation of the leaching residue. I would also like to thank Miguel for his contribution and assistance throughout this work. More generally, I am grateful to the entire Gemme team for welcoming me and making me feel part of the team during my master's thesis.

Finally, I would like to thank my family and friends for their unwavering support, encouragement, and for believing in me, even during the moments when I struggled to believe in myself.

Abstract

English version

Due to the increasing demand for lithium-ion batteries (LIBs), their recycling has become increasingly important from both economic and environmental perspectives. Furthermore, the presence of graphite during the leaching step can reduce the overall efficiency of the recycling process. As graphite is also included in the list of Critical Raw Materials (CRMs), its recovery and recycling are of particular importance.

This work investigates the influence of ions released from black mass—a heterogeneous mixture of cathode and anode active materials obtained after the size-reduction of spent LIBs—on the agglomeration behaviour of graphite. The ultimate objective is to promote the selective agglomeration of graphite and subsequently recover it by flotation or sedimentation.

First, the evolution of the zeta potential as a function of pH was investigated to identify the conditions under which graphite agglomeration is promoted in the presence of ions released from black mass when it is suspended in water or subjected to leaching. Based on these measurements, the pH range most favourable for the selective agglomeration of graphite was identified. In deionised water, this range was found to be between pH 3 and 5.

To evaluate the influence of pH on flotation performance, flotation tests were conducted on mechanically pre-treated black mass at different pH values. The results showed that the natural pH of the black mass in water provided the highest separation efficiency. However, the presence of PVDF resulted in the entrainment of cathode active materials (CAMs) into the froth. Therefore, the removal of the PVDF binder prior to flotation is recommended.

Batch sedimentation tests were also conducted to determine the settling velocities of graphite and NMC811 ($LiNi_{0.8}Mn_{0.1}Co_{0.1}O_2$) and to identify the pH and ion concentration conditions that maximise the difference between their settling behaviours. The results demonstrated that the presence of precipitates substantially reduced the settling velocities of both graphite and NMC811. Based on the most promising conditions identified during these experiments, continuous sedimentation tests were subsequently performed to selectively recover graphite in the underflow.

Using synthetic black mass, a graphite grade of 94.37% and a recovery of 54.3% were obtained at pH 10.5 in the presence of Ni^{2+} at a concentration of 0.02 M, after filtration of the solution to remove precipitates, and with an upward water velocity of 13.6 cm/min. In deionised water at pH 10.5, a graphite grade of 91.24% and a recovery of 90.02% were achieved at an upward water velocity of 6.65 cm/min.

Finally, continuous sedimentation tests were performed on mechanically pre-treated industrial black mass at pH 10.5 and on leaching residues at pH 5 to evaluate the applicability of the process to more representative industrial materials.

Version française

En raison de la demande croissante en batteries lithium-ion (BLIs), leur recyclage revêt une importance grandissante, tant d'un point de vue économique qu'environnemental. Par ailleurs, la présence de graphite lors de l'étape de lixiviation peut réduire l'efficacité globale du procédé de recyclage. Le graphite étant également inscrit sur la liste des matières premières critiques, sa récupération et son recyclage présentent un intérêt particulier.

Ce travail étudie l'influence des ions libérés par la black mass — un mélange hétérogène de matériaux actifs de cathode et d'anode obtenu après l'étape de réduction granulométrique des batteries lithium-ion en fin de vie — sur le comportement d'agglomération du graphite. L'objectif final est de favoriser l'agglomération sélective du graphite afin de permettre sa récupération sélective par flottation ou par sédimentation.

Dans un premier temps, l'évolution du potentiel zêta en fonction du pH a été étudiée afin d'identifier les conditions favorables à l'agglomération du graphite en présence des ions libérés par la black mass lorsqu'elle est mise en suspension dans l'eau ou soumise à une lixiviation. Sur la base de ces mesures, la gamme de pH la plus favorable à l'agglomération sélective du graphite a été déterminée. En eau déionisée, cette gamme se situe entre pH 3 et 5.

Afin d'évaluer l'influence du pH sur les performances de flottation, des essais de flottation ont été réalisés sur une black mass ayant subi un prétraitement mécanique, à différentes valeurs de pH. Les résultats ont montré que le pH naturel de la suspension de black mass dans l'eau permettait d'obtenir la meilleure efficacité de séparation. Cependant, la présence de PVDF (polyfluorure de vinylidène) a entraîné l'entraînement de matériaux actifs de cathode dans la mousse. Il est donc recommandé d'éliminer le liant PVDF avant l'étape de flottation.

Des essais de sédimentation en batch ont également été réalisés afin de déterminer les vitesses de sédimentation du graphite et du NMC811 ($LiNi_{0.8}Mn0.1Co_{0.1}O_2$), ainsi que d'identifier les conditions de pH et de concentration ionique permettant de maximiser la différence entre leurs comportements de sédimentation. Les résultats ont mis en évidence que la présence de précipités réduisait considérablement les vitesses de sédimentation du graphite et du NMC811. Sur la base des conditions les plus prometteuses identifiées lors de ces essais, des tests de sédimentation continue ont ensuite été réalisés afin de récupérer sélectivement le graphite dans le sous-produit de fond (underflow).

Avec une black mass synthétique, une teneur en graphite de 94,37 % et une récupération de 54,3 % ont été obtenues à pH 10,5, en présence de Ni^{2+} à une concentration de 0,02 M, après filtration de la solution afin d'éliminer les précipités, et pour une vitesse ascendante de l'eau de 13,6 cm/min. En eau déionisée à pH 10,5, une teneur en graphite de 91,24 % et une récupération de 90,02 % ont été obtenues pour une vitesse ascendante de 6,65 cm/min.

Enfin, des essais de sédimentation continue ont été réalisés sur une black mass industrielle ayant subi un prétraitement mécanique à pH 10,5, ainsi que sur des résidus de lixiviation à pH 5, afin d'évaluer l'applicabilité du procédé à des matériaux plus représentatifs des conditions industrielles.

Contents

1 Introduction **1**
- 1.1 Context . . . 1
- 1.2 Objectives . . . 2
- 1.3 Scientific strategy . . . 2

2 Background **4**
- 2.1 State of the art . . . 4
  - 2.1.1 Composition and functionning of LIBs . . . 4
  - 2.1.2 Routes to recycle batteries . . . 5
    - 2.1.2.1 Pyrometallurgical route . . . 6
    - 2.1.2.2 Mechanical and thermal pretreatment . . . 6
    - 2.1.2.3 Hydrometallurgical route . . . 7
- 2.2 Black mass flotation and pretreatment . . . 8
- 2.3 Zeta potential . . . 11
- 2.4 Sedimentation test . . . 12

3 Materials and methods **13**
- 3.1 Pristine materials used . . . 13
- 3.2 Black mass characterization . . . 13
  - 3.2.1 Sampling . . . 14
- 3.3 Leaching residue characterization . . . 15
- 3.4 Leaching procedure of the pristine material . . . 15
- 3.5 Zeta potential measurements . . . 16
- 3.6 Froth flotation experiments . . . 16
- 3.7 Batch sedimentation tests . . . 19
- 3.8 Continuous sedimentation test . . . 21
- 3.9 Characterization . . . 25
  - 3.9.1 ICP-OES . . . 25
  - 3.9.2 XRF . . . 25
  - 3.9.3 ISE fluoro analysis . . . 26
  - 3.9.4 Total organic carbon (TOC) analysis . . . 26

4 Results and discussion **27**
- 4.1 Zeta potential . . . 27
  - 4.1.1 Deionised water . . . 27
    - 4.1.1.1 Non-leached compounds . . . 27
    - 4.1.1.2 Leached compounds . . . 27
  - 4.1.2 Effect of ions presence . . . 29
    - 4.1.2.1 Effect of lithium ions presence . . . 29
    - 4.1.2.2 Effect of nickel ions presence . . . 30
    - 4.1.2.3 Effect of cobalt ions presence . . . 33
    - 4.1.2.4 Effect of manganese ions presence . . . 35
    - 4.1.2.5 Effect of aluminum ions presence . . . 38

4.1.3 Zeta potential summary . . . 40
4.2 Flotation tests . . . 41
4.2.1 Impact of washing pre-treatment . . . 41
4.2.2 Optimisation of the promoter concentration . . . 43
4.2.3 Impact of the pH . . . 44
4.2.4 Flotation tests summary . . . 48
4.3 Batch sedimentation tests . . . 48
4.3.1 Deionised water . . . 48
4.3.1.1 Impact of pH . . . 48
4.3.2 Effect of ions presence . . . 50
4.3.2.1 Effect of lithium ions presence . . . 50
4.3.2.2 Effect of nickel ions presence . . . 51
4.3.2.3 Effect of cobalt ions presence . . . 53
4.3.2.4 Effect of aluminum ions presence . . . 54
4.3.3 Batch sedimentation tests summary . . . 56
4.4 Continuous sedimentation tests . . . 57
4.4.1 Impact of pH in deionised water . . . 57
4.4.2 Impact of the studied ions . . . 59
4.4.3 Industrial black mass . . . 62
4.4.4 Continuous sedimentation tests summary . . . 64

5 Conclusion and perspectives **65**

A Appendix **68**
A.1 Values of the logarithm of the concentration for the solubility of ionic species 68
A.2 Characterization of the different flotation products . . . 71
A.3 Characterization of the continuous sedimentation products . . . 75

List of Figures

1 Charge and discharge cycle of a LIB. On the left there is the anode, containing graphite as active material and on the right there is the cathode, containing for example NMC as active material. The equations are the reduction-oxidation reactions happening during charging and discharging, Me can be replaced by NixCoyMnz (x+y+z = 1) since it is the metallic part in the cathode active material. [25] 5

2 Schematic overview of the possible routes to recycle lithium-ion batteries [9] 6

3 Summary of simplified behaviour of active particles from lithium-ion batteries during black mass froth flotation [9] 10

4 Schematic view of the electrical double layer [40] 11

5 Schematic representation of the zone settling and related Kynch curve [41] . 12

6 Flowsheet pretreatment of the black mass used, ©M. Batutiako 14

7 Representation of the flotation cell used and names of the different parts it is composed of [50] 17

8 The three flow diagrams for the flotation experiments (I) No washing pre-treatment, collector concentration set at 150gpt during the rougher stage, (II) With washing pre-treatment and no pH modification, (III) With washing and pH modification. The washing pre-treatment is realised during 15 minutes at 1500 rpm at a pulp density of 5.7%. During the pH modification step, the pH was modified to 7, 5 and 3. Tests (II) and (III) are performed at a concentration of Escaid^{TM}110 of 150gpt in the rougher stage and 75gpt in the scavenger stage and an MIBC concentration of 80gpt both in the rougher and scavenger stages 18

9 Schematic representation of the continuous sedimentation device, where A represents the feed being stirred, B a pump, C a funnel, D the micro-flottation cell, E a pump, F the inlet water at the wanted pH, G a pump, H the underflow product, I the overflow product 22

10 Picture of the continuous sedimentation device, where A represents the feed being stirred, B a pump, C a funnel, D the micro-flottation cell, E a pump, F the inlet water at the wanted pH, G a pump, H the underflow product, I the overflow product 23

11 Evolution of the zeta potential of graphite and NMC811 as a function of the pH in deionised water, using H_2SO_4 and $NaOH$ to regulate the pH. Error bars present the standard deviation of measurement error. The measurements were realised using the Zetasizer Nano Z ZEN2600, the concentration of the colloidal suspension equalled 0.02g/l at ambient temperature. 27

12 Evolution of the zeta potential of graphite and NMC811, leached and non-leached, as a function of the pH in deionised water, using H_2SO_4 and $NaOH$ to regulate the pH. Error bars present the standard deviation of measurement error. The measurements were realised using the Zetasizer Nano Z ZEN2600, the concentration of the colloidal suspension equalled 0.02g/l at ambient temperature 28

13 Evolution of the zeta potential of leached graphite and NMC811 as a function of the pH in deionised water, using H_2SO_4 and $NaOH$ to regulate the pH. Error bars present the standard deviation of measurement error. The measurements were realised using the Zetasizer Nano Z ZEN2600, the concentration of the colloidal suspension equalled 0.02g/l at ambient temperature. 28
14 Evolution of the zeta potential of leached graphite and NMC811 as a function of the pH in the presence of lithium ions, using H_2SO_4 and $NaOH$ to regulate the pH. Error bars present one standard deviation of measurement error. The measurements were realised using the Zetasizer Nano Z ZEN2600, the concentration of the colloidal suspension equalled 0.02g/l at ambient temperature. . 29
15 Difference between the zeta potential of leached graphite and the one of NMC811 as a function of the pH in the presence of lithium ions, using H_2SO_4 and $NaOH$ to regulate the pH. The measurements were realised using the Zetasizer Nano Z ZEN2600, the concentration of the colloidal suspension equalled 0.02g/l at ambient temperature. 30
16 Evolution of the zeta potential of leached graphite and NMC811 as a function of the pH in the presence of nickel ions, using H_2SO_4 and $NaOH$ to regulate the pH. Error bars present one standard deviation of measurement error. The measurements were realised using the Zetasizer Nano Z ZEN2600, the concentration of the colloidal suspension equalled 0.02g/l at ambient temperature. . 32
17 Difference between the zeta potential of leached graphite and the one of CAM as a function of the pH in the presence of nickel ions, using H_2SO_4 and $NaOH$ to regulate the pH. The measurements were realised using the Zetasizer Nano Z ZEN2600, the concentration of the colloidal suspension equalled 0.02g/l at ambient temperature. 32
18 Solubility of Ni^{2+} in equilibrium with $Ni(OH)_{2(s)}$, $[Ni_{tot,dis}]$ represents the total concentration of nickel species dissolved 33
19 Evolution of the zeta potential of graphite and NMC811 as a function of the pH in the presence of cobalts ions, using H_2SO_4 and $NaOH$ to regulate the pH. Error bars present one standard deviation of measurement error. The measurements were realised using the Zetasizer Nano Z ZEN2600, the concentration of the colloidal suspension equalled 0.02g/l at ambient temperature. . 34
20 Difference between the zeta potential of graphite and the one of NMC811 as a function of the pH in the presence of cobalt ions, using H_2SO_4 and $NaOH$ to regulate the pH. The measurements were realised using the Zetasizer Nano Z ZEN2600, the concentration of the colloidal suspension equalled 0.02g/l at ambient temperature. 35
21 Solubility of Co^{2+} in equilibrium with $Co(OH)_{2(s)}$,$[Co_{tot,dis}]$ represents the total concentration of cobalt species dissolved 35
22 Evolution of the zeta potential of leached graphite and NMC811 as a function of the pH in the presence of manganese ions, using H_2SO_4 and $NaOH$ to regulate the pH. Error bars present one standard deviation of measurement error. The measurements were realised using the Zetasizer Nano Z ZEN2600, the concentration of the colloidal suspension equalled 0.02g/l at ambient temperature. 37

23 Difference between the zeta potential of leached graphite and the one of CAM as a function of the pH in the presence of manganese ions, using H_2SO_4 and $NaOH$ to regulate the pH. The measurements were realised using the Zetasizer Nano Z ZEN2600, the concentration of the colloidal suspension equalled 0.02g/l at ambient temperature. 37
24 Solubility of Mn^{2+} in equilibrium with $Mn(OH)_{2,(s)}$, $[Mn_{tot,dis}]$ represents the total concentration of manganese species dissolved. 38
25 Evolution of the zeta potential of leached graphite and NMC811 as a function of the pH in the presence of aluminum ions, using H_2SO_4 and $NaOH$ to regulate the pH. Error bars present one standard deviation of measurement error. The measurements were realised using the Zetasizer Nano Z ZEN2600, the concentration of the colloidal suspension equalled 0.02g/l at ambient temperature. 39
26 Difference between the zeta potential of leached graphite and the one of CAM as a function of the pH in the presence of aluminum ions, using H_2SO_4 and $NaOH$ to regulate the pH. The measurements were realised using the Zetasizer Nano Z ZEN2600, the concentration of the colloidal suspension equalled 0.02g/l at ambient temperature. 40
27 Solubility of Al^{3+} in equilibrium with $Al(OH)_3(s)$, $[Al_{tot,dis}]$ represents the total concentration of aluminum species dissolved. 40
28 Grade and recovery of the carbon in the froth during the flotation, with and without washing. The test was performed in the GTK Labcell from Outotec. The washing was realised during 15 minutes at 1500 rpm and a pulp density of 5.7%. The rougher stage was realised during 19 minutes, with Escaid110 at a concentration of 150gpt conditioned during 2 minutes, and MIBC at a concentration of 80gpt conditioned during 1 minute, a flow rate of 4l/min and a rotation speed of 800rpm. The scavenger stage was realised during 12 minutes, with Escaid110 at a concentration of 75gpt conditioned during 2 minutes, and MIBC at a concentration of 80gpt conditioned during 1 minute. 42
29 Grade-recovery curve of the impurities in the froths during the flotation, without and with washing. The test was performed in the GTK Labcell from Outotec. The washing was realised during 15 minutes at 1500 rpm and a pulp density of 5.7%. The rougher stage was realised during 19 minutes, with Escaid110 at a concentration of 150gpt conditioned during 2 minutes, and MIBC at a concentration of 80gpt conditioned during 1 minute, a flow rate of 4l/min, a pulp density of 7.7% and a rotation speed of 800rpm. The scavenger stage was realised during 12 minutes, with Escaid110 at a concentration of 75gpt conditioned during 2 minutes, and MIBC at a concentration of 80gpt conditioned during 1 minute. 42

30 Pictures of the flotation cell, GTK Labcell from Outotec, in cases with and without washing, at 10 seconds after the beginning of the air flow. The washing was realised during 15 minutes at 1500 rpm and a pulp density of 5.7%. The rougher stage was realised during 19 minutes, with Escaid110 at a concentration of 150gpt conditioned during 2 minutes, and MIBC at a concentration of 80gpt conditioned during 1 minute, a flow rate of 4l/min and a rotation speed of 800rpm. The scavenger stage was realised during 12 minutes, with Escaid110 at a concentration of 75gpt conditioned during 2 minutes, and MIBC at a concentration of 80gpt conditioned during 1 minute. 43
31 Evolution of the cumulative recoveries and grades of carbon and NMC elements as a function of the promoter concentration, in the case with washing and without pH modification. The test was performed in the GTK Labcell from Outotec. The washing was realised during 15 minutes at 1500 rpm and a pulp density of 5.7%. The rougher stage was realised during 19 minutes, with Escaid110 at a concentration of 150, 350 and 500 gpt conditioned during 2 minutes, and MIBC at a concentration of 80gpt conditioned during 1 minute, a flow rate of 4l/min and a rotation speed of 800rpm, the pulp density was equalled to 7.7%. The scavenger stage was realised during 12 minutes, with Escaid110 at half the concentration during the rougher stage, conditioned during 2 minutes, and MIBC at a concentration of 80gpt conditioned during 1 minute. 44
32 Pictures of the flotation cell, GTK Labcell from Outotec, during the calibration of the pH, using H_2SO_4, at pH 2.57 and 4.75, before the addition of promoters, after the washing pre-treatment. The washing was carried out for 15 minutes at 1500 rpm with a pulp density of 5.7%. During the flotation test, the pulp density was equalled to 7.7%. 45
33 Evolution of the cumulative recoveries and grades of graphite and NMC elements as a function of the pH, in the case with washing, with a promoter concentration of 150 gpt. The pH, modified using H_2SO_4, at the beginning of the experiment was equal to 2.57, 4.75 and 6.55. The point at pH10.5 corresponds to the case without washing. The test was performed in the GTK Labcell from Outotec. The washing was realised during 15 minutes at 1500 rpm and a pulp density of 5.7%. The rougher stage was realised during 19 minutes, with Escaid110 at a concentration of 150gpt conditioned during 2 minutes, and MIBC at a concentration of 80gpt conditioned during 1 minute, a flow rate of 4l/min and a rotation speed of 800rpm, the pulp density was equalled to 7.7%. The scavenger stage was realised during 12 minutes, with Escaid110 at a concentration of 75gpt, conditioned during 2 minutes, and MIBC at a concentration of 80gpt conditioned during 1 minute. 47
34 Evolution of the zeta potential of graphite and NMC811 as a function of the pH in deionised water with 0.05M Li+ and with 0.005M Ni2+, using H_2SO_4 and $NaOH$ to regulate the pH. Error bars present the standard deviation of measurement error. The measurements were realised using the Zetasizer Nano Z ZEN2600, the concentration of the colloidal suspension equalled 0.02g/l at ambient temperature. 48

35 Evolution of the height of the suspension zone as a function of time for graphite and NMC811 at pH from 3 to 11. The graduated cylinder for graphite contains 600ml and the one of NMC811 120ml. In both cases, the pH was modified using H_2SO_4 and NaOH, the pulp density was equal to 7.7%. 49
36 Settling speed of graphite and NMC811, measured during a batch sedimentation test, at pH from 3 to 11, modified using H_2SO_4 and NaOH, with a pulp density equal to 7.7%. 50
37 Evolution of the height of the suspension zone as a function of time for graphite and NMC811 at pH6 and 9, the slopes are equal to the settling velocities of graphite NMC811, respectively, in the presence of Li^+ at a concentration of 0.1M. The pH was modified using H_2SO_4 and NaOH, the pulp density was equal to 7.7%. 51
38 Evolution of the height of the suspension zone as a function of time for graphite and NMC811 at pH 5 in the presence of nickel ions at a concentration of 0.02M. The pH was modified using H_2SO_4 and NaOH, the pulp density was equal to 7.7%. 52
39 Evolution of the height of the suspension zone as a function of time for graphite and NMC811 at pH10.5 without and with filtration of the precipitates in the presence of nickel ions at a concentration of 0.02M, the slopes are equal to the settling velocities of graphite and NMC811, respectively. The pH was modified using H_2SO_4 and NaOH, the pulp density was equal to 7.7%. 53
40 Evolution of the height of the suspension zone as a function of time for graphite and NMC811 at pH 5 without precipitates in the presence of cobalt ions at a concentration of 0.02M. The sedimentation test for graphtie was realised in a 600ml graduated cylinder and in a 120ml graduated cylinder for NMC811. The pH was modified using H_2SO_4 and NaOH, the pulp density was equal to 7.7%. 54
41 Evolution of the height of the suspension zone as a function of time for graphite and NMC811 at pH5 with and without filtration of the precipitates in the presence of aluminum ions at a concentration of 0.04M, the slopes are equal to the settling velocities of graphite and NMC811, respectively. The pH was modified using H_2SO_4 and NaOH, the pulp density was equal to 7.7%. . . . 55
42 Evolution of the height of the suspension zone as a function of time for graphite and NMC811 at pH11 with filtration of the precipitates in the presence of aluminum ions at a concentration of 0.04M. The pH was modified using NaOH, the pulp density was equal to 7.7%. 56
43 Continuous sedimentation test of synthetic black mass, composed of 80% of graphite and 20% of NMC811 , evolution of the grades and recoveries of the underflow product, as a function of the raising speed at pH5 in deionised water 58
44 Continuous sedimentation test of synthetic black mass, composed of 80% of graphite and 20% of NMC811 , evolution of the grades and recoveries of the underflow product, as a function of pH, modified using H_2SO_4 ad NaOH in deionised water. 59

45 C grade and recovery of the model black mass and leaching residue, continuous sedimentation test with a pulp density of 7.7% for the inlet flow, at pH5, modified using H_2SO_4 and NaOH and a raising speed of 10cm/min. 62
46 C grade and recovery of the model black mass and the mechanically pretreated black mass, continuous sedimentation test with a pulp density of 7.7% , at pH10.5, modified using NaOH, and a raising speed of 6.7cm/min 63

List of Tables

1 Lithium-ion battery constructive components and materials [11]. 4
2 Distributor and purity of the pristine minerals used 13
3 ICP and total organic carbon analysis of the mechanically pretreated black mass 14
4 ICP and total organic carbon analysis of the leaching residue 15
5 Operating conditions of the set (I) of tests : impact of the pH in deionised water, the pulp density is equal to 7.7% 20
6 Operating conditions of the set (II) of tests : impact of the pH in presence of ions, the pulp density is equal to 7.7% 21
7 Summary of the continuous sedimentation test realised, the synthetic black mass is composed of 80% of graphite and 20% of NMC811 24
8 ICP and ISE analyses of the flotation and washing waters at different pH (part 1) 47
9 ICP and ISE analyses of the flotation and washing waters at different pH (part 2) 47
10 Settling speed of graphite and NMC811, measured during a batch sedimentation test, at pH from 3 to 11, modified using H_2SO_4 and NaOH, with a pulp density equal to 7.7%. 50
11 Summary, settling speeds of graphite and NMC811 in the presence of ions at certain pH and concentration. The pH was modified using NaOH, the pulp density was equal to 7.7%. 57
12 Settling speed of graphite for pulp densities of 7.7% and 13% at pH = 5, in deionised water, the settling speed for a pulp density of 4.8% is approximated by a linear regression of the 2 settling speeds above. 58
13 Settling speed of graphite and NMC811, measured during a batch sedimentation test, as a function of the pH, modified using H_2SO_4 and NaOH, and raising speed in deionised water. 59
14 Grades, recoveries of the continuous sedimentation tests of synthetic black mass, composed of 80% of graphite and 20% of NMC811, and operating conditions, such as feed used, ions added, net raising speed and pH (part 1) . . 60
15 Grades, recoveries of the continuous sedimentation tests of synthetic black mass, composed of 80% of graphite and 20% of NMC811, and operating conditions, such as feed used, ions added, net raising speed and pH (part 2), the blank cases corresponds to a solid sample of insufficient mass to realise the XRF analysis. 61
16 Grades, recoveries of the continuous sedimentation tests of synthetic black mass, composed of 80% of graphite and 20% of NMC811, and operating conditions, such as feed used, ions added, net raising speed and pH (part 3), the blank cases corresponds to a solid sample of insufficient mass to realise the XRF analysis. 61

17 Grades, recoveries of the continuous sedimentation tests of synthetic black mass, composed of 80% of graphite and 20% of NMC811, and operating conditions, such as feed used, ions added, net raising speed and pH (part 4), the blank cases corresponds to a solid sample of insufficient mass to realise the XRF analysis. 61
18 Aluminum grade in both overflow and underflow and ratios of aluminum grade overflow/mass overflow and aluminum grade underflow/mass underflow for a continuous sedimentation test of synthetic black mass, composed of 80% of graphite and 20% of NMC811, performed at pH11, with a raising speed of 15cm/min in presence of aluminum at a concentration of 0.04M filtered to remove the precipitates 62
19 ICP analyses of the continuous sedimentation speed water, respectively for the test at pH10.5 with the black mass pretreated mechanically and for the test at pH5 with the leaching residue 64
20 Logarithm of concentration of nickel species at different pH, equilibrium constant for hydrolysis used from [62] and solubility constant used from [69] . . 68
21 Logarithm of concentration of manganese species at different pH. equilibrium constant for hydrolysis used from [63] and solubility constant used from [69] 69
22 Logarithm of concentration of manganese species at different pH. equilibrium constant for hydrolysis used from [64] and solubility constant used from [69] 69
23 Logarithm of concentration of aluminum species at different pH. equilibrium constant for hydrolysis used from [65] and solubility constant used from [69] 70
24 Grades, obtained using ICP-OES and total organic carbon analyses, and recoveries of the concentrates and tailings, in the cases without washing and with washing, with a concentration of escaid of 150, 350 and 500 gpt. The pH is unmodified in all cases 71
25 Cumulative grades and recoveries in the cases without washing and with washing, with a concentration of escaid of 150, 350 and 500 gpt. The pH is unmodified in all cases 72
26 Grades, obtained using ICP-OES and total organic carbon analyses, and recoveries of the concentrates and tailings, in the cases with washing and with and without pH modification, with a ph of 7, 5 and 3, in all cases the escaid concentration equals 150 gpt 73
27 Cumulative grades and recoveries in the cases with washing and with and without pH modification, with a ph of 7, 5 and 3, in all cases the escaid concentration equals 150 gpt 74
28 Grade, recoveries and operating conditions of the continuous sedimentation tests realised in deionised water with synthetic black mass, composed of 80% of graphite and 20% of NMC (part I) 75
29 Grade, recoveries and operating conditions of the continuous sedimentation tests realised in deionised water with synthetic black mass, composed of 80% of graphite and 20% of NMC (part II) 75

1 Introduction

1.1 Context

In the last years, lithium-ion batteries (LIBs) have become the main energy source of various electronic devices, from mobile phones to electric vehicles.
As a result of the wide application of these products, the quantity of spent LIBs has rapidly increased. As a consequence, considerable quantities of discarded waste were generated [1] [2] [3] [4]. Knowing that Co, Cu, Mn, battery-grade Ni and natural graphite are in the Critical Raw Material list [5] and that several elements are much more abundant in LIBs than in natural ores, the recycling of the spent LIBs is an absolute necessity [3].

Moreover, according to the EU legislation, 65% by weight of lithium-ion batteries must be currently recycled, and 70% by weight will have to be recycled by 2030 [6]. Knowing that graphite represents 14-22 wt.% of a LIB, its recycling will greatly increase the overall efficiency of LIB recycling [7].

Recycling graphite will result in a diversification of the graphite supply, which is currently dominated by China, which produces 95% of the spherical anode grade graphite used in LIBs. Strategies to develop a graphite supply chain for battery production are therefore being vigorously searched by other countries [8].

To reach those goals, it is necessary to develop more efficient strategies for the mechanical treatment of end-of-life batteries. Similarly to primary resources processing, the recovery of battery components strongly depends on particle size reduction and their liberation. However, the complex structure of LIBs poses significant challenges for separation operations and mechanical treatment [9]. LIBs are constituted of a succession of cells inside a metallic casing. Each cell is composed of two electrodes, a separator and an electrolyte. The cathode is composed of active particles such as lithium metal oxides (LMO), and a conductive agent, such as carbon black powder or acetylene black, which are coated onto aluminium foil by an organic binder, such as polyvinylidene fluoride (PVDF). The anode contains active particles composed of graphite that are coated on copper foil by an organic binder, styrene butadiene rubber (SBR). The organic electrolyte is composed of lithium salt ($LiPF_6$) and functional additives dissolved in an organic solvent. The separator is composed of polymeric material and its functional coating, composed of PVDF [10] [3].

Currently, the components that have a high economic value, such as Co,Ni, Cu and Li are the ones targeted by the recycling technologies [11]. To achieve an efficient separation process, well liberated compounds are necessary. In the case of LIBs, after comminution, the resulting fine, called "black mass", contains a heterogeneous mixture of cathode and anode active materials. Currently, the aim of the recycling process of black mass is to recover metals, which are components of great economic value, such as cobalt, nickel and copper. However, the heterogeneity of the black mass limits the performances of those recycling technologies [9]. Indeed, in pyrometallurgical technologies, graphite is generally used as a reducing agent and problems can occur during the process if the graphite content is too high. Moreover, due to the high temperature at which the process occurs, plastic covers and all organic compounds are incinerated and metals such as aluminum, manganese and lithium are lost in the slag.

Therefore, the overall efficiency of the process is reduced[12][10] [13] [14].

The hydrometallurgical recycling of spent LIBs involves an aqueous chemical treatment process to achieve high recovery rates and generate new cathode materials or other high-value products [15] [16]. However, graphite stays in the solid residue and unnecessary amounts of acid are consumd due to the porosity of graphite. Therefore, removing the graphite before the leaching could decrease the quantity of material to leach and the quantity of reagents consumed. Controlling the composition at metallurgical purification stages could minimize losses and operating costs. In order to recover graphite before the leaching step, flotation was investigated, due to the significant difference in wettability of the graphite, which is hydrophobic, and the cathode active materials, which are hydrophilic[17] [18] [19] [20].
Since the elements having a high economic value are recovered during the hydrometallurgical step, the separation of graphite could be realised after the hydrometallurgical step to minimize the losses of cathode active material (CAM).
Due to the zeta potential difference of CAM and graphite in deionised water [21] and therefore in agglomeration behaviour, sedimentation tests were investigated as a separation step for graphite and CAM, both before and after the leaching process.
Due to the presence of ions during the hydrometallurgical step, its impact on the flotation and settling behaviours of graphite and CAM was determined.

1.2 Objectives

The main objective of this work is to study the impacts of ions, such as Li^{+}, Co^{2+}, Ni^{2+}, Mn^{2+} and Al^{3+} on the selective agglomeration of graphite and its recovery using flotation and sedimentation once it is agglomerated. The sub-objectives are :

- To establish the evolution of the zeta potential of graphite and $Li(Ni_{0.8}Mn_{0.1}Co_{0.1})O_2$ (NMC811) as a function of pH in the presence of characteristics ions emanating from black mass when it is washed or leached.
- To determine the pH at which selective agglomeration of graphite is favoured. **to** study the impact of promoter concentration and pH on the flotation of graphite from black mass as well as the influence of ions present.
- To determine the settling speeds of graphite and NMC811 at the conditions at which graphite agglomeration is favoured.
- To selectively recover graphite by continuous sedimentation at the conditions at which the settling speeds differences are the most significant.

1.3 Scientific strategy

In order to fulfil this objective, the following experimental approach was followed.
First, the evolution of the zeta potential of graphite (NMC811) as a function of the pH was determined, in the presence of characteristics ions emanating from black mass when it is placed in water or leached.
Secondly, the pH at which selective agglomeration of graphite is favoured was determined.

Based on the differences of zeta potential in deionised water, flotation tests have been realised to study the impact of promoter concentration and pH on the flotation of graphite from black mass as well as the influence of ions present in flotation water. The optimal promoter concentration was determined at unmodified pH. Then, washing pretreatment of the black mass impact on flotation was studied. Thirdly, tests were realised at different pH (10.5, 9.5, 7, 5, 3) to determine its impact on graphite flotation.
Based on the zeta potential differences, batch sedimentation tests were also realised. The experimental conditions, such as pH and concentration of ion present, at which the highest zeta potential differences were observed, were selected to realise batch sedimentation tests, in order to see the link between a zeta potential difference, which induces a difference regarding the agglomeration behaviour, and a difference in the settling velocities. The optimal conditions, regarding pH and ion concentration, at which the settling velocities of CAM and graphite differ the most, were determined.
At those conditions, continuous sedimentation tests were realised, firstly with synthetic graphite and NMC to optimize the operational parameters such as the upward velocity, pH an ion concentration, secondly with real black mass and leaching residue.

The first part of this master thesis consists of a background of the LIBs recycling and black mass. It is followed by the materials and methods used. The black mass samples used as well as the equipment for the zeta potential measurement, flotation tests and batch and continuous sedimentation tests will be explained. The experimental protocols as well as the characterization techniques used will also be presented. In the third part, the results obtained during the experiments will be discussed. At the end, a conclusion and some perspectives are presented.

2 Background

2.1 State of the art

2.1.1 Composition and functionning of LIBs

In order to understand the challenges faced in the separation of the different battery components, it is important to understand their design and internal structure [9].

The weight percentage of the battery components and their most commonly used materials are given in Table 1. It can be seen that the anode, composed of graphite, accounts for 17 wt.%. Therefore its recycling will greatly increase the overall efficiency of LIBs recycling and help to achieve the 70% of recycling by weight required by the UE legislation in 2030.

Battery Component	**%w/w**	**Most Commonly Used Material**
Case	∼25%	Steel/plastics
Cathode	∼27%	$LiCoO_2$, $LiNi_xMn_yCo_zO_2$, $LiMn_2O_4$, $LiNiO_2$, $LiFePO_4$
Anode	∼17%	Graphite/$Li_4Ti_5O_{12}$
Copper and aluminium foils and current collectors	∼13%	Cu/Al
Electrolyte	∼10%	Solution of $LiPF_6$, $LiBF_4$, $LiClO_4$, and $LiSO_2$ dissolved in propylene carbonate, ethylene carbonate, or dimethyl sulfoxide
Separator	∼4%	Microporous polypropylene
Binder	∼4%	Polivinylidene Difluoride (PVDF)

Table 1: Lithium-ion battery constructive components and materials [11].

The major components of LIBs are: the shell, the cathode, the anode and the electrolyte [3] [10].

The shell is usually composed of low-carbon cold-rolled steel and stainless or nickel-plated cold-rolled steel. Its role is to serve as a protective layer, sustaining the external mechanical loading and providing an intact electrochemical reaction environment for battery charging/discharging [22].

The cathode is composed of an active material, which is a metal oxide containing lithium, such as $LiCoO_2$ (LCO), $LiTiO_2$ (LTO), $LiMn_2O_4$ (LMO), $LiFePO_4$ (LFP) or $LiNi_xCo_yMn_zO_2$ (x+y+z = 1) (NMC), binders, polyvinylidene fluoride (PVDF), and conductive agent, such as carbon black powder or acetylene black. All those compounds are mixed with a solvent in order to form a slurry. They are then coated onto the aluminum foil. [10] [3].

Similarly, the anode is also composed of an active material, generally graphite, a water soluble

binder such as styrene butadiene rubber (SBR), and both are coated onto the copper foil [10] [23]. Therefore, the anode is more easily liberated from its binder than the cathode.

The organic electrolyte is composed of a lithium salt, generally LiPF6 dissolved in an organic solvent, the most used are dimethyl carbonate (DMC) and methyl ethyl carbonate. The role of this electrolyte is to allow the transit of the lithium-ions between the cathode and the anode active materials [3] [10] [24].

Finally, the separator is composed of polyolefin-based materials, such as polyethylene (PE) and polypropylene (PP) and separates the electrodes in order to prevent a short circuit [3] [10] [24].

The LIB is a rechargeable battery containing several cells in which lithium ions move between the anode and the cathode. The cathode active material emits lithium ions to the anode during charging and receives them during discharging. On the other hand, the anode active material receives the lithium ions from the cathode during charging and emits them during discharging [25]. This cycle of charge and discharge is illustrated in Figure 1.

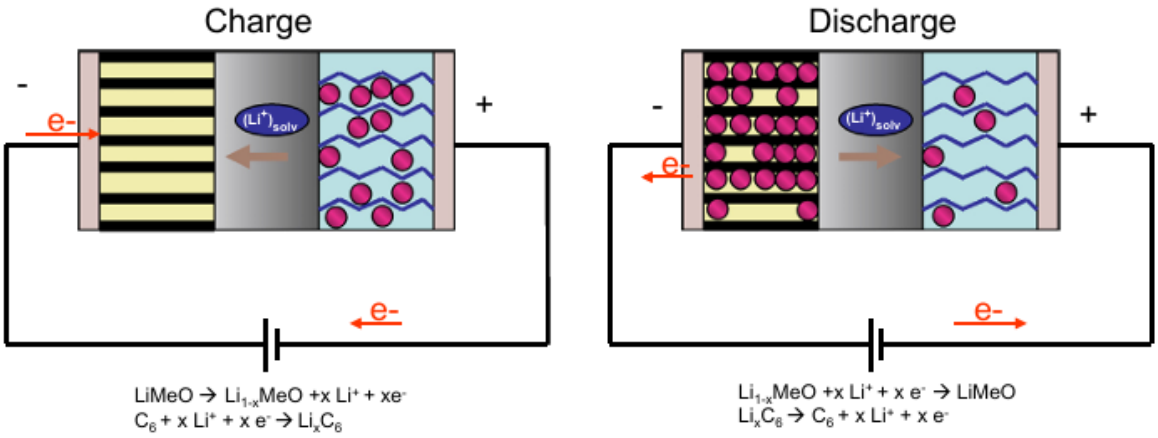

Figure 1: Charge and discharge cycle of a LIB. On the left there is the anode, containing graphite as active material and on the right there is the cathode, containing for example NMC as active material. The equations are the reduction-oxidation reactions happening during charging and discharging, Me can be replaced by NixCoyMnz (x+y+z = 1) since it is the metallic part in the cathode active material. [25]

2.1.2 Routes to recycle batteries

Nowadays,the components that have a high economic value, such as Co, Ni, Cu, and Li are the one targeted by the recycling technologies [11]. Those recycling methods are pyrometallurgy and hydrometallurgy [26]. They are schematised in Figure 2.

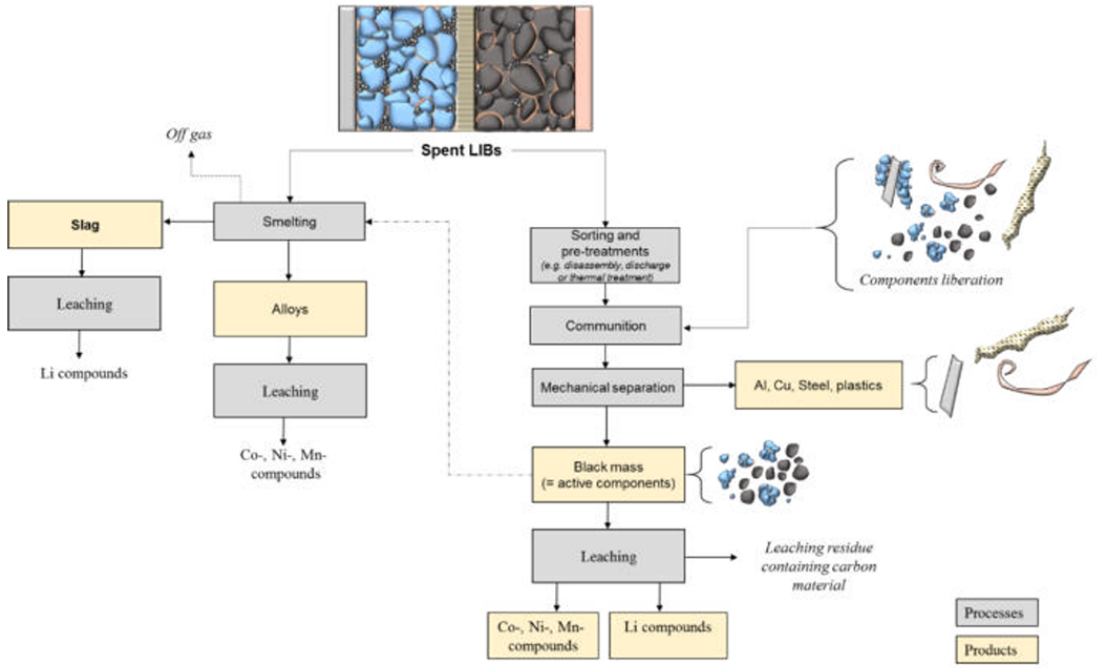

Figure 2: Schematic overview of the possible routes to recycle lithium-ion batteries [9]

2.1.2.1 Pyrometallurgical route

In pyrometallurgical processes, the cathode metals are reduced by the carbon present in the anode material, removing the need to separate the electrodes before the process. As it can be seen in Figure 3, three outcomes are produced by the reducing process : a Co alloy that contains Ni, Mn and Cu, depending on the feed material, a slag containing aluminum and lithium in the form of oxides, and burning gases, such as carbon dioxide, carbon monixide, water, organic fumes, etc. The alloys can be separated in component metals using hydrometallurgy and the metals lost in the slag are generally used as additives in the construction industry, since it is not profitable to recover them by hydrometallurgy. [11] [12]. Moreover, in existing processes treating primary resources such as Ni, Co and Cu ores, black mass can be incorporated as a secondary feed, by the dotted line in Figure 2 [9].

One advantage of pyrometallurgy is its robustness, which does not require pretreatment, such as discharging and dismantling, since many hazards potentials are eliminated during the smelting [12]. The disadvantages are the lower recycling efficiency compared to hydrometallurgy, high energy consumption and emission of burning gases [10] [13] [14] [12].

2.1.2.2 Mechanical and thermal pretreatment

Alternatively to the pyrometallurgical process, pretreatments can be realised to prepare the battery recycling. First of all, in the case of electric vehicle battery packs, the batteries are disassembled. Then, they are discharged for safety reasons, to avoid short-circuits and spontaneous combustion. Usually, the batteries are immersed in a 5% NaCl solution for 24h to deactivate the cells. They are then air dried naturally [14] [3]. A thermal process, such as

pyrolysis in the absence of oxygen or calcination in the presence of oxygen, can be applied before the crushing to thermally destroy the separator, electrolyte and binder, improving the recovery of anode and cathode active materials [27]. The comminution process is performed to liberate the electrode active particles and concentrate them in the fine fraction, called black mass. Sieving is performed to separate the black mass from the coarse fraction containing the electrode foils, plastic or metal casing, and separator materials. The coarse fraction can be further separated using magnetic and electrostatic separation [14] [26] [27].

2.1.2.3 Hydrometallurgical route

The hydrometallurgical recycling of LIBs involves an aqueous chemical treatment process comprising two main stages, such as leaching, which corresponds to the dissolution of metallic components mostly coming from the active material (mixture of cathodes and anodes), preferably with mineral acids, and separation/purification, which corresponds to the solid/liquid separation of the cake and the pregnant leached solution (PLS), the use of solvent extraction on the PLS, ion exchange, and precipitation to achieve high recovery rates and generate new cathode materials or other high-value products [15] [16].

The most commonly used acid to leach metals from LIBs is sulfuric acid due to its effectiveness, low-cost, and compatibility with metal separation techniques. In the leaching process, graphite stays in a solid residue after filtration [16] [28]. The reactions that occur when NMC is in contact with sulphuric acid are given by [28]:

$$2ALiNi_xMn_yCo_zO_2(s) + 3AH_2SO_4(aq)$$

$$\rightarrow 2AxNiSO4(aq) + 2AyMnSO4(aq) + 2AzCoSO4(aq) + ALi_2SO4(aq) + 3AH2O(aq) + A/2O_2(g)(1)$$

The second step corresponds to the use of solvent extraction, ion exchange, and precipitation to achieve high recovery rates and generate new cathode materials or other high-value products, in the form of precursor salts, such as $NiSO_4$, $CoSO_4$ and Li_2CO_3 [15] [16] [29]

Compared with pyrometallurgical approaches, hydrometallurgical processes are more flexible and offer several advantages, such as low energy consumption, high product purity, and reduced CO_2 emissions[15] [16] [28].
However, hydrometallurgy needs mechanical pretreatment, the processes are relatively complex and achieve lower throughputs [16] [15] . It also requires an extensive use of chemicals and generates secondary streams of hazardous liquid waste that need to be managed carefully [15].

Removing the graphite before the leaching could decrease the quantity of material to leach, increasing the recycling efficiency and decrease the quantity of reagents consumed, due to graphite porosity. In order to recover graphite before the leaching step, flotation was investigated, due to the significant difference in wettability of the graphite, which is hydrophobic

and the cathode active materials, which are hydrophilic[17][18] [19] [20].

2.2 Black mass flotation and pretreatment

In the mining industry, flotation is a physico-chemical separation process that uses the difference in surface properties of the valuable minerals and the unwanted gangue minerals [30]. It can also be used in the recycling industry to separate materials that have a significant difference in wettability, such as graphite, which is hydrophobic, and lithium transition metal oxides (LMOs), cathode active materials, which are hydrophilic, from the black mass [17] [18] [19] [20]. The selective attachment of valuable materials to air bubbles, called "true-flotation" is the most important mechanism and represents the majority of particles that are recovered in the concentrate [30].

Although this mechanism is dominant for the recovery of valuable material, the separation efficiency is also dependent on the degree of entrainment and physical entrapment, which occur simultaneously to true flotation. Mechanical entrainment is a mechanism by which particles suspended in water reach the froth phase and are removed together with the particles recovered by true flotation. It is directly proportional to water recovery and is increased with fine particle sizes [30]. Entrapment is a mechanism by which fine hydrophilic particles become physically entangled within hydrophobic particles or bubble-particle agglomerates and are thus transported to the froth phase. It is often referred to as aggregation [30].

In a mechanical flotation cell, an agitator is present to provide enough turbulence in the pulp (the combination of water and solid, the quantity of solid present in the cell is termed "pulp density") to promote collision of particles and bubbles, resulting in the attachment of valuable particles to bubbles and their transport to the surface, where they will be recovered in the froth. This process is only applicable to relatively fine particles because, if they are too large, the particle weight will be higher than the adhesion between the particle and the bubble, therefore the bubble will not be able to lift the particle [30].

In direct flotation, the valuable material is floated and the unwanted material is left in the pulp or tailing, as opposed to reverse flotation, where the unwanted material is floated.

The attachment of valuable particles to air bubbles is only possible if the particles are hydrophobic. When they reach the surface, the air bubbles can only continue to carry the particles if they can form a stable froth. If they cannot, they will burst and drop the particles. To achieve these conditions, several compounds, known as flotation reagents, can be used [30]. The flotation reagents are divided into 3 categories. The collectors adsorb on the particle surfaces, making them hydrophobic, and promoting bubble attachment The frothers help to maintain the froth stable. Finally, regulators control the flotation process, either by activating or depressing particles attachment to air bubbles or by controlling the pH of the system [30].

The surfaces of non-polar minerals, such as graphite, are characterised by relatively weak molecular bonds. The minerals are composed of covalent molecules linked together by Van der Waals forces, and non-polar minerals are hydrophobic since their surfaces don't attach to the water dipoles. Even though it is possible to float graphite without reagent, its hydrophobicity

is generally increased by the use of non-ionic hydrocarbon collectors, their adsorption is due to intermolecular Van der Waals forces [20] [31]. On the contrary, minerals with strong covalent bond or ionic surface bonding are polar and exhibit high free energy values at the polar surface. These minerals are naturally hydrophilic since the polar surfaces react strongly with water molecules [30].

Therefore, flotation has drawn interest to separate the anode composed of graphite and the cathode active materials, composed of LMOs, due to their wettability differences, graphite being hydrophobic and LMOs being hydrophilic [17] [18] [19] [20]. Two chemical reagents typically reported in literature to float black mass are kerosene, as a promoter to increase graphite's hydrophobicity, and methyl isobutyl carbinol (MIBC) as a frother, to stabilize the froth [20].

However, the flotation of the real black mass is hard to realise since the particles are coated with hydrophobic polymeric binders, which promote the attachement of LMOs particles to air bubbles [20] [32] [17] [18] [19].
In addition to true flotation, entrainment and entrapment are also present and decrease the flotation performance [20]. The presence of entrainment was proved by a linear correlation between the lithium metal oxides recovery and water recovery The agglomeration of graphite and LMOs particles might result in entrapment [20].
In order to reduce entrapment, a pre-conditioning, such as attrition, is recommended [20] [33]. Selective flocculation of cathode active materials could be realised in order to reduce entrainment [20] [21].
Flocculation was realised by Rinne et al. at pH around 5 using modelised black mass. The reagents used were cationic polyacrylamide flocculant to agglomerate the cathode and a dispersant (0.5wt. % SHMP) to avoid the formation of heteroflocs and MIBC as a frother. In the absence of ultrafine fine particles, the battery-grade graphite reached 99.4%. In the presence of ultrafine particles, the grade equalled to 98.2%. When the ultrafine feed was flocculated, the grade increased to 98.4%, although a drop in recovery was observed. When a dispersant was applied in addition to a flocculant, the recovery could be increased while maintaining a 98.4% grade. It has been shown that branched flocculants provided improved selectivity over linear flocculants. Those results suggest that particle size needs to be controlled to recover battery-grade graphite, with a grade higher than 99% [21].

Finally, Vanderbruggen et al. have also shown that even though oily type promoters strongly interact with the spheroidized graphite particles, which increases the collection efficiency of graphite, they also promote the collection of lithium transition metal oxide fine particles on bubbles. This highlights the need of a more selective promoter or depressants to increase the separation efficiency between the black mass components [20].

As a summary, the different behaviours occurring during the flotation of black mass are illustrated in Figure 3.

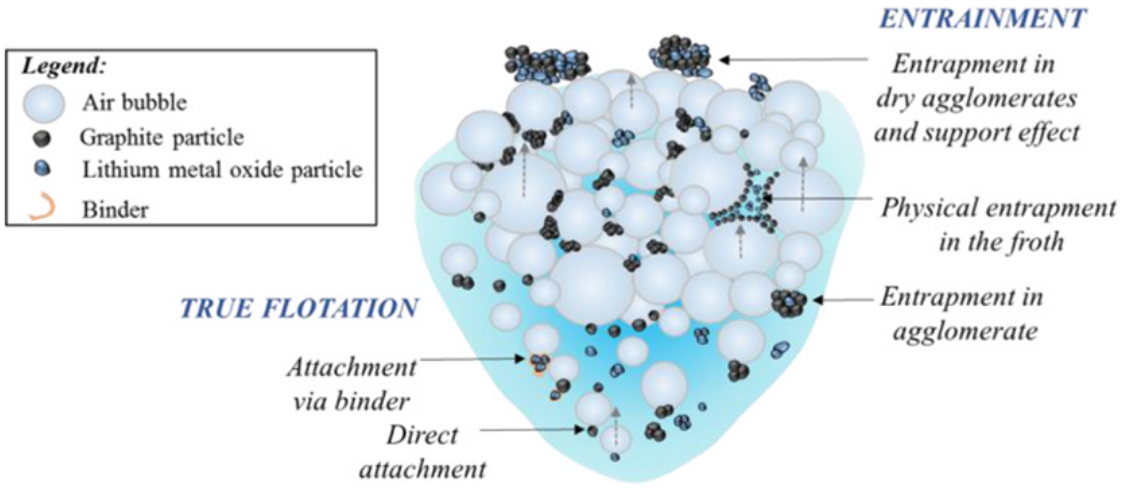

Figure 3: Summary of simplified behaviour of active particles from lithium-ion batteries during black mass froth flotation [9]

Due to the negative impact of the organic binder presence on the flotation performances, several pre-treatments to remove the binder and improve the flotation performance were investigated. These include chemical dissolution with Fenton reagent [18], mechanically-induced stress such as mechanical grinding [17], cryogenic grinding [34], and thermal treatment [19].

After being modified by Fenton's reagent, a combination of Fe^{2+} and H_2O_2 with a ratio 1/120, and a liquid/solid ratio 75/1, the original wettability of LiCoO2 and graphite was regained. The content of cobalt was 39.91 wt.% [18].

Concerning mechanical grinding, under the optimum grinding conditions of 5 min, the concentrate grade of LiCoO2 and graphite are, respectively, 97.19% and 82.57%, and their recovery rate are, respectively, 49.32% and 73.56% [17]. Cryogenic grinding of mechanically treated electrode material in a ball mill cooled with liquid nitrogen was realised at -196 °C and resulted in an improved concentrate grade up to 91.75% LCO with a recovery of 89.83% [34].

Even though these results are good, these techniques were limited to lab-scale application, due to difficulties in up-scalability. Furthermore, the mechanical grinding process breaks the spheroidized anode graphite, which hinders its direct use in battery applications [35]. Because of its effectiveness and the ease with which it can be scaled up for industrial applications, thermal treatment at temperatures between 400 °C and 600 °C under vacuum, inert gas, or air atmospheres has become the most widely studied technique [35]. Previous studies reported high recovery rates of LMOs in the cell product, ranging from 80% to 98%, while graphite recovery in the froth product reached approximately 95–98% [19][36] [37] [33].

2.3 Zeta potential

Selective agglomeration of graphite could increase the overall selectivity of the flotation process.

The study of the zeta potential is used to identify the pH at which agglomeration occurs and gives an information about the surface charge of the particle. Therefore, selective reagent can be used, anionic if the zeta potential is positive or cationic if it is negative [29]. The zeta potential can be used to determine the stability of a particle. When solid particles are dispersed in a liquid, which is called a colloidal system, the liquid layer surrounding those particles is composed of an inner and a diffuse region. The inner region, composed of a thin layer of ions having the opposite charge of the surface of the particle, is called the Stern layer. In the diffuse region, called the diffuse layer, the ions are less bound together. There is a theoretical boundary inside which the ions and the particle form a stable entity. Ions within that boundary move with the particle, as it travels through a medium due to Brownian motion or sedimentation. This layer is called the double layer. Ions beyond the boundary don't move and stay with the bulk dispersant. The zeta potential is the potential at this boundary. Therefore, a particle with a negative zeta potential will bound with positively charged surfaces and vice-versa [38] [39].

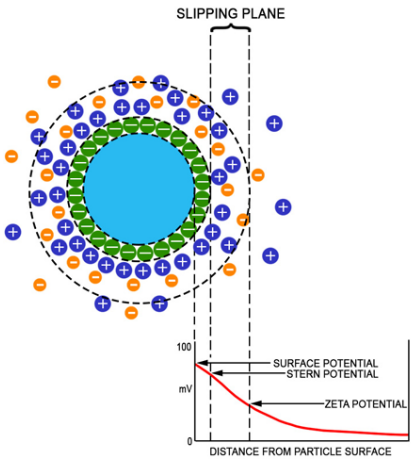

Figure 4: Schematic view of the electrical double layer [40]

The magnitude of the zeta potential is used to determine the stability of a colloidal suspension. If the entire particles in suspension have a highly positive or negative zeta potential, the particles will repel each other due to repulsive electrostatic forces between particles with the same charge. On the contrary, if the zeta potential is low, there will be no repulsion forces and therefore the particles will flocculate. If the value of the zeta potential is higher than $\pm$ 30 mV, the system is considered stable. On the contrary, if the value of the zeta potential is lower than $\pm$ 10 mV, the particles will agglomerate[38] [40] [39].

When measuring a zeta potential in an aqueous media, the pH must be specified since it affects the zeta potential. Indeed, when acid is added to a colloidal solution, the particles will become more positive if the acidic protons are specifically adsorbed. On the contrary, when base is added the particle will become more negative if the ions are specifically adsorbed.

Due to these effects on the charge of the particles, one point can be observed at which the zeta potential equals zero for a certain pH, it is called the isoelectric point. Since the colloidal system is the least stable, it is generally the point where aggregation will occur [39] [38].

2.4 Sedimentation test

Sedimentation tests were performed to determine the settling velocity of graphite and NMC811. When the concentration of solids in suspension is above 500mg/l, the flocculated particles increasingly lose their individual mobility and can no longer move relatively to each other. Therefore, they settle in zones with an interface formed between the liquid supernatant and the entangled flocs [41]. The settling velocity of flocs is noticeably different from that of the individuals particles and depends especially on the concentration of solids.

Generally, four zones can be observed during an experiment, as represented in [41].

- a : which is the clarification zone, where the liquid is clear,
- b : zone of homogeneous suspension of same concentration as the starting suspension,
- c : transition zone of increasing concentration, where it is generally assumed that no coalescence occurs, not always observable,
- d : compression zone : where sludge thickens.

The time-dependent height of the interface between first zones a and b and later zones a and d constitute the so-called Kynch curve. Kynch has hypothesized that the sedimentation velocity of a layer of particles only depends on its concentration of solids, and does not depend on the dynamics of formation of this layer. This assumption is valid for suspensions that do not show a too strong heterogeneity of the size and shape of the particles, as it is the case here. The slowing down in the velocity in the compression zone is therefore due to the increase in concentration [41]. Based on this assumption, the settling speed is determined at each instant by the local tangent to the Kynch curve : $v_d = -(dh/dt)_i$ [41]. Therefore, the average velocity is given by the slope of the Kynch curve.

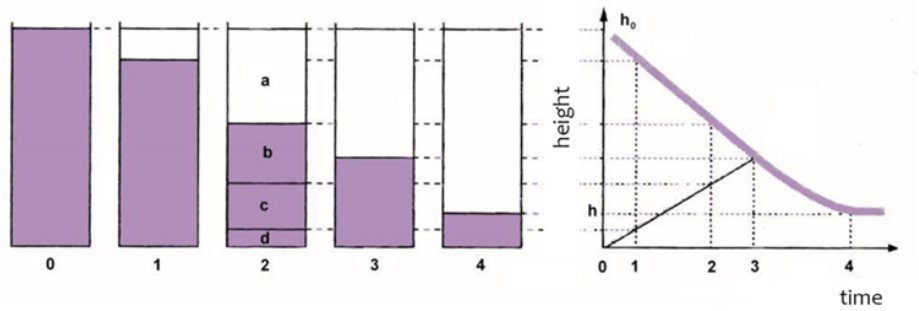

Figure 5: Schematic representation of the zone settling and related Kynch curve [41]

3 Materials and methods

3.1 Pristine materials used

During the zeta potential measurements and batch sedimentation tests, pristine materials are used. During the continuous sedimentation tests, synthetic black mass was used. Due to a lack of cathode material, the 14g of feed used were composed of 11g of graphite and 3g of NMC811, which corresponds to the quantity percentage of carbon present in the leaching residue. The distributor and purity of the pristine graphite and NMC811 used to model the synthetic black mass are shown in Table 2.

Distributor	**Mineral**	**Purity (%)**
ProGraphite [42]	Synthetic graphite anode material	99.96
Gelon [43]	NMC811	99.5

Table 2: Distributor and purity of the pristine minerals used

3.2 Black mass characterization

The black mass was provided by an industrial partner. It was obtained using the pre-treatment showed in Figure 6. First, the modules are discharged. The discharged modules undergo shredding and volatile component vaporisation to remove organic solvents and exhaust gas. After that, a sieving of 300 μm is realized. The undersize fraction composed the black mass 11A. The oversize fraction undergoes zigzag separation. The heavy fraction will be further separated. The light fraction will undergo milling and another sieving step at 300 μm. The undersize fraction composed black mass 11B. The black mass 11A is richer in carbon and the black mass 11B is richer in NMC content and impurities. The representative black mass corresponds to the mixing of black mass 11A and 11B with a ratio 47%/53%. Initially, 3.5kg of each black mass, 11A and 11B, were taken. In order to make sure that the particle size is suitable for flotation, both samples were sieved using a 150 μm sieve. After the sieving, the mass of black mass 11A was 2.4kg and that of black mass 11B 3.2kg.

The feed composition is given in Table 3. It can be seen that the composition of aluminum equals 0.65%. This comes probably from the aluminum foil. The 30% of nickel, 3.8% of cobalt and 1.96% of manganese come from the NMC cathode. It can be noticed that the cathode is rich in Ni. The 0.66% of copper probably comes from the copper foil and the 0.34% of iron from the shell. The 0.39% of phosphorous comes presumably from the electrolyte, the 3% of fluorine from the binder and the electrolyte and the 4.04 % of lithium from the cathode and the electrolyte.
The 33.05% of carbon comes probably from the anode, in the form of graphite and from the carbon black. The black mass is from the same batch of modules. Therefore, a mixture is not expected. However, since NMC811 formulations are at the discretion of the manufacturers, mixtures or transformations may be found in them, which could explain why the grades of Ni, Mn and Co do not respect the usual ratios for NMC cathode.

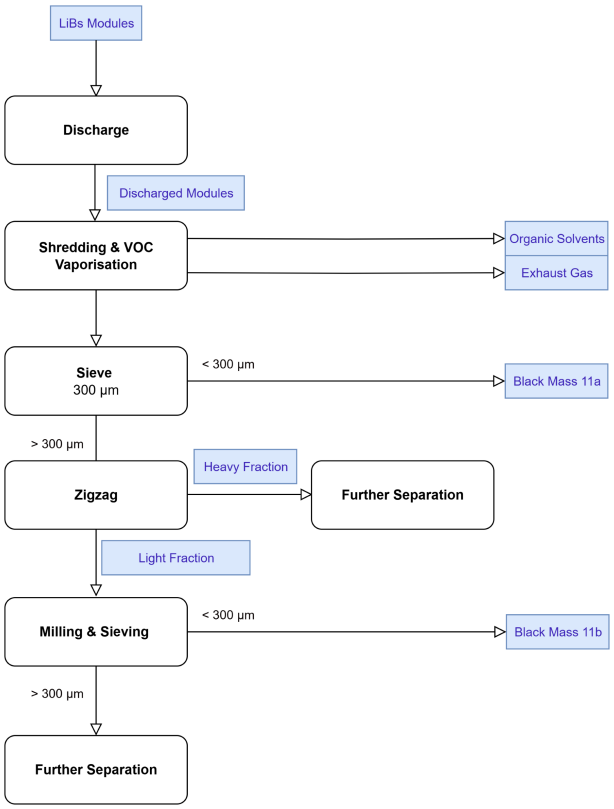

Figure 6: Flowsheet pretreatment of the black mass used, ©M. Batutiako

	Al	Co	Cu	F	Fe	Li	Mn	Ni	P	C
Feed composition	0.65%	3.80%	0.66%	3.00%	0.34%	4.04%	1.96%	30.14%	0.39%	33.05%

Table 3: ICP and total organic carbon analysis of the mechanically pretreated black mass

3.2.1 Sampling

The representativity of the samples strongly influences the reliability of the results. Indeed, all the samples must have the same properties as the initial feed in order to be able to compare properly the effect of several flotation parameters without the influence of the feed composition. Due to the heterogeneity of the particles, both in terms of size and density, the sampling of the black mass is challenging and was done carefully in order to obtain the most representative samples.

After the sieving, the mass of black mass 11A was 2.4kg and that of black mass 11B 3.2kg. First, the black mass 11A and 11B were split separately in 8 using a rotary spitter. One sub-sample of 300g of each black mass was taken for feed analysis. Therefore, for black mass 11A, the recombination of the 7 remaining sub-samples, resulting in one sub-sample of 1219g and one of 912g. In order to respect the 47/53 ratio, the sub-samples of black mass 11B

must weight 1375 and 1029g. Therefore, from the 8 sub-samples of roughly 400g, 2 were set aside. Concerning the remaining 6, in order to obtain the wanted masses, black mass was transferred from one sub-sample to the other, making the assumption that the transfer is representative due to the small size of the particles. After that, the corresponding sub-sampels were mixed manually, respecting the 47/53 ratio. A second splitting was realised for each sub-samples and 8 sub-samples of 325g and 245g were obtained. In order to obtain the wanted 100g samples, those sub-samples were split using a riffle splitter. Splitting the 245g in 2, 20g were removed to obtain the wanted 100g sub-sample. Splitting the 320g in 4, the 20g missing in each sample was provided by the extra 20g removed from the 245g samples. Due to the small size of the particles, the assumption was made that this step was representative.

3.3 Leaching residue characterization

In order to evaluate the possibility to obtain a high-purity graphite by recovering it after the leaching step, a leaching residue was produced. The black mass 11AB was leached during 4 hours in a 30L reactor using sulphuric acid provided by VWR chemicals (H_2SO_4, 95-97%, Prod No. 2090-290 [44]) and iron sulphate heptahydrate, provided by VWR chemicals ($FeSO_4.7H_2O$, 98%, Prod No. A15178.0E [45]). 2mol of sulphuric acid were used for 1mol of equivalent NMC, the pulp density was 15% and 790kg of iron sulphate were used per ton of black mass [46]. The elemental composition of the leaching residue is shown in Table 4. Analyzing the values, it can be seen that the carbon content accounts for almost 80%. Comparing to the composition before lixiviation, as shown in Table 3,it can be seen that composition of all elements excepted carbon is reduced. This is expected since the leaching step brings the NMC compounds in solution and that the graphite does not react during the lixiviation. Since the fluorine and phosphorus content are not significantly reduced in Table 4, it can be assumed that the PVDF is still present.

Al	**Co**	**Cu**	**F**	**Fe**	**Li**	**Mn**	**Ni**	**P**	**C**
0.16%	0.64%	0.05%	2.88%	0.77%	0.15%	1.10%	4.78%	0.23%	79.65%

Table 4: ICP and total organic carbon analysis of the leaching residue

3.4 Leaching procedure of the pristine material

In order to evaluate the impact of lixiviation on the zeta potential of the particles, a lixiviation was realised on the pristine graphite and NMC811. The duration of the test was 4 hours, 14ml of sulphuric acid at a purity of 96% were added for the graphite and 19ml were added for the NMC811 to keep the pH around 0.8, which is the pH of the solution containing graphite. In both cases, 200ml of water were used and 31.5g of iron sulphate heptahydrate. Since 0.26 mol of sulphuric acid and 0.11 mol of iron sulphate heptahydrate were used for 0.41mol of NMC, the reaction was not complete. The test was realised to evaluate the zeta potential of the particles that are not completely leached, as they are present in the leaching residue.

3.5 Zeta potential measurements

The zeta potential's evolution of graphite and NMC811 regarding the pH was determined using the Zetasizer Nano Z ZEN2600. The pH was adjusted using H_2SO_4 and NaOH from 3 to 11. The pristine materials were mixed with deionised water to produce a colloidal suspension of 0.02 g/l. To take into account the statistical variance, 3 individual measurements were taken for each samples and an average value was calculated.

After that, the zeta potential measurements were realised at the same conditions, using the graphite and NMC811 leached.

In order to evaluate the impact of different ions present in water flotation of black mass, several solutions were prepared. Lithium sulphate monohydrate, supplied by Thermo Fisher Scientific ($Li_2SO_4.H_2O$, 99%, Product No A10410.36) [47] was used at a concentration of Li^+ of 0.1 and 0.05M, which corresponds to a concentration of, respectively, 0.7 and 0.35 g/l. Nickel sulphate hexahydrate ($NiSO_4.6H_2O$, 98%, Product No VWRC25895.294) was used at a concentration of Ni^{2+} of 0.2, 0.1, 0.05 and 0.025M, which corresponds to a concentration of, respectively, 1.17, 0.59, 0.29 and 0.15g/L. Manganese (II) sulphate tetrahydrate, supplied by Thermo Fisher Scientific ($MnSO_4.4H_2O$, 99%, Product No B22081.22) was used at a concentration of Mn^{2+} of 0.2, 0.1, 0.05 and 0.025M, which corresponds, respectively, to a concentration of 1.10, 0.55, 0.27 and 0.14 g/l. Cobalt (II) sulphate heptahydrate, supplied by Thermo Fisher Scientific ($CoSO_4.7H_2O, 98\%$, Product No A16201.36) [48] at a concentration of Co^{2+} of 0.2, 0.1 and 0.025M, which corresponds, respectively, to a concentration of 1.18, 0.59, 0.29 and 0.15g/l. Aluminum sulphate about 14 hydrate, supplied by VWR^{TM} ($Al_2(SO_4)_3.14H_O$, 99.88%, Product No 21070.297) [49] was used at a concentration of Al^{3+} of 0.4, 0.2, 0.1 and 0.05M, which corresponds, respectively, to a concentration of 1.08, 0.54, 0.27 and 0.13 g/l.

3.6 Froth flotation experiments

The flotation experiments were realised using a laboratory mechanically stirred cell (GTK Labcell from Outotec). The Magotteaux bottom driven cell was also used. The rotor is not bound to the cell but the rotor and the stator are attached to a shaft and must be slided down to allow the rotor to mix properly the cell content. The rotation speed is imposed using the control panel, the air flow is controlled using the rotameters. The rotor and shaft height control allows to slide the rotor and shaft down and to lock it to the hollow on the right side of the flotation machine. The waterpistol was used to clean the rotor and shaft before and after the experiments. Since the scrapping was realised manually, the skimmers were not used.

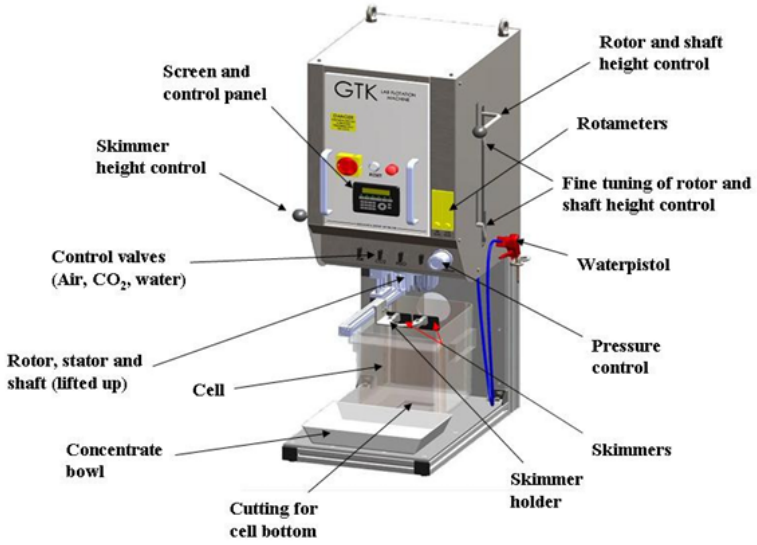

Figure 7: Representation of the flotation cell used and names of the different parts it is composed of [50]

Escaid^{TM} 110, supplied by ExxonMobil(Hydrocarbon fluid, Product No. 20171206) was used as a promoter to enhance the natural hydrophobicity of graphite surfaces. Escaid^{TM} is a low odor dearomatised hydrocarbon fluid which poses low risk to worker safety.[51] [52] Methyl isobutyl carbinol (MIBC) from Thermo Fisher Scientific (C6H14O, 99%, Product No A13435.AP) was used as a frother to increase froth stability. [53] Sulphuric acid supplied by Grosseron (H_2SO_4, 95%, Product No 20704.320) was used to reduce the pH. [54]

The washing pre-treatment was realised at a rotation speed of 1500 rpm, during 15 minutes with a pulp density of 5.7%. In order to increase the quantity of ions dissolved in the water, a 2L cell was used for the washing and a 1.3L cell was used for the flotation. The flotation experiments were realised at a rotation speed of 800 rpm, with an air flowrate of 4l/min and a pulp density of 7.7%.
Three sets of experiments were realised, as illustrated in Figure 8. In the first, the pH was not modified and the promoter concentration was varied to optimised it. 3 tests were performed, respectively at, 150, 350 and 500 gpt of Escaid^{TM}. The frother concentration was 80 gpt.
In the second set of experiments, the promoter concentration was set at 150 gpt, the frother concentration was set at 80 gpt and the pH was decreased, using H_2SO_4 to determine its effect. 3 tests were performed, beginning at roughly pH 7, 5 and 3 at the moment when the Escaid^{TM} is added. For all experiments, the Escaid^{TM} was conditioned for 2 minutes, the MIBC was conditioned for 1 minute and then the first rougher concentrate was floated for 7 minutes.
The second rougher concentrate was floated during 9 minutes. After a conditionning time of 1 minute, the half of the initial promoter quantity was added and conditioned during 1 minute. The initial frother quantity was added and the frother was conditioned during 1 minute. Then, the scavenger concentrate was floated for 9 minutes.

During the experiment, water was added to compensate the water retrieved during the flotation, in order to maintain a pulp level constant.

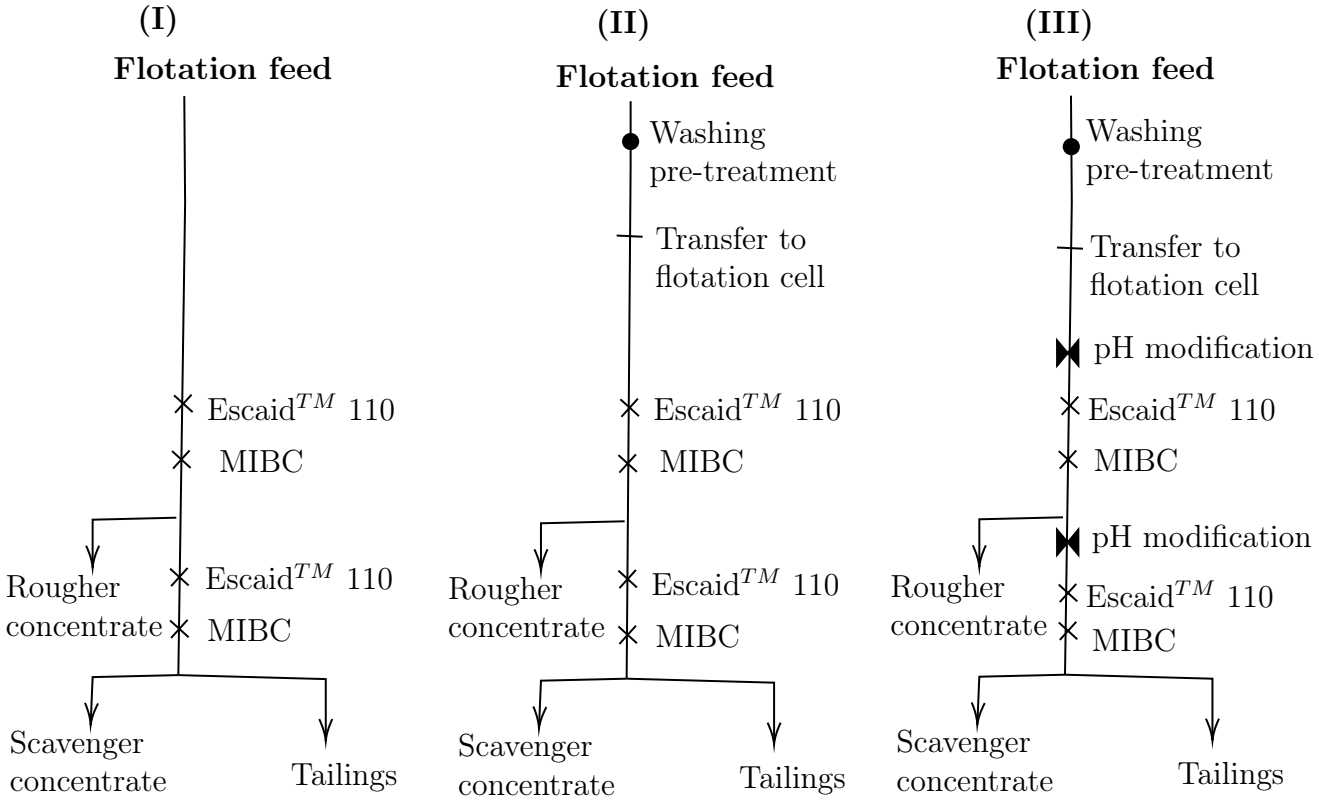

Figure 8: The three flow diagrams for the flotation experiments (I) No washing pre-treatment, collector concentration set at 150gpt during the rougher stage, (II) With washing pre-treatment and no pH modification, (III) With washing and pH modification. The washing pre-treatment is realised during 15 minutes at 1500 rpm at a pulp density of 5.7%. During the pH modification step, the pH was modified to 7, 5 and 3. Tests (II) and (III) are performed at a concentration of Escaid^{TM}110 of 150gpt in the rougher stage and 75gpt in the scavenger stage and an MIBC concentration of 80gpt both in the rougher and scavenger stages

After the washing, the slurry was filtered using a filter 15-20 μm Labomoderne (Ref. FL1163). Then, was water used to put the filtered slurry in solution in the 1L cell and reach the 7.7 % pulp density.
A filtration was realised using a 2-4 μm filter supplied by Labomoderne (Ref. FL5408). After filtration, the solids were dried in an oven at 45 °C during 12h. The filtration was done for safety reasons, to pack the black mass inside the filter and avoid dust in the oven.
Samples of flotation water were taken and sent to ICP-OES and ISE analysis. After the drying, the solid samples were weighted and sent to ICP-OES and total organic carbon analysis. Due to a lack of time to realise all the analyses, the 2 rougher concentrates were combined. When the scavenger concentrate mass was below 5g, it was also combined with the rougher concentrates. This is the case for the flotation experiments at pH 5 and 3.

The quantity of reagents added is given by :

$$r(i)[\mu l] = d(i)[g/t] \cdot 10^{-6}[t/g] \cdot \frac{1}{D(i)[g/l]} \cdot M$$

where

- r is the quantity of the reagent i added
- d is the dosage of the reagent i
- D is the density of the reagent i
- M is the mass of the black mass in the flotation cell

The concentrations of acid used were 5 and 20 vol.%, which equals to 0.072 and 0.36 mol/l. To minimise the quantity of acid added, the 20 vol. % acid was used to decrease the pH to 3 and the 5 vol. % acid was used to decrease the pH to 5 and 7. Since the pH increased during all the experiments after the addition of acid, for the experiments at pH 7, 5, 3, the rougher stages started respectively at pH 6.55, 4.75 and 2.57 and ended at pH 7.7, 6.53 and 5.54. During the conditionning of the scavenger stage, acid was added to decrease the pH and start at the pH close to the pH at which the rougher started. For the experiments at pH 7, 5, 3, the scavenger stage started respectively at pH 6.74, 4.67 and 2.55 and ended at pH 7.78, 6.32 and 4.57.

The flotation performance of the different tests was evaluated based on the grade, recovery, mass pull and water pull.
The recovery is given by :

$$R(i) = \frac{G_P(i) \cdot M_P}{G_F(i)_F}$$

where :

- R(i) is the recovery of the component i
- $G_P(i)$ is the grade of the component i in the overflow product
- M_P is the overflow product mass
- $G_F(i)$ is the grade of the component i in the feed
- M_F is the feed mass

3.7 Batch sedimentation tests

In order to determine the impact of the pH on the settling speed, settling tests were performed at pH 3, 5, 7, 9 and 11 on synthetic graphite and NMC811. Since the quantity of graphite available was higher, in order to obtain more reliable results those tests were performed in a

graduated cylinder of 600ml. Concerning the NMC811, since the quantity available was more limited, all the tests were realised in a graduated cylinder of 120 ml. For all the experiments, the pulp density was set to 7.7% since it is the pulp density fixed during the flotation tests and the pH was fixed using H_2SO_4 and $NaOH$.

Due to a lack of graphite material, except for the experiment in the presence of cobalt ions, all the following experiment will be realised in a graduated cylinder of 120ml for the graphite. As it will be explained in subsubsection 4.3.1, due to the significant settling speed difference at pH5 in deionised water, settling tests were performed in the presence of ions, such as Co^{2+} at a concentration of 0.2M, Ni^{2+} at a concentration of 0.2M, Al^{3+} at a concentration of 0.4M, with and without filtration. Indeed, as it will be explained in subsection 4.1 and subsection 4.3, the presence of precipitates on the particles reduces the zeta potential and settling speed differences. Therefore, a filtration was realised before the settling tests at the conditions at which precipitation could occur in order to evaluate the impact of the ions in solution. In order to better understand the impact of precipitation, two settling tests were realised with Al^{3+} at a concentration of 0.4M, with and without filtration at pH 6.

Due to the significant zeta potential difference at pH6 and 9 at a concentration of Li^+ equalled to 0.05M, settling tests were performed at those conditions, once again in a 120ml graduated cylinder with a pulp density of 7.7%, fixing the pH with H_2SO_4 and $NaOH$. The Li^+ solution was filtered before the tests in order to measure the highest settling speed difference.

Due to the significant zeta potential difference at pH10.5 at a concentration of Ni^{2+} equalled to 0.02M, settling tests were performed at those conditions. In order to evaluate the impact of the precipitation, two settling tests were realised, with and without the filtration of the Ni^{2+} solution before the settling test.

Similarly, since due to the significant zeta potential difference at pH11 at a concentration of Al^{3+} equalled to 0.04M, settling tests were performed at those conditions. The Al^{3+} solution was filtered before the tests in order to measure the highest settling speed difference. As a summary, the operational conditions used during the tests are listed in Table 5 and Table 6.

Material	**Ions**	**pH**
Graphite	Deionised water	Modified to 3, 5, 7, 9, 11
NMC811	Deionised water	Modified at 3, 5, 7, 9, 11

Table 5: Operating conditions of the set (I) of tests : impact of the pH in deionised water, the pulp density is equal to 7.7%

Material	**Ions**	**pH**	**Filtration of precipitates**
Graphite	Li^+ 0.1M	6, 9	No
NMC811	Li^+ 0.1M	6, 9	No
Graphite	Ni^{2+} 0.02M	5, 10.5	No
NMC811	Ni^{2+} 0.02M	5, 10.5	No
Graphite	Ni^{2+} 0.02M	5, 10.5	Yes
NMC811	Ni^{2+} 0.02M	5, 10.5	Yes
Graphite	Co^{2+} 0.02M	5	Yes
NMC811	Co^{2+} 0.02M	5	Yes
Graphite	Al^{3+} 0.04M	3.8, 5, 6	No
NMC811	Al^{3+} 0.04M	3.8, 5, 6	No
Graphite	Al^{3+} 0.04M	5, 6, 11	Yes
NMC811	Al^{3+} 0.04M	5, 6, 11	Yes

Table 6: Operating conditions of the set (II) of tests : impact of the pH in presence of ions, the pulp density is equal to 7.7%

During all the tests, solid sample was put into solution and mixed, increasing slowly the rotation speed until no more particles were viisble at the top of the beaker. At that moment the content was transfered in the graduated cylinder and mixed until no particles were sticked at the bottom. Then, the sedimentation test started. The time started to be measured at the moment at which the separation between the clarification area and the settling zone reached 110 ml, and the time at which each 10 ml were reached was evaluated. To take into account the statistical variance, each test was realised 2 times, 3 if the differences were too significant, and an average value for each time was calculated. The evolution of the height of the suspension zone, converted in cm as a function of time, in minute,s was plotted. Since the settling speed is reduced when the pulp density increases, the settling speed was determined as the slope of the average values for the top-half of the cylinder.

3.8 Continuous sedimentation test

A schematic representation of the continuous sedimentation device is shown in Figure 9. The feed(A), which is stirred in a beaker during the experiment with a pulp density of 7.7% is pumped (B) and goes in the micro flotation cell (D) by a funnel (C). The water at the wanted pH (F) is pumped (E) and goes in the micro flotation cell by side, at a height below the half of a cell to maximize the effect of the water to entrain selectively the particles. The entrained particles go to the overflow (I) and the others settle at the bottom of the micro flotation cell. At the end of the experiment, those particles are pumped (G) to the underflow (H). To improve the understanding, a picture is shown in Figure 10. Before the beginning og the test, the feed in conditioned during 20 minutes at 600 rpm to ensure a good mixing and the formation of agglomerates. The mixing continues during the entire test. The pump pumping the feed is set to the lowest speed, 0.4cm/min, to allow the feed to enter in the cell

gently, allowing the particles to be entrained by the water or to settle selectively. In order to always have water entering in the microflotation cell and therefore to avoid the presence of bubbles, the water in the overflow is filtered during the test and reintroduced in the water beaker (F). Before the beginning of the test, deionised water at fixed pH is introduced until the outlet of the funnel. Therefore, when the test begins, the water will reach the top of the cell at the time when the feed enters the cell.

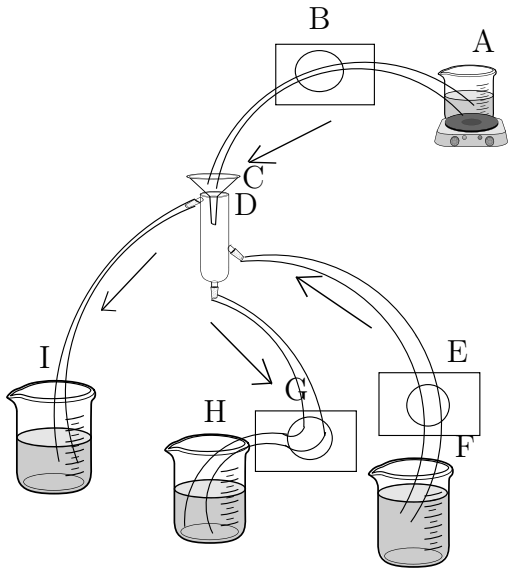

Figure 9: Schematic representation of the continuous sedimentation device, where A represents the feed being stirred, B a pump, C a funnel, D the micro-flottation cell, E a pump, F the inlet water at the wanted pH, G a pump, H the underflow product, I the overflow product



Figure 10: Picture of the continuous sedimentation device, where A represents the feed being stirred, B a pump, C a funnel, D the micro-flottation cell, E a pump, F the inlet water at the wanted pH, G a pump, H the underflow product, I the overflow product

As it will be explained in subsection 4.4, the upward speed, which corresponds to the velocity of the inlet water (F) in Figure 9 equals to the lowest settling speed of graphite and NMC811

determined during the batch sedimentation test, to take into account the reduction of pulp density in the microflotation cell compared to the 7.7% pulp density in the beaker. Therefore, the upward speed of water is higher than the lowest settling speed, therefore those particles are entrained in the overflow and the particles with a settling speed higher than the water speed will settle at the bottom of the cell. The average duration of the test is one hour and a half.

As it will be explained in subsection 4.4, tests were first realised at pH5 in deionised water since the settling speed difference was the highest. To evaluate the impact of the upward speed, 3 tests, at an upward speed of 7.8, 10 and 16.2 cm/min were realised at pH5. 16.2 cm/min corresponds to the velocity at a pulp density of 4.8%, the one if the entire 14g of feed are in the flotation cell. However, as it will be explained, the grades and recoveries were higher at a lower upward speed. At pH7, the upward speed was set to 8cm/min. As it will be explained, due to the high settling speed differences in the presence of nickel and aluminum at pH10.5 and 11, respectively, a continuous sedimentation test was realised in deionised water at pH10.5 and the upward speed was set to 6.7 cm/min. Then, two continuous sedimentation tests were realised in the presence on nickel ions, with a filtration of the precipitates, at an upward speed of 6.7 and 13.6 cm/min and a continuous sedimentation test in the presence of aluminum ions, with a filtration of the precipitates, was realised at an upward speed of 15cm/min. All those tests were realised using synthetic black mass.

Due to the good results obtained at pH 5 and 10.5 in deionised water, a continuous sedimentation test was realised using leaching residue at pH5 and a black mass pretreated mechanically at pH 10.5, respectively at a raising speed of 10 and 6.7cm/min.

For more clarity, the operational conditions of the continuous sedimentation tests are shown in Table 7.

Black mass	**Pulp density of the feed (%)**	**Ions**	**Raising speed (cm/min)**	**pH**
Synthetic	7.7	Deionised water	7.8	5
Synthetic	7.7	Deionised water	10	5
Synthetic	7.7	Deionised water	16.2	5
Synthetic	7.7	Deionised water	8	7
Synthetic	7.7	Deionised water	6.65	10.5
Synthetic	7.7	Ni2+ filtered	6.65	10.5
Synthetic	7.7	Al3+ filtered	15	11
Synthetic	7.7	Ni2+ filtered	13.6	10.5
Mechanically pretreated	7.7	Deionised water	6.6	10.5
Leaching residue	7.7	Deionised water	10	5

Table 7: Summary of the continuous sedimentation test realised, the synthetic black mass is composed of 80% of graphite and 20% of NMC811

3.9 Characterization

In order to obtain the wanted elemental compositions of the different samples, several analytical techniques are used. Both Inductively Coupled Plasma Optical Emission spectroscopy (ICP) and X-rays fluorescence (XRF) analyses are used to obtain the composition of every elements present in black mass except carbon and fluorine in solid samples. ICP is also used to obtain the quantitative composition of liquid samples. In order to obtain the carbon content in the solid samples, total organic carbon analysis (TOC) is used. The fluorine composition in solid samples is obtained by XRF and by ion-selective electrode (ISE) analysis in the liquid samples. XRF is a qualitative method, compared to ICP. However, due to a lack of time, some analysis were only realised using XRF.

3.9.1 ICP-OES

ICP-OES is an analytical technique used to determine quantitatively the elemental composition of various samples. Contrary to the XRF anaylis, standard solutions are used during the ICP analysis to make it quantitative [55]. Therefore, contrary to the XRF analysis, the exact composition will be provided only regarding the elements asked to be analysed. By using standard solutions with known concentrations, this relationship can be accurately established.
It uses a high-temperature argon plasma, a gas containing a significant number of argon ions, typically from 8,000 to 10,000 K, to excite atoms in a sample, causing them to emit light at specific wavelengths that are measured to identify and quantify elements [55].
In practice, the plasma is formed by seeding the argon gas passing through a plasma torch with electrons. The electrons are accelerated and collide with argon atoms releasing more electrons and forming argon ions. Elements, in the form of atoms, are introduced into the plasma. A proportion of theses atoms will be become ionized within the plasma. When an atom or ion is excited within the plasma, its electrons move from a lower to higher energy level, releasing energy in the form of photons at specific wavelengths, characteristic of their respective elements, as they transition back to their initial 'ground' state [56] [55]. Since solid samples cannot be introduced into the plasma directly, an acidic digestion is used in this case, using aqua regia (a mix of HNO_3 and HCl) [57]. The liquid samples are diluted, since an elevated content of dissolved solids can cause suppression or drift of the signal [58].

3.9.2 XRF

XRF is an analytical technique that uses the interaction of X-rays with a material to determine qualitatively its elemental composition. Contrary to ICP, it can be used on both liquids and solids. Firstly, primary X-rays knock out an electron from one of the orbitals surrounding the nucleus within an atom of the material. Therefore, a hole is produced in the orbital, resulting in a high energy, unstable configuration for the atom. In order to restore equilibrium, an electron from a higher energy level, outer orbital, falls into the hole. Since this is a lower energy position, the excess energy is emitted in the form of fluorescent X-rays. The energy difference between the expelled and replacement electrons is characteristic of the element atom in which the fluorescence process is occurring. Thus, the energy of the emitted fluorescent X-ray is directly linked to a specific element being analyzed [59].

3.9.3 ISE fluoro analysis

An ion-selective electrode (ISE) works by generating a small voltage that changes predictably with the concentration of a specific ion in a solution. The electrode contains a specialized membrane that only responds to one type of ion, fluoride in this case.
When the target ion interacts with the electrode's membrane, an electrical signal proportional to how much ion is present develops across it [60].

3.9.4 Total organic carbon (TOC) analysis

Total Organic Carbon (TOC) is a measure of the amount of carbon found in samples. It was only used for solid samples in this case. The organic carbon present in the sample is oxidized to form CO_2, which is quantitatively measured, using non-dispersive infrared (NDIR) detection, which measures the infrared absorption of CO molecules [61].

4 Results and discussion

4.1 Zeta potential

4.1.1 Deionised water

4.1.1.1 Non-leached compounds

In deionised water, the evolution of the zeta potential of graphite and NMC811 as a function of the pH is shown in Figure 11. The evolution is similar to the one found by Rinne et al. [21]. It can be seen that, at pH between 3 and 5, the zeta potential of graphite is between -15 mV and 0mV and the zeta potential of CAM is more negative. The zeta potential values between which agglomeration is taking place vary among the sources, comprised between +/-10mV [39] or +/-30mV [38]. However, using both sources, it can be assumed that the graphite tends to agglomerate more than cathode active material in the region of pH 3 to 5. In order to evaluate the link between zeta potential, agglomeration and therefore settling speed, the evolution of the settling speed as a function of pH will be establised for graphite and NMC. It is expected that the graphite agglomerates more than NMC in the region of pH 3 to 5 and therefore, has a higher settling speed.

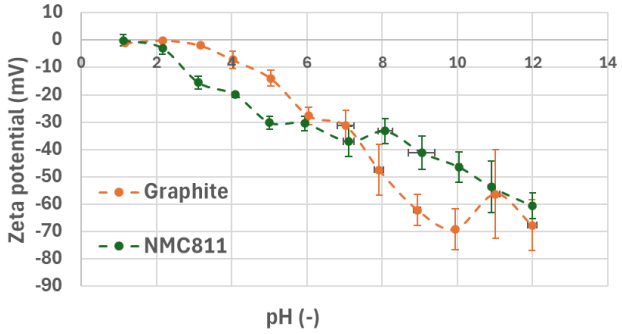

Figure 11: Evolution of the zeta potential of graphite and NMC811 as a function of the pH in deionised water, using H_2SO_4 and $NaOH$ to regulate the pH. Error bars present the standard deviation of measurement error. The measurements were realised using the Zetasizer Nano Z ZEN2600, the concentration of the colloidal suspension equalled 0.02g/l at ambient temperature.

4.1.1.2 Leached compounds

The evolution of the zeta potential of graphite and NMC811, leached and non-leached, is shown in Figure 12. Analyzing the graphs it can be seen that, as expected, the zeta potential of graphite is not affected by the leaching. The difference at alkaline pH can be explained by the important standard deviation at those pHs. On the contrary, the NMC811 is affected by the leaching. This is also expected since the cathode compounds are leached, therefore the structure of the particles is expected to change during the leaching. The difference is the most important at acidic pH, between 2 and 5, at those pHs the NMC811 is leached.

The leaching happening during the zeta potential test can modify the zeta potential of the particles. Since the leaching alters the surface of NMC811 particles, it could explain the fact that hydrogen and hydroxide ions seem to have a higher impact, respectively at acidic and alkaline pH. Similarly to the case with graphite, since the standard deviations are significant at alkaline pH, it is harder to quantify the impact of leaching.

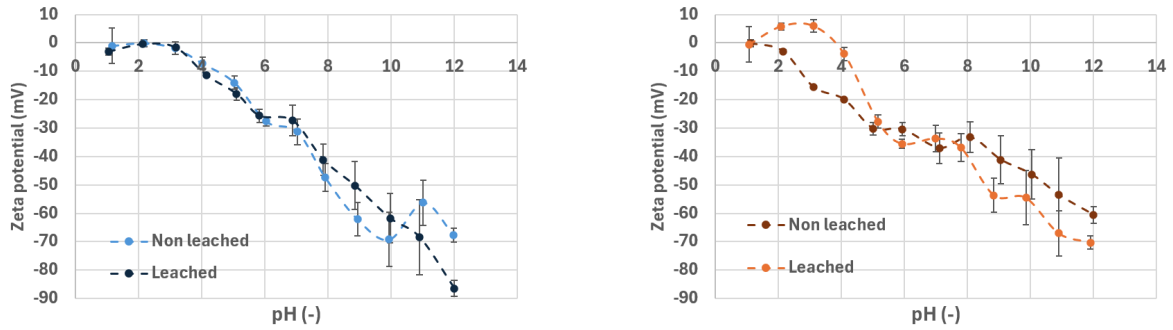

(a) Graphite (b) NMC811

Figure 12: Evolution of the zeta potential of graphite and NMC811, leached and non-leached, as a function of the pH in deionised water, using H_2SO_4 and $NaOH$ to regulate the pH. Error bars present the standard deviation of measurement error. The measurements were realised using the Zetasizer Nano Z ZEN2600, the concentration of the colloidal suspension equalled 0.02g/l at ambient temperature

To make the comparison between the zeta potential of leached graphite and NMC811, their evolution as a function of pH is shown in Figure 13. It can be seen that zeta potential difference is greatly reduced in the case of leached graphite and NMC811.

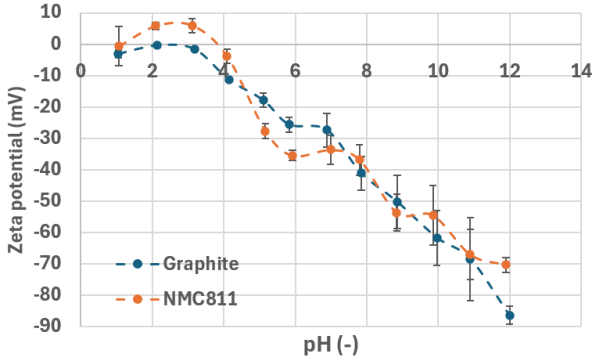

Figure 13: Evolution of the zeta potential of leached graphite and NMC811 as a function of the pH in deionised water, using H_2SO_4 and $NaOH$ to regulate the pH. Error bars present the standard deviation of measurement error. The measurements were realised using the Zetasizer Nano Z ZEN2600, the concentration of the colloidal suspension equalled 0.02g/l at ambient temperature.

4.1.2 Effect of ions presence

4.1.2.1 Effect of lithium ions presence

The evolution of the zeta potential as a function of the pH, in the presence of lithium ions, of graphite and NMC811 are shown in Figure 14. Analyzing the graphs, it can be seen that the zeta potential is higher in the presence of lithium ions, and that the ions effect is more marked in the alkaline region. Indeed, since the lowest zeta potential are around -30mV at pH11 for both species, agglomeration is expected to occur in the whole pH-range between 3 and 11.
In order to facilitate the comparison between the zeta potential of graphite and NMC811, Figure 15, shows the evolution of difference between the zeta potential of graphite and the one of NMC811 as a function of the pH in the presence of lithium ions. It can be seen that the zeta potential difference between the graphite and NMC811 is negative between pH 4 and 7, with the highest difference at pH 6 and a concentration of lithium ions equalled to 0.05M. On the contrary, the zeta potential difference is positive in the alkaline region, with the highest difference at pH9 and a concentration of lithium ions equalled to 0.05M. Therefore, the zeta potential of graphite is more negative than the one of NMC811 in the acidic region and less negative in the alkaline region.

It can be seen that the difference is the highest for the lowest concentration. It could be explained by the precipitation of lithium on both surfaces, therefore the zeta potential measured would be the one of lithium hydroxide for both graphite and NMC811 when the concentration is high enough for all particles to be completely covered by the precipitate.
Since the difference between both zeta potentials is the highest at pH = 6 and 9, batch sedimentation tests will be realised at those pH.

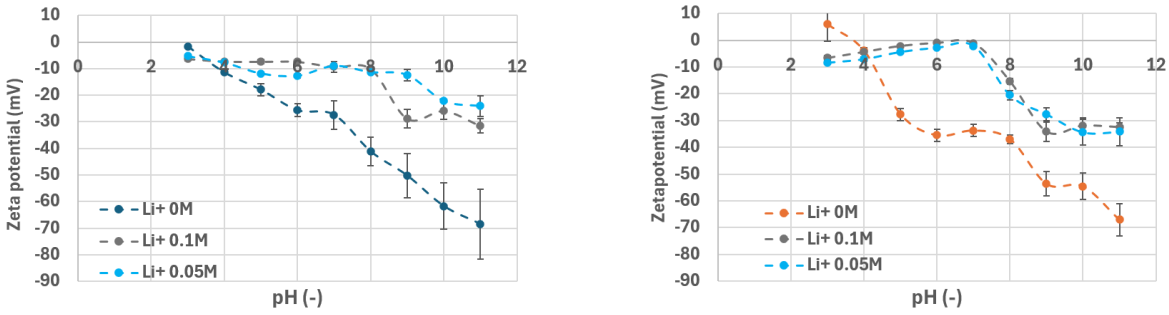

(a) Graphite

(b) NMC811

Figure 14: Evolution of the zeta potential of leached graphite and NMC811 as a function of the pH in the presence of lithium ions, using H_2SO_4 and $NaOH$ to regulate the pH. Error bars present one standard deviation of measurement error. The measurements were realised using the Zetasizer Nano Z ZEN2600, the concentration of the colloidal suspension equalled 0.02g/l at ambient temperature.

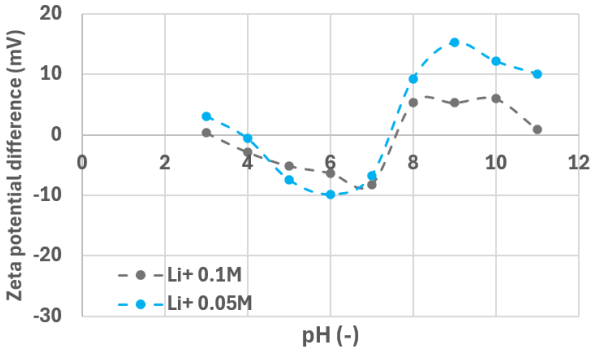

Figure 15: Difference between the zeta potential of leached graphite and the one of NMC811 as a function of the pH in the presence of lithium ions, using H_2SO_4 and $NaOH$ to regulate the pH. The measurements were realised using the Zetasizer Nano Z ZEN2600, the concentration of the colloidal suspension equalled 0.02g/l at ambient temperature.

4.1.2.2 Effect of nickel ions presence

The evolution of the zeta potential as a function of the pH, in the presence of nickel ions, of graphite and NMC811 are shown in Figure 16.

Concerning both compounds, the difference is more marked in the alkaline region. The impact of nickel ions is higher than one of lithium ions, which could be explained by the fact that nickel is a bivalent cation and a monovalent one.
In order to facilitate the comparison between the zeta potential of graphite and NMC811, Figure 17, shows the evolution of the difference between the zeta potential of graphite and the one of CAM as a function of the pH in the presence of nickel ions. Since the difference between both zeta potentials is the highest at pH = 11, batch sedimentation tests will be realised at that pH. It can be seen that the difference is the highest for the lowest nickel concentration. It could be explained by the precipitation of nickel on both surfaces, therefore the zeta potential measured would be the one of nickel hydroxide for both graphite and NMC811 when the concentration is high enough for all particles to be completely covered by the precipitate. This could explain why the zeta potential difference at pH11 at the concentration of 0.02M is not more negative than the one at a concentration of 0.01M, as it would be expected by the decrease of the difference when the concentration of nickel ions increases from 0.025 to 0.01M.
In order to know the pH at which the nickel ions precipitate, the solubility of Ni^{2+} in equilibrium with $Ni(OH)_{2(s)}$ and the distribution of Ni species can be calculated.

The five nickel species considered are : Ni^{2+}, $Ni(OH)^{+}$, $Ni(OH)_2$, $Ni(OH)_3^{-}$, $Ni(OH)_4^{2-}$

The equations considered are :

$$Ni(OH)_2 \leftrightarrow Ni^{2+} + 2OH^-, \qquad Kps_{NI(OH)_2} = 5.48 \cdot 10^{-16}[62] \tag{2}$$
$$Ni^{2+} + H_2O \leftrightarrow NiOH^+ + H^+, \qquad k1 = 1.26 \cdot 10^{-10}[62] \tag{3}$$
$$Ni^{2+} + 2H_2O \leftrightarrow Ni(OH)_2 + 2H^+, \qquad k2 = 10^{-19}[62] \tag{4}$$
$$Ni^{2+} + 3H_2O \leftrightarrow Ni(OH)_3^- + 3H^+, \qquad k3 = 6.31 \cdot 10^{-30}[62] \tag{5}$$
$$Ni^{2+} + 4H_2O \leftrightarrow Ni(OH)_4^{2-} + 4H^+, \qquad k4 = 1 \cdot 10^{-44}[62] \tag{6}$$

From Equation 2, the following expression is obtained : $[Ni^2+] = Kps^{'}(Ni(OH)_2) \cdot [H^+]^2$, where $Kps^{'}(Ni(OH)_2) = Kps_{NI(OH)_2} \cdot k_w^{-2}, \qquad k_w = 10^{-14}$
Therefore, it is possible to express the equations Equation 2 to Equation 6 as a function of pH :

$$[Ni^{2+}] = Kps^{'}(Ni(OH)_2) \cdot 10^{-2pH} \tag{7}$$
$$[Ni(OH)^+] = k1 \cdot Kps^{'}(Ni(OH)_2) \cdot 10^{-pH} \tag{8}$$
$$[Ni(OH)_2] = k2 \cdot Kps^{'}(Ni(OH)_2) \tag{9}$$
$$[Ni(OH)3^-] = k3 \cdot Kps^{'}(Ni(OH)_2) \cdot 10^{pH} \tag{10}$$
$$[Ni(OH)_4^{2-}] = k4 \cdot Kps^{'}(Ni(OH)_2) \cdot 10^{2pH} \tag{11}$$

The total concentration of nickel species dissolved is given by

$$[Ni_{(tot,diss)} = [Ni^{2+} + [Ni(OH)^+] + [Ni(OH)_2] + [Ni(OH)_3^-] + [Ni(OH)_4^{2-}]$$

The evolution of the logarithm of the nickel concentration as a function of pH is shown in Figure 18, the precise values are shown in Table 20. Analysing Figure 18 and Table 20, it can be seen that the precipitation of Ni^{2+} is taking place between pH 8 and 12 for the concentration of 0.02M. Those pHs correspond to the ones at which the zeta potential difference is the highest at the lowest concentration in nickel ions. The precipitation of $Ni(OH)_{2(s)}$ on the particles could explain why the zeta potential is close to 0 at alkaline pH.

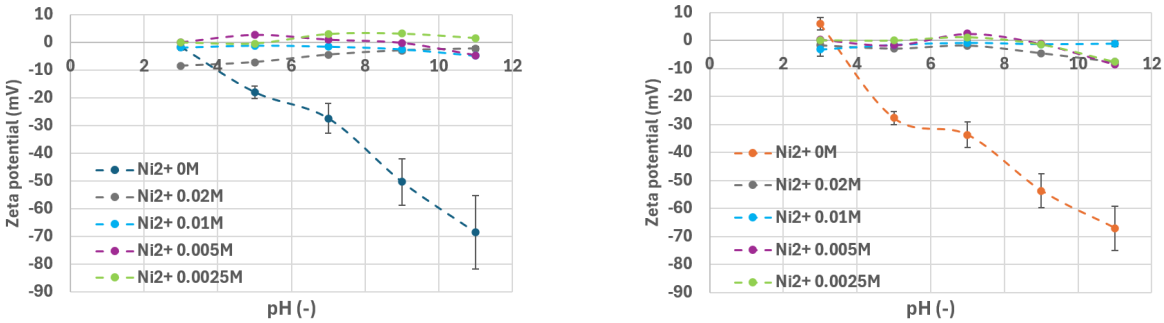

(a) Graphite (b) NMC811

Figure 16: Evolution of the zeta potential of leached graphite and NMC811 as a function of the pH in the presence of nickel ions, using H_2SO_4 and $NaOH$ to regulate the pH. Error bars present one standard deviation of measurement error. The measurements were realised using the Zetasizer Nano Z ZEN2600, the concentration of the colloidal suspension equalled 0.02g/l at ambient temperature.

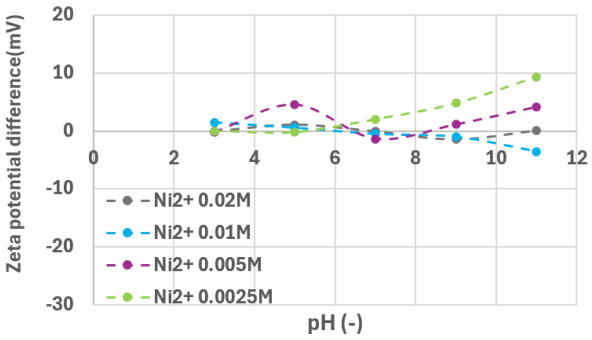

Figure 17: Difference between the zeta potential of leached graphite and the one of CAM as a function of the pH in the presence of nickel ions, using H_2SO_4 and $NaOH$ to regulate the pH. The measurements were realised using the Zetasizer Nano Z ZEN2600, the concentration of the colloidal suspension equalled 0.02g/l at ambient temperature.

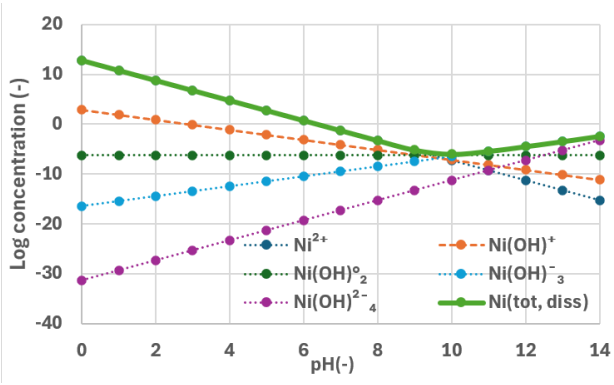

Figure 18: Solubility of Ni^{2+} in equilibrium with $Ni(OH)_{2(s)}$, $[Ni_{tot,dis}]$ represents the total concentration of nickel species dissolved

4.1.2.3 Effect of cobalt ions presence

The evolutions of the zeta potential as a function of the pH, in the presence of cobalt ions, of graphite and NMC811 are shown in Figure 19.

Concerning both compounds, the difference is more marked in the alkaline region.
In order to facilitate the comparison between the zeta potential of graphite and NMC811, Figure 20, shows the evolution of the difference between the zeta potential of graphite and the one of NMC811 as a function of the pH in the presence of cobalt ions. It can be seen that the difference is the highest for the highest ion concentration. As seen in Figure 19, the zeta potential of NMC811 is more increased than the one of graphite in the presence of cobalt ions. Since the difference is the highest at pH at which the cobalt does not precipitate given its concentration, it makes sense that the highest the ion concentration in the solution, the highest the zeta potential difference. The fact that the zeta potential is the same at alkaline pH could be explained by the precipitation of cobalt on both surfaces, therefore the zeta potential measured would be the one of cobalt hydroxide for both graphite and NMC811.
Since the difference between both zeta potentials is the highest at pH = 5, batch sedimentation tests will be realised at that pH. Similarly to nickel, in order to know the pH at which the cobalt ions precipitate, the solubility of Co^{2+} in equilibrium with $Co(OH)_{2(s)}$ and the distribution of Co species can be calculated. The five cobalt species considered are : Co^{2+}, $Co(OH)^{+}$, $Co(OH)_2$, $Co(OH)_3^{-}$, $Co(OH)_4^{2-}$ The equations considered are :

$$Co(OH)_2 \leftrightarrow Co^{2+} + 2OH^-, \qquad Kps_{Co(OH)_2} = 5.92 \cdot 10^{-14}[63] \tag{12}$$

$$Co^{2+} + H_2O \leftrightarrow CoOH^+ + H^+, \qquad k1 = 2.45 \cdot 10^{-10}[63] \tag{13}$$

$$Co^{2+} + 2H_2O \leftrightarrow Co(OH)_2 + 2H^+, \qquad k2 = 1.7 \cdot 10^{-20}[63] \tag{14}$$

$$Co^{2+} + 3H_2O \leftrightarrow Co(OH)_3^- + 3H^+, \qquad k3 = 9.77^{-33}[63] \tag{15}$$

$$Co^{2+} + 4H_2O \leftrightarrow Co(OH)_4^{2-} + 4H^+, \qquad k4 = 5.01 \cdot 10^{-47}[63] \tag{16}$$

From Equation 12, the flowing expression is obtained : $[Co^2+] = Kps^{'}(Co(OH)_2) \cdot [H^+]^2$, where $Kps^{'}(Co(OH)_2) = Kps_{Co(OH)_2} \cdot k_w^{-2}, \qquad k_w = 10^{-14}$

Therefore, it is possible to express the equations Equation 12 to Equation 16 as a function of pH :

$$[Co^{2+}] = Kps'(Co(OH)_2) \cdot 10^{-2pH} \tag{17}$$

$$[Co(OH)^{+}] = k1 \cdot Kps'(Co(OH)_2) \cdot 10^{-pH} \tag{18}$$

$$[Co(OH)_2] = k2 \cdot Kps'(Co(OH)_2) \tag{19}$$

$$[Co(OH)3^{-}] = k3 \cdot Kps'(Co(OH)_2) \cdot 10^{pH} \tag{20}$$

$$[Co(OH)_4^{2-}] = k4 \cdot Kps'(Co(OH)_2) \cdot 10^{2pH} \tag{21}$$

The total concentration of cobalt species dissolved is given by

$$[Co_{(tot,diss)} = [Co^{2+} + [Co(OH)^{+}] + [Co(OH)_2] + [Co(OH)_3^{-}] + [Co(OH)_4^{2-}]$$

The evolution of the logarithm of the cobalt concentration as a function of pH is shown in Figure 21, the precise values are shown in Table 21. Analyzing Figure 21, it can be seen that the precipitation of Co^{2+} is taking place between pH 9 and 14 for the concentration of 0.02M. The precipitation of $Co(OH)_{2(s)}$ on the particles could explain why the zeta potential is close to 0 at alkaline pH.

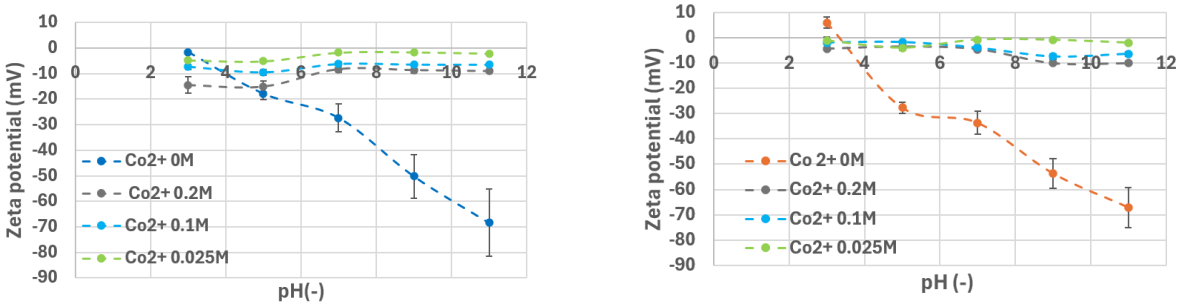

(a) Graphite

(b) NMC811

Figure 19: Evolution of the zeta potential of graphite and NMC811 as a function of the pH in the presence of cobalts ions, using H_2SO_4 and $NaOH$ to regulate the pH. Error bars present one standard deviation of measurement error. The measurements were realised using the Zetasizer Nano Z ZEN2600, the concentration of the colloidal suspension equalled 0.02g/l at ambient temperature.

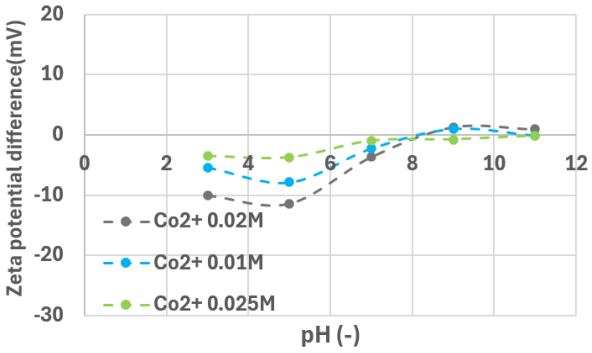

Figure 20: Difference between the zeta potential of graphite and the one of NMC811 as a function of the pH in the presence of cobalt ions, using H_2SO_4 and $NaOH$ to regulate the pH. The measurements were realised using the Zetasizer Nano Z ZEN2600, the concentration of the colloidal suspension equalled 0.02g/l at ambient temperature.

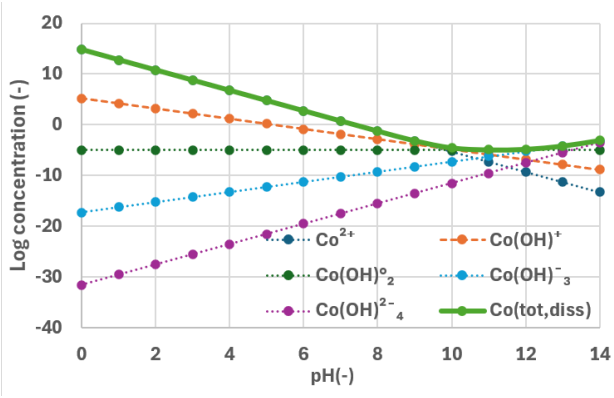

Figure 21: Solubility of Co^{2+} in equilibrium with $Co(OH)_{2(s)}$,$[Co_{tot,dis}]$ represents the total concentration of cobalt species dissolved

4.1.2.4 Effect of manganese ions presence

The evolution of the zeta potential as a function of the pH, in the presence of manganese ions, of graphite and NMC811 are shown in Figure 22.

Concerning both compounds, the difference is more marked in the alkaline region.
In order to facilitate the comparison between the zeta potential of graphite and NMC811, Figure 23, shows the evolution of the difference between the zeta potential of graphite and the one of CAM as a function of the pH in the presence of manganese ions. It can be seen that the zeta potential of manganese at 0.005M at pH 11 seems strange compared to the other measures and should be verified. Analysing the other values, the difference between the zeta potential of graphite and NMC811 seems negligible. Therefore, the effect of manganese ions will not be evaluated during settling tests. Indeed similar zeta potential could indicate a similar aggregation and therefore a similar settling behaviour.

As previously, in order to know the pH at which the manganese ions precipitate, the solubility of Mn^{2+} in equilibrium with $Mn(OH)_{2(s)}$ and the distribution of Mn species can be calculated. The five manganese species considered are : Mn^{2+}, $Mn(OH)^{+}$, $Mn(OH)_2$, $Mn(OH)_3^-$, $Mn(OH)_4^{2-}$ The equations considered are :

$$Mn(OH)_2 \leftrightarrow Mn^{2+} + 2OH^-, \qquad Kps_{Mn(OH)_2} = 2 \cdot 10^{-13}[64] \tag{22}$$

$$Mn^{2+} + H_2O \leftrightarrow MnOH^+ + H^+, \qquad k_1 = 2.63 \cdot 10^{-11}[64] \tag{23}$$

$$Mn^{2+} + 2H_2O \leftrightarrow Mn(OH)_2 + 2H^+, \qquad k_2 = 6.61^{-23}[64] \tag{24}$$

$$Mn^{2+} + 3H_2O \leftrightarrow Mn(OH)_3^- + 3H^+, \qquad k_3 = 4.57^{-35}[64] \tag{25}$$

$$Mn^{2+} + 4H_2O \leftrightarrow Mn(OH)_4^{2-} + 4H^+, \qquad k_4 = 5.25 \cdot 10^{-49}[64] \tag{26}$$

From Equation 22, the flowing expression is obtained : $[Mn^2+] = Kps^{'}(Mn(OH)_2) \cdot [H^+]^2$, where $Kps^{'}(Mn(OH)_2) = Kps_{Mn(OH)_2} \cdot k_w^{-2}, \qquad k_w = 10^{-14}$
Therefore, it is possible to express the equations Equation 22 to Equation 26 as a function of pH :

$$[Mn^{2+}] = Kps^{'}(Mn(OH)_2) \cdot 10^{-2pH} \tag{27}$$

$$[Mn(OH)^+] = k_1 \cdot Kps^{'}(Mn(OH)_2) \cdot 10^{-pH} \tag{28}$$

$$[Mn(OH)_2] = k_2 \cdot Kps^{'}(Mn(OH)_2) \tag{29}$$

$$[Mn(OH)3^-] = k_3 \cdot Kps^{'}(Mn(OH)_2) \cdot 10^{pH} \tag{30}$$

$$[Mn(OH)_4^{2-}] = k_4 \cdot Kps^{'}(Mn(OH)_2) \cdot 10^{2pH} \tag{31}$$

The total concentration of manganese species dissolved is given by

$$[Mn_{(tot,diss)} = [Mn^{2+} + [Mn(OH)^+] + [Mn(OH)_2] + [Mn(OH)_3^-] + [Mn(OH)_4^{2-}]$$

The evolution of the logarithm of the manganese species concentration as a function of pH is shown in Figure 24, the precise values are shown in Table 22. Analyzing Figure 24, it can be seen that the precipitation of Mn^{2+} is taking place between pH 9 and 14 for the concentration of 0.02M. The precipitation of $Mn(OH)_{2(s)}$ on the particles could explain why the zeta potential is close to 0 at alkaline pH.

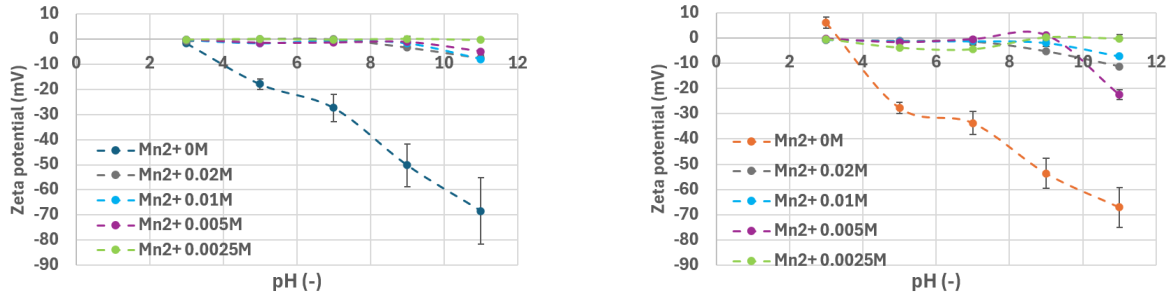

(a) Graphite (b) NMC811

Figure 22: Evolution of the zeta potential of leached graphite and NMC811 as a function of the pH in the presence of manganese ions, using H_2SO_4 and $NaOH$ to regulate the pH. Error bars present one standard deviation of measurement error. The measurements were realised using the Zetasizer Nano Z ZEN2600, the concentration of the colloidal suspension equalled 0.02g/l at ambient temperature.

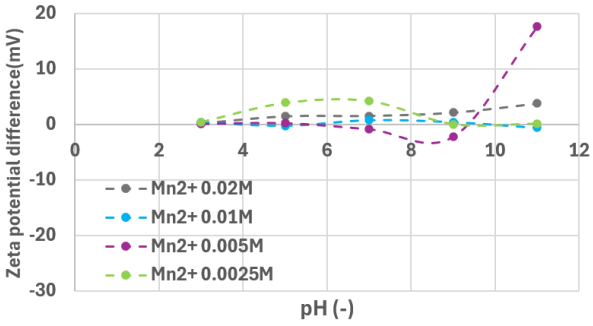

Figure 23: Difference between the zeta potential of leached graphite and the one of CAM as a function of the pH in the presence of manganese ions, using H_2SO_4 and $NaOH$ to regulate the pH. The measurements were realised using the Zetasizer Nano Z ZEN2600, the concentration of the colloidal suspension equalled 0.02g/l at ambient temperature.

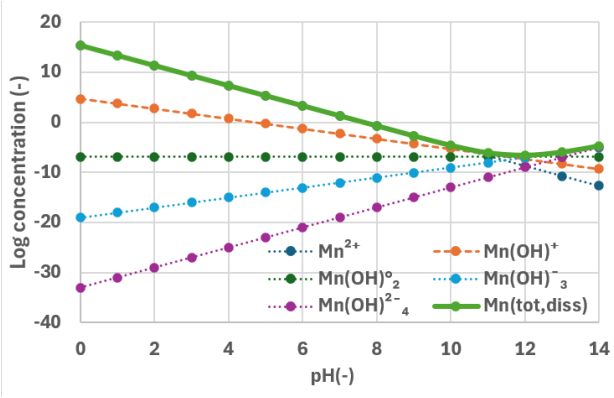

Figure 24: Solubility of Mn^{2+} in equilibrium with $Mn(OH)_{2,(s)}$, $[Mn_{tot,dis}]$ represents the total concentration of manganese species dissolved.

4.1.2.5 Effect of aluminum ions presence

The evolution of the zeta potential as a function of the pH, in the presence of aluminum ions, of graphite and NMC811 are shown in Figure 25.

Concerning both compounds, the difference is more marked in the alkaline region. It can be assumed that hydrogen ions already increase the zeta potential in the acidic region.
It can be seen that the zeta potiential of both compounds decreases more in the alkaline region in the presence of aluminum ions compared to the cases with other ions. In order to facilitate the comparison between the zeta potential of graphite and NMC811, Figure 26, shows the evolution of the difference between the zeta potential of graphite and the one of CAM as a function of the pH in the presence of aluminum ions.

Since the difference between both zeta potentials is the highest at pH = 11, batch sedimentation tests will be realised at that pH. Due to the significant difference in zeta potential at low aluminum ions concentration, a significant difference in the agglomeration behaviour can be expected.

As previously, in order to know the pH at which the aluminum ions precipitate and the different aluminum species present at each pH, the solubility of Al^{3+} in equilibrium with $Al(OH)_{3(s)}$ and the distribution of Al species can be calculated. The five aluminum species considered are : Al^{3+}, $Al(OH)^2+$, $Al(OH)_2^+$, $Al(OH)_3$, $Al(OH)_4^-$ The equations considered are :

$$Al(OH)_3 \leftrightarrow Al^{3+} + 3OH^-, Kps_{Al(OH)_3} = 3 \cdot 10^{-34}[65] \quad (32)$$

$$Al^{3+} + H_2O \leftrightarrow AlOH^{2+} + H^+, \quad k_1 = 1.05 \cdot 10^{-5}[65] \quad (33)$$

$$Al^{3+} + 2H_2O \leftrightarrow Al(OH)_2^+ + 2H^+, \quad k_2 = 2.34^{-11}[65] \quad (34)$$

$$Al^{3+} + 3H_2O \leftrightarrow Al(OH)_3 + 3H^+, \quad k_3 = 2.19^{-16}[65] \quad (35)$$

$$Al^{3+} + 4H_2O \leftrightarrow Al(OH)_4^- + 4H^+, \quad k_4 = 1.23 \cdot 10^{-23}[65] \quad (36)$$

From Equation 32, the flowing expression is obtained : $[Al^3+] = Kps^{'}(Al(OH)_3) \cdot [H^+]^3$, where $Kps^{'}(Al(OH)_3) = Kps_{Al(OH)_3} \cdot k_w^{-3}$,$_w = 10^{-14}$

Therefore, it is possible to express the equations Equation 32 to Equation 36 as a function of pH :

$$[Al^{3+}] = Kps'(Al(OH)_3) \cdot 10^{-3pH} \tag{37}$$

$$[Al(OH)^{2+}] = k_1 \cdot Kps'(Al(OH)_3) \cdot 10^{-2pH} \tag{38}$$

$$[Al(OH)_2^{+}] = k_2 \cdot Kps'(Al(OH)_3) \cdot 10^{-pH} \tag{39}$$

$$[Al(OH)_3] = k_3 \cdot Kps'(Al(OH)_3) \tag{40}$$

$$[Al(OH)_4^{-}] = k_4 \cdot Kps'(Al(OH)_3) \cdot 10^{pH} \tag{41}$$

The total concentration of aluminum species dissolved is given by

$$[Al_{(tot,diss)} = [Al^{3+} + [Al(OH)^{2+}] + [Al(OH)_2^{+}] + [Al(OH)_3] + [Al(OH)_4^{-}]$$

The evolution of the logarithm of the aluminum species concentration as a function of pH is shown in Figure 27, the precise values are shown in Table 23. Analyzing Figure 27 and Table 23, it can be seen that aluminum precipitates between pH 3.5 and 13 for a concentration of 0.04M.

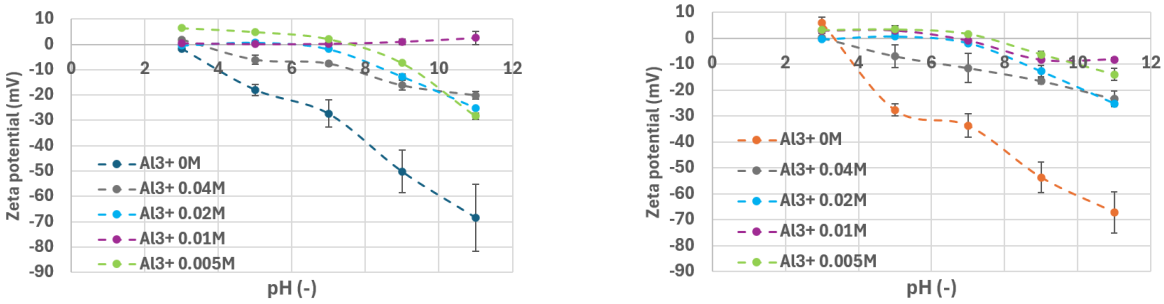

(a) Graphite

(b) NMC811

Figure 25: Evolution of the zeta potential of leached graphite and NMC811 as a function of the pH in the presence of aluminum ions, using H_2SO_4 and $NaOH$ to regulate the pH. Error bars present one standard deviation of measurement error. The measurements were realised using the Zetasizer Nano Z ZEN2600, the concentration of the colloidal suspension equalled 0.02g/l at ambient temperature.

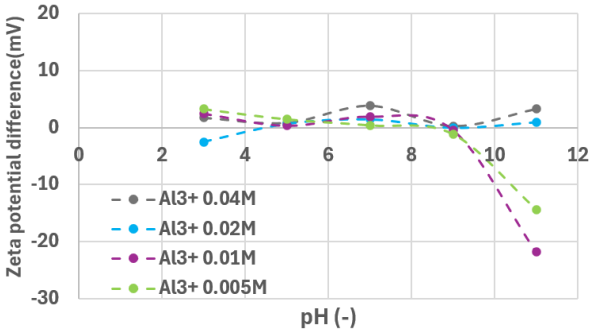

Figure 26: Difference between the zeta potential of leached graphite and the one of CAM as a function of the pH in the presence of aluminum ions, using H_2SO_4 and $NaOH$ to regulate the pH. The measurements were realised using the Zetasizer Nano Z ZEN2600, the concentration of the colloidal suspension equalled 0.02g/l at ambient temperature.

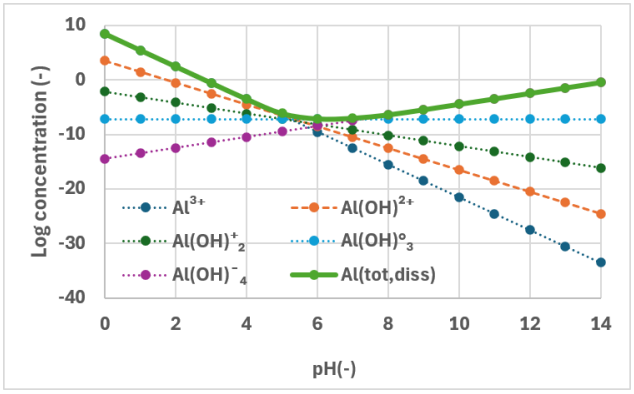

Figure 27: Solubility of Al^{3+} in equilibrium with $Al(OH)_3(s)$, $[Al_{tot,dis}]$ represents the total concentration of aluminum species dissolved.

4.1.3 Zeta potential summary

In deionised water, it was shown that the zeta potential of graphite is close to zero between pH 3 and 5, whereas that of NMC811 remains significantly different from zero. Under these conditions, graphite is therefore expected to agglomerate more readily than NMC811, resulting in a higher settling velocity.

To better understand the influence of pH on particle agglomeration and, consequently, on the flotation and settling behaviour of graphite and NMC811, flotation and settling tests will be conducted over a range of pH values. Based on the zeta potential measurements, pH 5 is expected to provide one of the most favourable conditions for achieving a significant difference in settling velocity between the two materials. Therefore, additional settling tests in the presence of aluminium and nickel ions will be performed at this pH.

The effect of cobalt ions will also be investigated. Since the largest difference in zeta potential between graphite and NMC811 was observed at pH 5 in the presence of 0.2 M cobalt ions, a

settling test will be conducted under these conditions.

The results obtained in the presence of dissolved ions indicate that precipitation can reduce the difference in zeta potential between the two species. When precipitates form, both graphite and NMC811 can become covered by the same precipitated phase, resulting in more similar surface properties. Consequently, lower ion concentrations, provided that they still produce a significant difference in zeta potential, are expected to be more favourable for separation. To minimise the influence of precipitates on the settling behaviour, the ionic solutions adjusted to the desired pH can be filtered before the settling tests.

Based on the zeta potential results, additional conditions will also be investigated. Significant differences between the zeta potentials of graphite and NMC811 were observed at pH 11 in the presence of nickel and aluminium ions; therefore, settling tests will be performed under these conditions after filtration of any precipitates. Similarly, lithium ions produced larger differences in zeta potential at pH 6 and 9, and settling tests will consequently be conducted at these pH values, with the solutions filtered before use.

Finally, no settling tests will be conducted in the presence of manganese ions. As the difference in zeta potential between graphite and NMC811 was not significant under the conditions investigated, and considering the limited time available, manganese was not considered a priority for further experimental work.

4.2 Flotation tests

4.2.1 Impact of washing pre-treatment

The washing pre-treatment was realised to increase the graphite grade. It has been shown that reducing the lithium ion concentration by performing washing pretreatment decreases the recovery of cathode materials by entrainment, therefore increasing the graphite grade [66].

To evaluate the impact of washing, Figure 28 and Figure 29 can be analysed. The Ni, Mn and Co are presented separately, but their behaviour during the flotation is similar, as it can be seen in the graphs. The values of the grades and recoveries, both with and without washing, can be found in Table 24 and Table 25. It can be noticed that the recovery and the grade of graphite are greater in the case without washing. The recoveries of 80% in the case without washing and 60% in the case with washing indicate that the flotation is not performing well. This can be explained by the fact that the hydrodynamism is not good in the 1L cell, since it is a small one. Therefore, wall effects and more entrainment are induced. Even without washing, the recovery of nickel is high. In the case with washing, the recovery of cathode materials is lower, but it is not really representative since the black mass was treated mechanically, which means that the PVDF binder is still present and the small size of the flotation cell induces entrainment. In [66], the black mass was pre-treated thermally. This could explain why the washing pre-treatment was benefic in that case since the lithium ions are much more present when the black mass is pre-treated thermally compared to mechanically. Indeed, roughly 2600mg/L of Li^+, which corresponds to 0.37mol/l, were in solution for thermally pre-treated black mass and only 0.04mol/l of Li^+ were in solution for mechanically pretreated black

mass, as it can be seen in Table 8.

From Figure 30, views of the flotation cell can be seen in both cases. The height of the charged froth was much higher in the case without washing, which could explain the higher recovery.

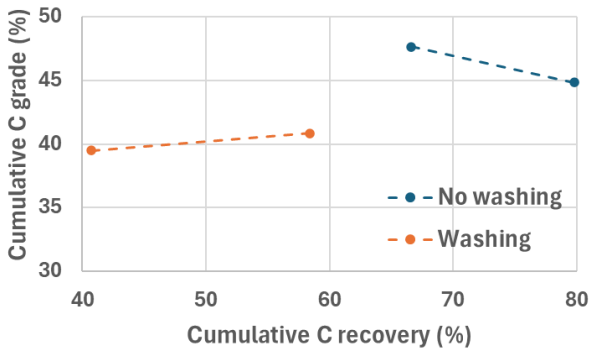

Figure 28: Grade and recovery of the carbon in the froth during the flotation, with and without washing. The test was performed in the GTK Labcell from Outotec. The washing was realised during 15 minutes at 1500 rpm and a pulp density of 5.7%. The rougher stage was realised during 19 minutes, with Escaid110 at a concentration of 150gpt conditioned during 2 minutes, and MIBC at a concentration of 80gpt conditioned during 1 minute, a flow rate of 4l/min and a rotation speed of 800rpm. The scavenger stage was realised during 12 minutes, with Escaid110 at a concentration of 75gpt conditioned during 2 minutes, and MIBC at a concentration of 80gpt conditioned during 1 minute.

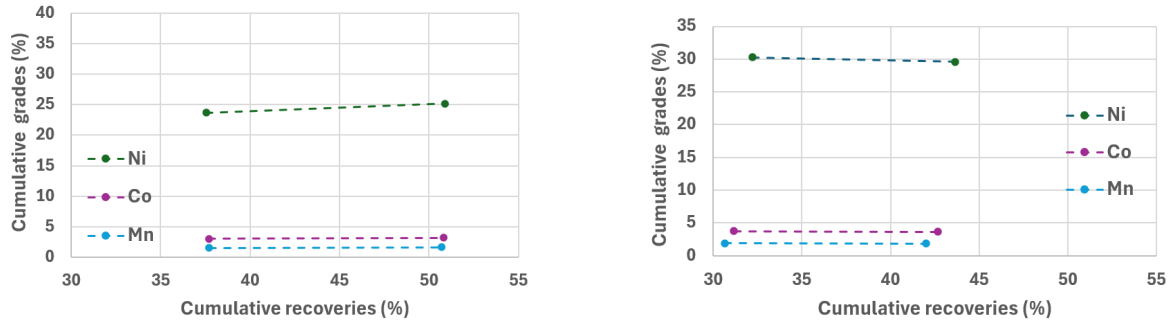

(a) Without washing

(b) With washing

Figure 29: Grade-recovery curve of the impurities in the froths during the flotation, without and with washing. The test was performed in the GTK Labcell from Outotec. The washing was realised during 15 minutes at 1500 rpm and a pulp density of 5.7%. The rougher stage was realised during 19 minutes, with Escaid110 at a concentration of 150gpt conditioned during 2 minutes, and MIBC at a concentration of 80gpt conditioned during 1 minute, a flow rate of 4l/min, a pulp density of 7.7% and a rotation speed of 800rpm. The scavenger stage was realised during 12 minutes, with Escaid110 at a concentration of 75gpt conditioned during 2 minutes, and MIBC at a concentration of 80gpt conditioned during 1 minute.



(a) No washing (b) Washing

Figure 30: Pictures of the flotation cell, GTK Labcell from Outotec, in cases with and without washing, at 10 seconds after the beginning of the air flow. The washing was realised during 15 minutes at 1500 rpm and a pulp density of 5.7%. The rougher stage was realised during 19 minutes, with Escaid110 at a concentration of 150gpt conditioned during 2 minutes, and MIBC at a concentration of 80gpt conditioned during 1 minute, a flow rate of 4l/min and a rotation speed of 800rpm. The scavenger stage was realised during 12 minutes, with Escaid110 at a concentration of 75gpt conditioned during 2 minutes, and MIBC at a concentration of 80gpt conditioned during 1 minute.

4.2.2 Optimisation of the promoter concentration

The evolution of the cumulative recoveries and grades as a function of the escaid concentration are shown respectively in Figure 31. The values of the grades and recoveries, for the different promoter concentration, in the case without washing, can be found in Table 24 and Table 25. It can be seen that the recovery of both graphite and NMC increases with the promoter concentration. This can be explained by the fact that the promoter adsorbs on PVDF which increases the true flotation of NMC. It can be assumed that the recovery of cathode materials decreases at 350gpt of escaid because graphite floats faster, since the graphite recovery increases. Since the black mass was treated mechanically, the dosage of promoter must be low since, after adsorbing on graphite, it will adsorb on the cathode materials where PVDF residues are present. Therefore, more NMC are floated due to true flotation. The grade of graphite increases when the promoter concentration increases from 150 to 350 gpt but decreases when it increases to 500 gpt. Like for the recovery, the grade of Ni, Co and Mn is minimum at 350 gpt and increases when the promoter concentration equals 500 gpt. Analysing both graphs, it can be observed that the graphite grade is maximised at 350gpt, when the recovery of NMC elements is minimised. Therefore, in order to maximise both recovery and grade, the promoter concentration of 350 gpt seems the most appropriate.

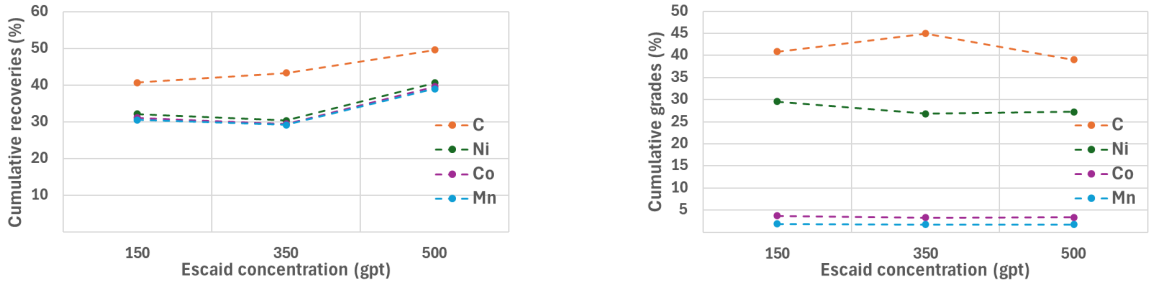

(a) Cumulative recoveries

(b) Cumulative grades

Figure 31: Evolution of the cumulative recoveries and grades of carbon and NMC elements as a function of the promoter concentration, in the case with washing and without pH modification. The test was performed in the GTK Labcell from Outotec. The washing was realised during 15 minutes at 1500 rpm and a pulp density of 5.7%. The rougher stage was realised during 19 minutes, with Escaid110 at a concentration of 150, 350 and 500 gpt conditioned during 2 minutes, and MIBC at a concentration of 80gpt conditioned during 1 minute, a flow rate of 4l/min and a rotation speed of 800rpm, the pulp density was equalled to 7.7%. The scavenger stage was realised during 12 minutes, with Escaid110 at half the concentration during the rougher stage, conditioned during 2 minutes, and MIBC at a concentration of 80gpt conditioned during 1 minute.

4.2.3 Impact of the pH

As explained previously, the pH increased during all the experiments. This can be explained by the leaching reactions taking place when the cathode active material is in contact with sulphuric acid, as follows :

$$2LiMO_{2(s)} + 3H_2SO_4 \rightarrow 2MSO_{4(aq)} + Li_2SO_{4(aq)} + 3H2O + 12O_{2(g)} \tag{42}$$

where M represents nickel, cobalt and manganese [67]
FFurthermore the electrolyte residues, such as Li_2CO_3, react with the acid to produce CO_2 [68] :

$$Li_2CO_3 + 2H^+ \rightarrow H_2O + 2Li^+ + CO_2 \tag{43}$$

Moreover, graphite and NMC surface sites are capable of adsorbing protons, which increases the pH. This is illustrated in Figure 11 by the increase of zeta potential when the ph decreases. In conclusion, the system reacts as a buffer and the increase of the pH corresponds to a return at an equilibrium state imposed by the neutralisation capacity of the black mass.

Therefore, the pH indicated corresponds to the pH at which the flotation started. For the experiments at pH 7, 5, 3, this corresponds respectively to pH 6.55, 4.75 and 2.57 and the pH at which the rougher stage ended was 7.7, 6.53 and 5.54.
For the experiments at pH 7, 5, 3, the scavenger stage started respectively at pH 6.74, 4.67 and 2.55 and ended at pH 7.78, 6.32 and 4.57.

It can be noticed that the difference between the start and end pH increases when the starting pH decreases. This can be explained by the chemical reactions Equation 42 and

Equation 4.2.3 which are more present at lower pH. Indeed, Table 8 and Table 9 show a higher elemental concentration in water at pH 3 and 5, indicating that leaching is happening at those pH.

The presence of bubbles is noticed during the conditioning period during which the pH was adjusted, as it can be seen in Figure 32. It can be noticed that there are more bubbles in the case where the pH is lower.

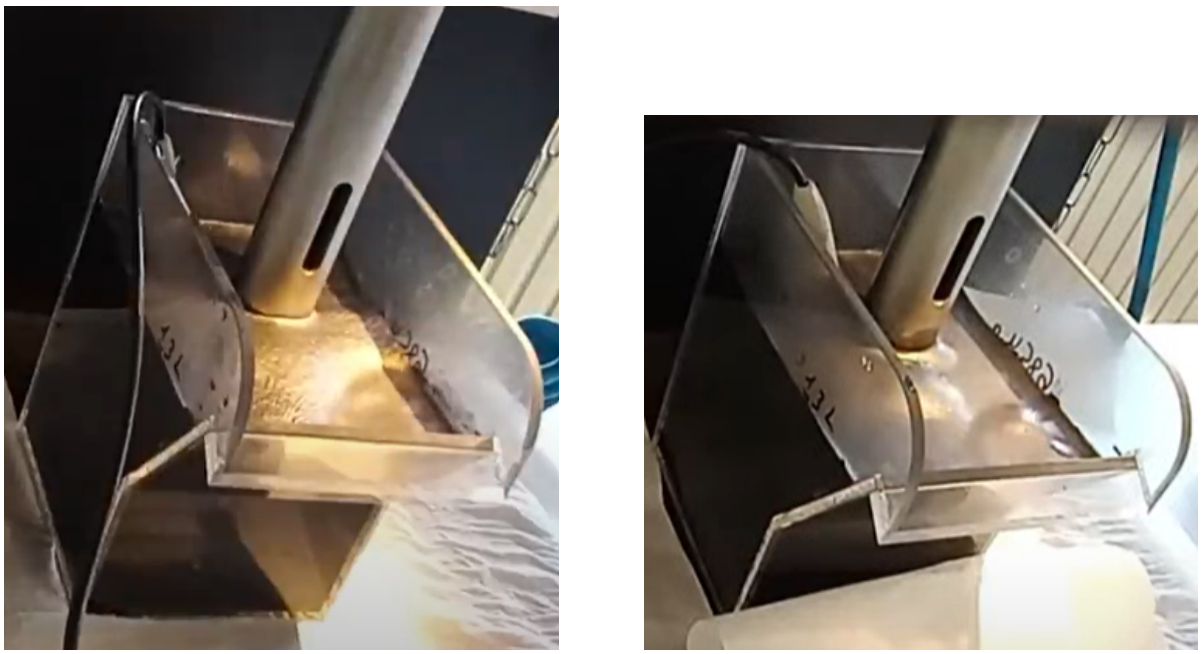

(a) pH 2.57 (b) pH 4.75

Figure 32: Pictures of the flotation cell, GTK Labcell from Outotec, during the calibration of the pH, using H_2SO_4, at pH 2.57 and 4.75, before the addition of promoters, after the washing pre-treatment. The washing was carried out for 15 minutes at 1500 rpm with a pulp density of 5.7%. During the flotation test, the pulp density was equalled to 7.7%.

Table 8 and Table 9 show the analyses of flotation water using both ICP and ISE characterization methods. The aluminum ion in the black mass originates from the cathode foil, the copper from the anode foil, the iron from the battery shell , the phosphorous from the electrolyte and the fluorine from the electrolyte and the PVDF binder. The lithium contribution comes from the cathode active material and the electrolyte.

The evolution of the concentrate recovery and grade as a function the pH are shown respectively in Figure 33. The values of the grades and recoveries, for the different pH can be found in Table 26 and Table 27. It can be seen that the recoveries of graphite, Ni, Co and Mn decrease when the pH decreases. This could be explained by several factors.
First of all, the zeta potential of the graphite in deionised water is close to -10 mV at pH 5, which corresponds to the limit at which agglomeration begins and close to 0 mV, where the agglomeration is supposed to be the highest, at pH 3. [38] Therefore, if graphite particles agglomerate, they will be bigger and tend to sink, which could explain the decrease

in graphite recovery. Therefore, since the zeta potential of NMC in deionised water is close to -30mV, the assumption can be made that the cathode particles are trapped in graphite agglomerates, since the graphite particles are bigger. This could explain the decrease of NMC recovery.

Moreover, looking at the results of ICP and ISE analyses of both washing and flotation waters, it can be seen that the ion content of all elements excepted phosphorus increases when the pH decreases, which can be explained by the leaching process. The most present elements in flotation water at pH 3 and 5 are lithium, nickel and aluminum. Those are therefore expected to have the highest impact. Analyzing the zeta potential of graphite and NMC in the presence of Li^+ 0.05 M, Ni^{2+}, Mn^{2+}, Co^{2+} 0.0025M and Al^{3+} 0.005M, in Figure 34, it can be seen that, except for cobalt in the case of graphite, the zeta potential increases when ions are added. Since cobalt is less present than lithium, nickel and aluminum in the flotation water, it is expected that those ions will have a greater impact on the zeta potential of graphite and therefore on its settling behaviour. It can also be noticed that the zeta potential of both graphite and NMC are close to 0 at pH 3 and 5 in the presence of Ni^{2+} and Mn^{2+} 0.0025M and Al^{3+} 0.005M. This could explain the decrease of both graphite and cathode recoveries since they will tend to agglomerate. Since the concentration of ions is lower in the flotation water at pH 5, their impact would be lower, which could explain why the recovery decreases, but not as much as at pH 3.

Moreover, at acidic pH, the graphite is being somewhat depressed and the froth is less stable, due to all the ions present in solution.

Therefore, since the pH of the mechanical pre-treated black mass in solution equals 10.5 before the washing and 9.5 after, the decrease of the pH could be one explanation to the decrease of the recoveries and grades after the washing.

Therefore, the optimum pH seems to be the natural pH. Considering the costs, it makes sense to float at natural pH. Indeed, if no acid is added, the operating costs (opex) are reduced, which makes the experiment more profitable.

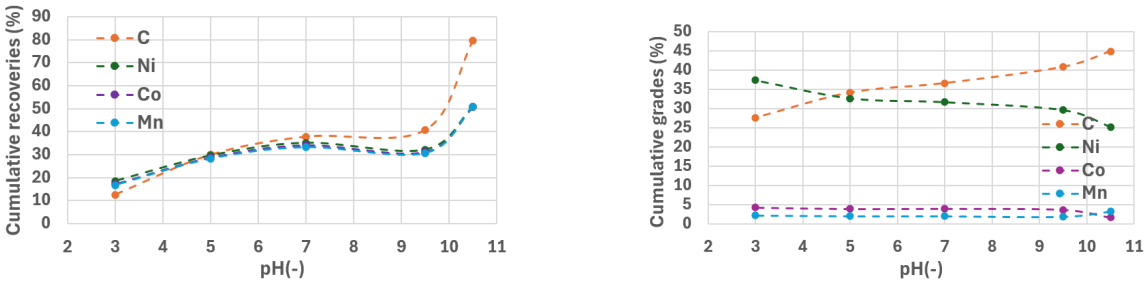

(a) Cumulative recoveries

(b) Cumulative grades

Figure 33: Evolution of the cumulative recoveries and grades of graphite and NMC elements as a function of the pH, in the case with washing, with a promoter concentration of 150 gpt. The pH, modified using H_2SO_4, at the beginning of the experiment was equal to 2.57, 4.75 and 6.55. The point at pH10.5 corresponds to the case without washing. The test was performed in the GTK Labcell from Outotec. The washing was realised during 15 minutes at 1500 rpm and a pulp density of 5.7%. The rougher stage was realised during 19 minutes, with Escaid110 at a concentration of 150gpt conditioned during 2 minutes, and MIBC at a concentration of 80gpt conditioned during 1 minute, a flow rate of 4l/min and a rotation speed of 800rpm, the pulp density was equalled to 7.7%. The scavenger stage was realised during 12 minutes, with Escaid110 at a concentration of 75gpt, conditioned during 2 minutes, and MIBC at a concentration of 80gpt conditioned during 1 minute.

Samples	**Al (mol/l)**	**Co(mol/l)**	**Cu (mol/l)**	**Fe(mol/l)**	**Li (mol/l)**
washing water	2.3E-04	<3.4E-05	<3.1E-05	<3.6E-05	4.1E-02
flotation water pH 9.5	7.4E-05	N/D	N/D	<3.6E-05	6.1E-03
flotation water pH 7	1.4E-04	<3.4E-05	<3.1E-05	<3.6E-05	8.9E-03
flotation water pH 5	1.3E-03	2.1E-04	<3.1E-05	<3.6E-05	1.2E-02
flotation water pH3	3.4E-03	9.2E-04	1.5E-04	9.4E-05	2.1E-02

Table 8: ICP and ISE analyses of the flotation and washing waters at different pH (part 1)

Samples	**Mn (mol/l)**	**Ni(mol/l)**	**P(mol/l)**	**F (mol/l)**
washing water	<3.6E-05	8.4E-05	4.1E-03	1.5E-02
flotation water pH 9.5	<3.6E-05	<3.4E-05	1.3E-04	8.4E-04
flotation water pH 7	<3.6E-05	1.0E-04	1.7E-04	5.0E-03
flotation water pH 5	1.7E-04	9.7E-04	1.1E-04	7.4E-03
flotation water pH3	5.5E-04	4.6E-03	1.2E-04	1.4E-02

Table 9: ICP and ISE analyses of the flotation and washing waters at different pH (part 2)

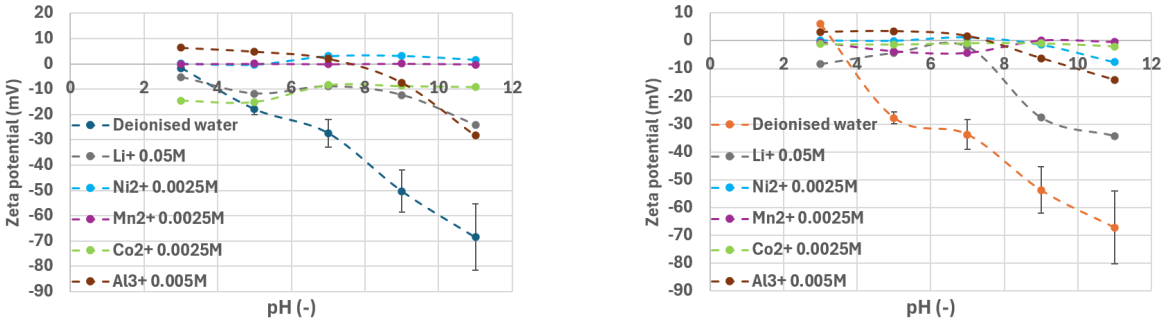

(a) Graphite

(b) NMC811

Figure 34: Evolution of the zeta potential of graphite and NMC811 as a function of the pH in deionised water with 0.05M Li+ and with 0.005M Ni2+, using H_2SO_4 and $NaOH$ to regulate the pH. Error bars present the standard deviation of measurement error. The measurements were realised using the Zetasizer Nano Z ZEN2600, the concentration of the colloidal suspension equalled 0.02g/l at ambient temperature.

4.2.4 Flotation tests summary

The impact of the washing, the promotor concentration and the pH have been studied. It has been shown that the recovery and the grade of graphite decrease when washing is applied as a pre-treatment.
The promotor concentration of 350gpt seems the most appropriate, to maximise both grade and recovery.
It can be concluded that the flotation at acidic pH is not concluant and the operating costs will be higher. Therefore, it is adviced to float at natural pH, in order to consume less acid and to obtain better results.

It must be kept in mind that the floated black mass was only mechanically treated. Therefore, the organic binder was still present which explains the lower selectivity compared to pyrolysed black mass. Removing the PVDF binder before flotation is suggested. It can be done using pyrolysis [19] [36] [37] or using a solvent, such as a Fenton reagent (a combinaison of Fe^{2+} and H_2O_2) [18].

4.3 Batch sedimentation tests

4.3.1 Deionised water

4.3.1.1 Impact of pH

The evolution of the height of the suspension zone as a function of time for graphite and NMC811 at pH from 3 to 11, is shown in Figure 35. It can be seen that in both cases the evolutions are linear. Therefore, linear regressions can be realised and the opposite of the slopes correspond to the settling speeds. The values are shown in Table 13. It can be seen that the settling speed of graphite is constant between pH 3 and 5, the pH at which the zeta potential is between 0 and - 15mV, as shown in Figure 11. At pH above 5, the settling speed

decreases when the pH increases.
Concerning NMC811, it can be seen that the settling speed is the highest at pH3, which corresponds to the pH at which the zeta potential equals -15 mV, which is sufficiently close to zero to assume that NMC811 is agglomerated at that pH. At pH above 3, the zeta potential decreases consequently and therefore the settling speed decreases also. It can be seen that, compared to graphite the settling speed of NMC811 is almost constant at pH above 5.

Even though the zeta potential of graphite is more negative than the one of NMC811 in the alkaline region, the settling speed of graphite will always be higher. This could be explained by the particle size, graphite particles being bigger than the cathode particles. Indeed, the D90 of graphite is comprised between 25 and 30 μm [42] and the one of NMC811 is comprised between 18 and 22 μm [43].

To make the comparison easier, the evolution of the settling speed of both, graphite and NMC811 as a function of pH are shown in Figure 36. It can be seen that the settling speed of CAM is much lower than the one of graphite. It can be seen that the settling speed difference is the highest at pH 5, which was expected since the zeta potential of graphite is sufficiently close to 0 and the one of NMC811 is not subsubsection 4.1.1. Therefore, continuous sedimentation test will be realised at pH 5 in deionised water and in the presence of nickel, aluminum and cobalt to evaluate their impact. Since the higher zeta potential difference in the presence of lithium is at pH6 and 9, the test at pH5 will not be realised.

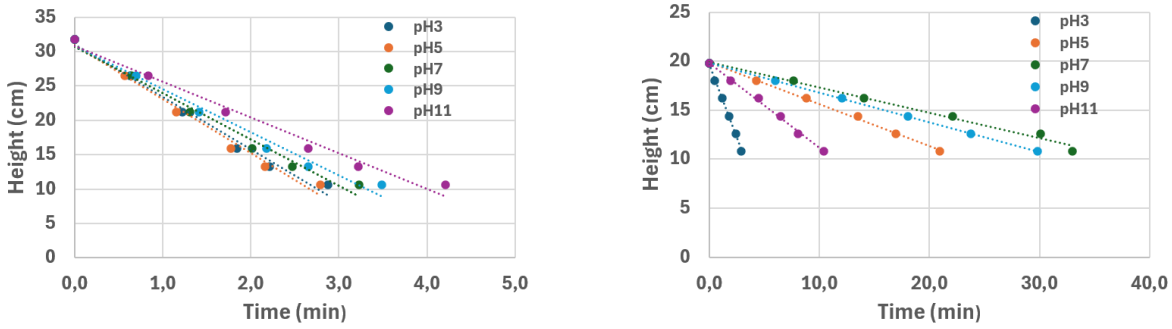

(a) Graphite

(b) NMC

Figure 35: Evolution of the height of the suspension zone as a function of time for graphite and NMC811 at pH from 3 to 11. The graduated cylinder for graphite contains 600ml and the one of NMC811 120ml. In both cases, the pH was modified using H_2SO_4 and NaOH, the pulp density was equal to 7.7%.

pH (-)	Graphite settling speed (cm/min)	NMC811 settling speed (cm/min)
3	8.64	2.99
5	8.98	0.43
7	7.85	0.30
9	7.31	0.26
11	5.99	0.87

Table 10: Settling speed of graphite and NMC811, measured during a batch sedimentation test, at pH from 3 to 11, modified using H_2SO_4 and NaOH, with a pulp density equal to 7.7%.

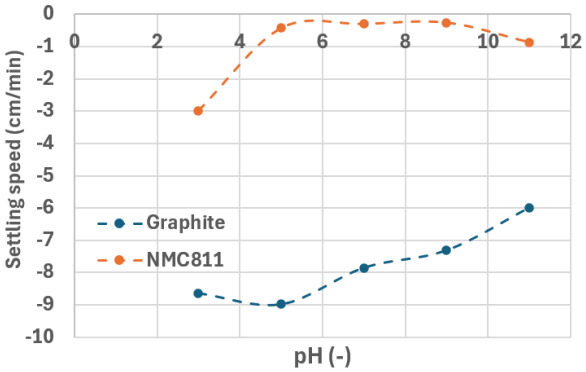

Figure 36: Settling speed of graphite and NMC811, measured during a batch sedimentation test, at pH from 3 to 11, modified using H_2SO_4 and NaOH, with a pulp density equal to 7.7%.

4.3.2 Effect of ions presence

4.3.2.1 Effect of lithium ions presence

As explained in paragraph 4.1.2.1, batch sedimentation tests have been realised at pH 6 and 9 in the presence of Li^+ to evaluate the impact of the zeta potential difference regarding the settling speed.

The evolution of the height of graphite and NMC811 at pH6 and 9 in the presence of Li^+ at a concentration of 0.1M are shown in Figure 37. Since the evolutions are linear, a linear regression can be realised and the opposite of the slope corresponds to the settling speed. Therefore, at pH6 the graphite settling speed is equal to 10.32cm/min and the NMC811 is equal to 9.28 cm/min. At pH9, the graphite settling speed is equal to 9.62cm/min and the NMC811 is equal to 13.08 cm/min.
Analyzing those values, it can be seen that the difference between the settling speed is significantly reduced compare to the one in deionised water. Therefore, continuous sedimentation test will not be realised using lithium. Comparing the settling speed in the presence of

lithium ions with the ones obtained in deionised water, as shown in Figure 35, it can be seen that the settling velocity of graphite increases a little and that the settling of NMC increases much more.

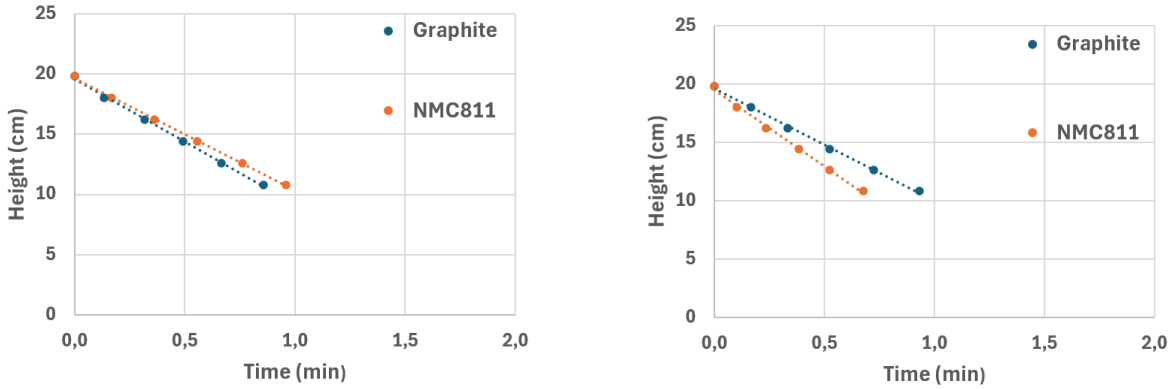

(a) pH 6

(b) pH 9

Figure 37: Evolution of the height of the suspension zone as a function of time for graphite and NMC811 at pH6 and 9, the slopes are equal to the settling velocities of graphite NMC811, respectively, in the presence of Li^+ at a concentration of 0.1M. The pH was modified using H_2SO_4 and NaOH, the pulp density was equal to 7.7%.

4.3.2.2 Effect of nickel ions presence

As explained in subsubsection 4.1.1 and subsubsection 4.3.1, since the highest settling speed difference between graphite and NMC811 is at pH5 in deionised water, a settling test was realised at pH5 with a concentration of 0.02M of Ni^{2+}. As seen in Figure 18, nickel ions do not precipitate at those conditions, therefore no filtration has been realised. The evolution of the height of the suspension zone as a function of time for graphite and NMC811 is shown in Figure 38. Since the evolution is linear, a linear regression can be realised and the opposite of the slope corresponds to the settling speed. Therefore, the settling velocity of graphite equals 7.48cm/min and the one of NMC811 equals 9.48cm/min at pH5 in the presence of nickel ions at a concentration of 0.02M.
It can be seen that the settling speeds are close and that once again, based on Figure 35, the graphite settling speed is almost unchanged compared to the NMC811 settling speed which is significantly increased. Since the settling speeed difference is noticeably decreased in the presence of Ni^{2+}, the continuous settling test at pH5 should be realised with the leaching residue since the majority of the nickel has been recovered in the liquid phase.

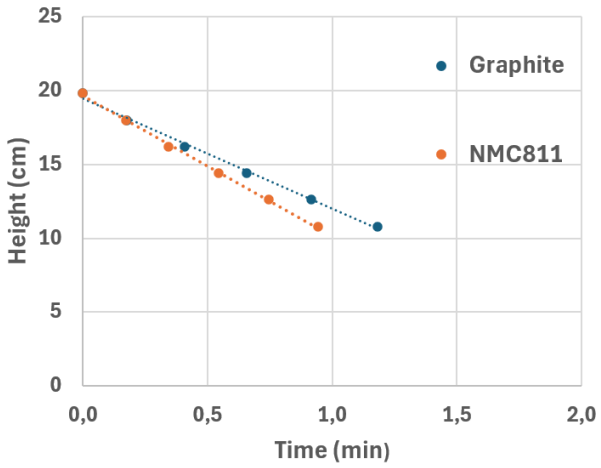

Figure 38: Evolution of the height of the suspension zone as a function of time for graphite and NMC811 at pH 5 in the presence of nickel ions at a concentration of 0.02M. The pH was modified using H_2SO_4 and NaOH, the pulp density was equal to 7.7%.

As explained in paragraph 4.1.2.2, the highest zeta potential difference in the presence of Ni^{2+} is at pH11 and a concentration of 0.02M. It has been shown that, nickel precipitates at those conditions and the zeta potential difference is lower at higher nickel concentrations, indicating that the precipitates could reduce the difference in the agglomeration behaviour of graphite and NMC811 . Since it has been shown, in subsubsection 4.2.1 that the pH of the industrial pretreated black mass in water equals 10.5, the settling tests were realised at pH10.5. In order to determine the impact of the precipitated ions on the surfaces of graphite and NMC811, the evolution of the height of the suspension zone for graphite and NMC811 in the presence of Ni^{2+} at a concentration of 0.02M, with and without filtration of the precipitates is shown in Figure 39. Since the evolutions are linear, a linear regression can be realised and the opposite of the slope obtained corresponds to the settling speed. Therefore, in the case without filtration, the graphite settling speed is equal to 0.61cm/min and the NMC811 is equal to 1.26 cm/min. In the case with filtration, the graphite settling speed is equal to 4.96cm/min and the NMC811 is equal to 13.19 cm/min.
Analyzing the values, it can be seen that the settling speed is much lower when the precipitates are present. It is assumed that since all the surfaces are recovered by the same particles, they all have the same charge. Therefore, they repel each other, which reduces the settling speed.
Due to the significant settling speed difference at pH 10.5 when the precipitates are filtrated, the continuous sedimentation test will be realised at those conditions. It can be noticed that the settling speed of NMC811 is much higher than the one of graphite, therefore, the graphite is expected to be entrained in the overflow and the NMC811 recovered in the underflow.

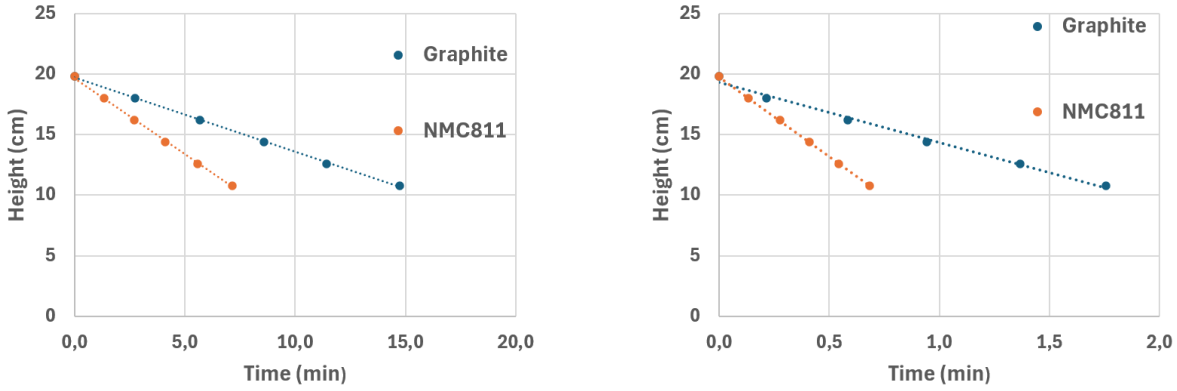

(a) No filtration of precipitates

(b) Filtration of precipitates

Figure 39: Evolution of the height of the suspension zone as a function of time for graphite and NMC811 at pH10.5 without and with filtration of the precipitates in the presence of nickel ions at a concentration of 0.02M, the slopes are equal to the settling velocities of graphite and NMC811, respectively. The pH was modified using H_2SO_4 and NaOH, the pulp density was equal to 7.7%.

4.3.2.3 Effect of cobalt ions presence

As explained in paragraph 4.1.2.3,since the zeta potential difference between graphite and NMC811 in the presence of cobalt ions is the highest at pH = 5 and a concentration of Co^{2+} which equals 0.02M, the batch sedimentation test was done at those conditions. Analyzing Figure 21, it can be seen that cobalt ions do not precipitate at those conditions. Therefore, the filtration was not realised.
The evolutions of the height of the suspension zone as a function of time for graphite and NMC811 at pH 5 without precipitates in the presence of cobalt ions at a concentration of 0.02M are shown in Figure 40. Since the evolutions are linear, a linear regression can be realised and the opposite of the corresponding slope corresponds to the settling speed. Therefore, the settling speed of graphite equals 8.55 cm/min and the one of NMC811 equals 3.68 cm/min.
Analyzing the values, it can be seen that the settling speed of graphite is higher than the one of NMC811. Comparing those values with the ones obtained in deionised water Figure 35, it can be seen that, similarly to lithium and nickel ions, the cobalt ions significantly increase the settling speed of NMC811 and do not impact significantly the one of graphite. As with lithium and nickel, it can be seen that the settling speed difference is reduced in the presence of cobalt ions compared to the case in deionised water.

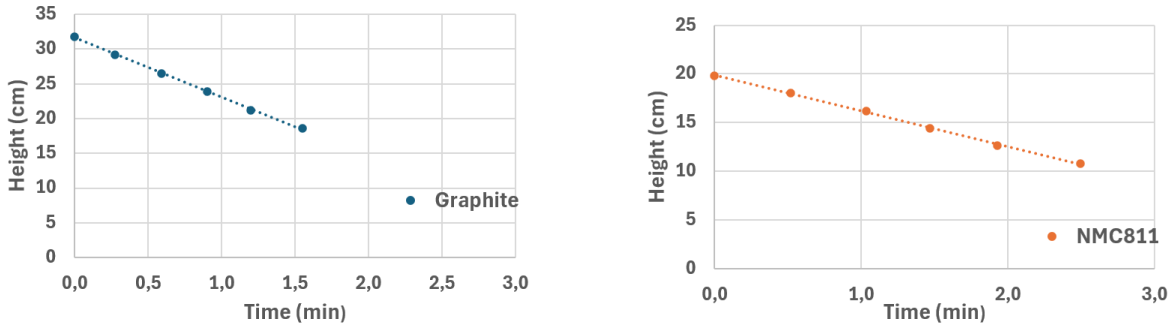

(a) Graphite (b) NMC811

Figure 40: Evolution of the height of the suspension zone as a function of time for graphite and NMC811 at pH 5 without precipitates in the presence of cobalt ions at a concentration of 0.02M. The sedimentation test for graphtie was realised in a 600ml graduated cylinder and in a 120ml graduated cylinder for NMC811. The pH was modified using H_2SO_4 and NaOH, the pulp density was equal to 7.7%.

4.3.2.4 Effect of aluminum ions presence

As explained in subsubsection 4.1.1 and subsubsection 4.3.1, since the highest settling speed difference between graphite and NMC811 is at pH5 in deionised water, a settling test was realised at pH5 with a concentration of 0.04M of Al^{3+}. In order to better understand the impact of precipitates, the test was performed with and without filtration. The evolutions of the height of the suspension zone as a function of time for graphite and NMC811 at pH5 with and without filtration of the precipitates in the presence of aluminum ions at a concentration of 0.04M, are shown in Figure 41. Since the evolutions are linear, a linear regression can be realised and the settling speed is given by the opposite of the slope. Therefore, in the case without filtration, the settling speeds of graphite and NMC811 equals to 0.19 and 0.37cm/min, respectively. In the case with filtration the settling speeds of graphite and NMC811 equals to 0.29 and 1.08cm/min, respectively.
Since the difference is not significative, it can be asumed that the precipitates are still present. Analyzing Figure 27, it can be seen that, if the pH increases slightly, the quantity of aluminum dissolved is solution is decreased. This could explain the presence of precipitates after filtration.

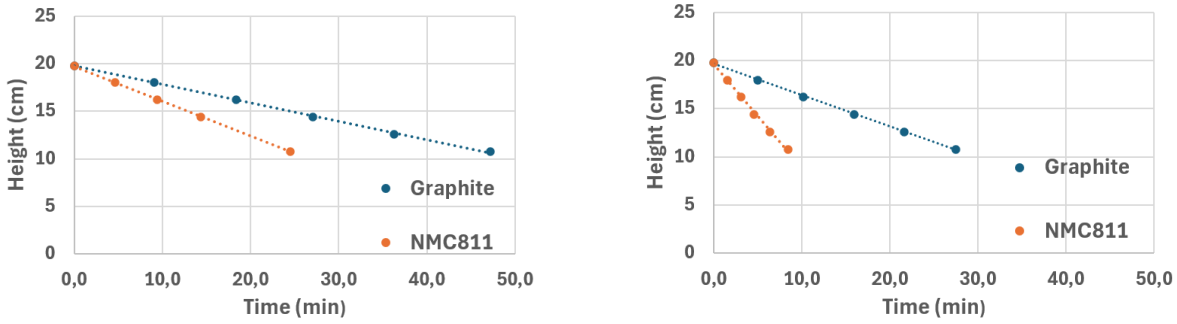

(a) Without filtration

(b) With filtration

Figure 41: Evolution of the height of the suspension zone as a function of time for graphite and NMC811 at pH5 with and without filtration of the precipitates in the presence of aluminum ions at a concentration of 0.04M, the slopes are equal to the settling velocities of graphite and NMC811, respectively. The pH was modified using H_2SO_4 and NaOH, the pulp density was equal to 7.7%.

As explained in paragraph 4.1.2.5, the highest zeta potential difference in the presence of Al^{3+} is at pH11. It has been shown that, aluminum precipitates at those conditions and the zeta potential difference is lower at higher aluminum concentrations, indicating that the precipitates could reduce the difference in the agglomeration behaviour of graphite and NMC811. Since the zeta potential difference was noticeably higher at pH11 compared to pH10.5 in the presence of aluminum ions, the sedimentation test was performed at pH11. In order to maximise the settling speed difference, the filtration was realised before the sedimentation test.

The evolutions of the height of the suspension zone as a function of time for graphite and NMC811 at pH11 with filtration of the precipitates in the presence of aluminum ions at a concentration of 0.04M are shown in Figure 42. It can be seen that the evolution is linear. Therefore, a linear regression can be realised and the settling speed is given by the opposite of the slope obtained. Therefore, the settling speed is equal to 7.26 cm/min for graphite and 22.77cm/min for NMC811.

Once again based on Figure 35, it can be noticed that the settling speed of graphite is almost unchanged and the settling speed of NMC811 is greatly increased, from 0.87 to 22.77cm/min. Since the settling speed difference is significant, a continuous sedimentation test will be performed at those conditions. The graphite is expected tobe recovered in the overflow and the NMC811 in the underflow.

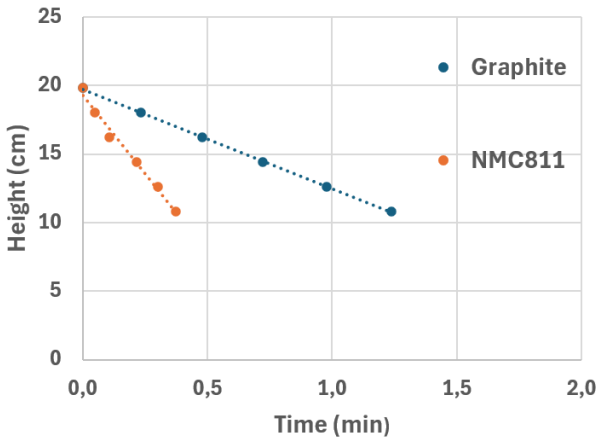

Figure 42: Evolution of the height of the suspension zone as a function of time for graphite and NMC811 at pH11 with filtration of the precipitates in the presence of aluminum ions at a concentration of 0.04M. The pH was modified using NaOH, the pulp density was equal to 7.7%.

4.3.3 Batch sedimentation tests summary

Based on the difference in the zeta potential of graphite and NMC811, several settling tests were performed. As expected, in deionised water the higher settling speed difference between graphite and NMC811 occurs at pH5, at which the zeta potential of graphite is sufficiently close to 0 to agglomerate and the one of NMC811 sufficiently below 0 to avoid agglomeration.

A summary of the settling speed obtained in the presence of ions is shown in Table 11. Since at pH5, Co^{2+} and Ni^{2+} at a concentration of 0.02M do not precipitate, filtration was not realised those conditions. Analyzing Table 11, it can be seen that, as expected based on the zeta potential experiments, the settling speed difference is lower in the presence of precipitates. It can also be seen that, at pH5, the settling speed differences are lower in the presence of ions compared to the case in deionised water. Therefore, the continuous sedimentation test of leaching residue could be performed at pH5 in deionised water since the majority of the NMC811 are removed and pH5 corresponds to its pH when it is in solution in deionised water. First, continuous sedimentation tests will be performed at pH5 in deionised water to determine the optimal raising speed.
Analyzing the values in Table 11, it can also be seen that the settling speed difference at pH10.5 and 11 in the presence of respectively, Ni^{2+} and Al^{3+} are significant. Therefore, a sedimentation test will be realised at pH10.5 in deionised water and then in the presence of Ni^{2+} filtrated and at pH11 in the presence of Al^{3+} filtrated to compare the effects of those ions and determine the optimal raising speed.

	Operating conditions			settling speed (cm/min)	
	pH	ion	concentration (M)	graphite	NMC811
No filtration	5	Co^{2+}	0.02	8.55	3.68
No filtration	5	Al^{3+}	0.04	0.19	0.37
Filtration	5	Al^{3+}	0.04	0.29	1.08
No filtration	5	Ni^{2+}	0.02	7.48	9.48
Filtration	6	Li^{+}	0.05	10.36	9.28
Filtration	9	Li^{+}	0.05	9.62	13.08
No filtration	10.5	Ni^{2+}	0.02	0.61	1.26
Filtration	10.5	Ni^{2+}	0.02	4.96	13.19
Filtration	11	Al^{3+}	0.04	7.26	22.77

Table 11: Summary, settling speeds of graphite and NMC811 in the presence of ions at certain pH and concentration. The pH was modified using NaOH, the pulp density was equal to 7.7%.

4.4 Continuous sedimentation tests

4.4.1 Impact of pH in deionised water

As seen in Figure 35, the highest difference in the settling speeds of graphite and NMC811 occurs at pH5. Therefore, the first tests will be realised at pH5 to maximise the separation. In the batch sedimentation test, the pulp density equals 7.7%. Due to a lack of pure graphite and NMC811, the continuous sedimentation test will be realised using 14g of feed, respectively 11g of graphite and 3g of NMC811 and a cell containing 280ml of water. Therefore, the maximum pulp density equals 4.8%.
Since the test is continuous, the solid fraction in the cell will always be lower. Therefore, the settling speed of graphite corresponding to a pulp density of 4.8% is lower than the actual settling velocity of graphite in the cell. Due to the reduction of the pulp density, the NMC811 settling speed will also increase. Therefore, the raising speed is fixed at the velocity corresponding to a pulp density of 4.8% to take into account the change of speed due to the change in the settling velocity. At pH5, the settling velocities were measured at a pulp density of 7.7% and 13%. A linear regression is therefore realised to approximate the velocity at 4.8%. The values obtained are shown in Table 12. After the test, the mass in the underflow, 7g, was much lower than expected, since 11g of graphite were in the feed. Therefore, the raising speed was reduced to 10 and 7.8 cm/min to optimise it. The evolution of the grades and recoveries of the underflow as a function of the settling speed are respectively shown in Figure 43. The values are shown in Table 28 and Table 29. Analyzing both graphs, it can be seen that, if the settling speed is too high, a majority of the feed will be entrained in the overflow. On the contrary, if the settling speed is too low, all the feed will sink in the underflow. The optimum settling speed is 10cm/min, since it maximises both grades and recovery and minimises the recovery of the NMC elements. The recoveries of nickel, cobalt and manganese should be almost the same, as it was the case for the flotation tests subsection 4.2. The differences could be explained by losses or imprecision since the analyses are realised using XRF in this

case.

Pulp density	Settling speed (cm/min)
7.7%	8.98
13%	3.91
4.8%	16.3

Table 12: Settling speed of graphite for pulp densities of 7.7% and 13% at pH = 5, in deionised water, the settling speed for a pulp density of 4.8% is approximated by a linear regression of the 2 settling speeds above.

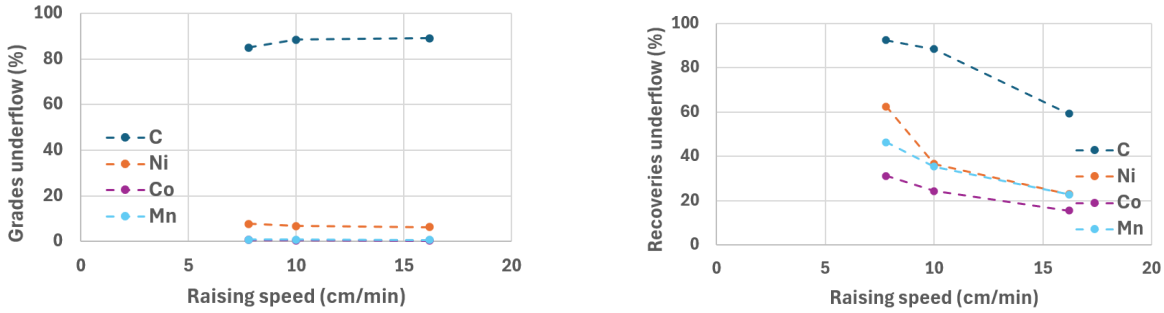

(a) Grades

(b) Recoveries

Figure 43: Continuous sedimentation test of synthetic black mass, composed of 80% of graphite and 20% of NMC811 , evolution of the grades and recoveries of the underflow product, as a function of the raising speed at pH5 in deionised water

Analyzing the settling speeds obtained for graphite and NMC811 as a function of pH during the batch sedimentation test, shown in Table 13 it can be seen that 10 cm/min corresponds to a raising speed close to the settling speed of graphite at pH5. Therefore, since the pulp density in the continuous sedimentation test is lower than that in the batch sedimentation test, it can be assumed that the settling speed of NMC811 increases consequently and becomes higher than the settling speed of graphite at the pulp density of 7.7%. Since the settling speed of graphite also increases, it will still be higher than the one of NMC811. This could explain the good results at 10 cm/min. Since the difference between the zeta potential of graphite and NMC811 in the presence of aluminum and nickel ions is the highest at pH11, and that the natural pH of the black mass pretreated mechanically is 10.5, a continuous sedimentation test will be realised in deionised water at pH10.5. A continuous sedimentation test will also be realised at pH7. For all the tests in deionised water, the raising speed will be equal to the settling speed of graphite at that pH and for a pulp density of 7.7%.

	Graphite	NMC811	Raising speed
pH (-)	(cm/min)	(cm/min)	(cm/min)
5	8.98	0,43	10
7	7.85	0.30	8
10.5	6.7	0.87	6.7

Table 13: Settling speed of graphite and NMC811, measured during a batch sedimentation test, as a function of the pH, modified using H_2SO_4 and NaOH, and raising speed in deionised water.

The evolution of the grades and recoveries of the underflow as a function of pH, when the settling speed is the one in Table 13, is shown respectively in Figure 44. The grades are almost constant with the pH and the recovery of NMC elements is much higher at pH7. Therefore, the leaching residue will be used for the continuous sedimentation test at pH5 and the black mass pre-treated mechanically will be used for the continuous sedimentation test at pH10.5. Once again, the recoveries of nickel, cobalt and manganese should be almost the same, as it was the case for the flotation tests subsection 4.2. The differences could be explained by losses or the imprecision of the characterization method since the analyses are realised using XRF in this case.

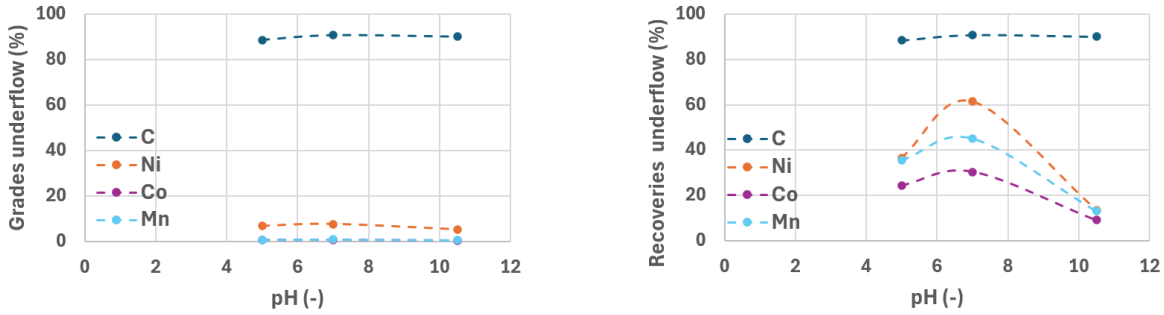

(a) Grades

(b) Recoveries

Figure 44: Continuous sedimentation test of synthetic black mass, composed of 80% of graphite and 20% of NMC811 , evolution of the grades and recoveries of the underflow product, as a function of pH, modified using H_2SO_4 ad NaOH in deionised water.

4.4.2 Impact of the studied ions

As seen in paragraph 4.3.2.2 and paragraph 4.3.2.4, the difference in settling speed of graphite and NMC compounds is significant at pH10.5 for Ni^{2+} and pH11 for Al^{3+}.
First of all, a test was performed at a raising speed of 6.7 cm/min in the presence of Ni^{2+} filtered to evaluate the impact of its presence compared to the case in deionised water. As it can be seen in Table 14, the grade and recovery of carbon are a little lower than the ones in deionised water at that settling speed. In order to optimise the impact of Ni^{2+}, as in the case with deionised water, the raising speed was set at 13.5cm/min, which corresponds

to the settling speed of the compound with the lower settling speed at a pulp density of 7.7%, which is NMC811 in this case. It can be seen that, even though the recovery in the underflow is quite low, the recovery is 94.37%, which is the highest so far. Since the settling speed of graphite is much lower than the one of NMC811, one could expect that it is mostly entrained in the overflow. However, analysing Figure 18, it can be seen that the concentration of Ni^{2+} in solution is lower at pH10 than at pH11. Therefore, the decrease of pH during the experiment results in the precipitation of Ni^{2+} on the particles, which decrease their settling speed and could explain the lower recovery of graphite in the overflow. Moreover, analysing Table 15, it can be seen that there is two times more nickel in the product than in the feed, which could be explained by the precipitation of nickel on the particles.

Concerning the aluminum, since a raising speed of 23cm/min seemed to be too high, it was set to 15cm/min, which corresponds to the double of the settling speed of graphite, which has the highest settling speed in this case. Once again, since the settling speed of graphite is much lower than the one of NMC811, one could expect that the graphite will be recovered in the overflow, which is the case. However, even though the settling speed difference is high, the grade in the overflow reaches only 70% and in the underflow 76%. Aluminum precipitates were observed on the beakers and on the particles after the test, even if filtration has been performed. Due to the duration of the test, more than one hour, the carbon dioxide acidified the solution, which, as seen in Figure 27, increased the quantity of precipitates. The grades of aluminum present in the products are shown in Table 18. Realising the ratios of the aluminum grade in the overflow and the mass of the product in the overflow, and in the underflow respectively, it can be seen that, proportionally, the aluminum precipitates more on NMC811 than on graphite. This could explained the lower grade in the overflow than the one expected due to the high settling speed differences obtained. The lower recovery could be explained by the precipitation of aluminum on graphite particles which, as seen previously, decreases the settling velocities. A batch sedimentation test should be realised with a lower concentration of aluminum to see if the settling speed difference is still significant. If it is the case, a continuous sedimentation test could be performed to see if the lower concentration increases the efficiency of the settling test by decreasing the quantity of aluminum precipitates.

Operational conditions			**Carbon in underflow**		**Carbon in overflow**	
Ions	Raising speed	pH	Grade UF	Recovery UF	Grade OF	Recovery OF
	(cm/min)	(-)	(%)	(%)	(%)	(%)
Deionised water	6.65	10.5	91.24	90.02	39.69	9.98
Ni2+ filtered	6.65	10.5	87.16	90.33	44.58	9.67
Ni2+ filtered	13.6	10.5	94.37	54.30	67.50	45.70
Al3+ filtered	15	11	76.35	29.80	69.48	70.20

Table 14: Grades, recoveries of the continuous sedimentation tests of synthetic black mass, composed of 80% of graphite and 20% of NMC811, and operating conditions, such as feed used, ions added, net raising speed and pH (part 1)

Operational conditions			**Nickel in underflow**		**Nickel in overflow**	
Ions	Raising speed	pH	Grade UF	Recovery UF	Grade OF	Recovery OF
	(cm/min)	(-)	(%)	(%)	(%)	(%)
Deionised water	6.65	10.5	5.31	13.64		
Ni2+ filtered	6.65	10.5	7.47	42.31		
Ni2+ filtered	13.6	10.5	34.30	112.26	20.00	97.82
Al3+ filtered	15	11	8.97	25.88	11.20	83.65

Table 15: Grades, recoveries of the continuous sedimentation tests of synthetic black mass, composed of 80% of graphite and 20% of NMC811, and operating conditions, such as feed used, ions added, net raising speed and pH (part 2), the blank cases corresponds to a solid sample of insufficient mass to realise the XRF analysis.

Operational conditions			**Manganese in underflow**		**Manganese in overflow**	
Ions	Raising speed	pH	Grade UF	Recovery UF	Grade OF	Recovery OF
	(cm/min)	(-)	(%)	(%)	(%)	(%)
Deionised water	6.65	10.5	0.60	13.08		
Ni2+ filtered	6.65	10.5	0.85	41.23		
Ni2+ filtered	13.6	10.5	2.45	51.44	2.24	70.28
Al3+ filtered	15	11	1.05	19.43	1.25	59.89

Table 16: Grades, recoveries of the continuous sedimentation tests of synthetic black mass, composed of 80% of graphite and 20% of NMC811, and operating conditions, such as feed used, ions added, net raising speed and pH (part 3), the blank cases corresponds to a solid sample of insufficient mass to realise the XRF analysis.

Operational conditions			**Cobalt in underflow**		**Cobalt in overflow**	
Ions	Raising speed	pH	Grade UF	Recovery UF	Grade OF	Recovery OF
	(cm/min)	(-)	(%)	(%)	(%)	(%)
Deionised water	6.65	10.5	0.44	9.10		
Ni2+ filtered	6.65	10.5	0.60	27.28		
Ni2+ filtered	13.6	10.5	4.28	83.77	1.66	48.55
Al3+ filtered	15	11	0.75	12.97	0.94	42.02

Table 17: Grades, recoveries of the continuous sedimentation tests of synthetic black mass, composed of 80% of graphite and 20% of NMC811, and operating conditions, such as feed used, ions added, net raising speed and pH (part 4), the blank cases corresponds to a solid sample of insufficient mass to realise the XRF analysis.

Grade aluminum overflow(%)	Ratio aluminum grade/overflow mass(%/g)	Grade aluminum underflow (%)	Ratio aluminum grade/underflow mass (%/g)
3.01	0.33	1.33	0.26

Table 18: Aluminum grade in both overflow and underflow and ratios of aluminum grade overflow/mass overflow and aluminum grade underflow/mass underflow for a continuous sedimentation test of synthetic black mass, composed of 80% of graphite and 20% of NMC811, performed at pH11, with a raising speed of 15cm/min in presence of aluminum at a concentration of 0.04M filtered to remove the precipitates

4.4.3 Industrial black mass

It was explained in subsubsection 4.4.1, that since the best results in deionised water are at pH5 and 10.5, the continuous sedimentation test could be performed at pH5 for the leaching residue and at pH10.5 for the black mass pre-treated mechanically. The conditions are the same as the one in subsubsection 4.4.1, 10cm/min at pH5 and 6.7 at pH10.5. The solid mass was 14g to reach the pulp density of 7.7% in the feed.
The grade and recovery of C, in the underflow and overflow, at pH5, both for the leaching residue and the model black mass, are shown in Figure 45. It can be seen that, both recovery and grade in the underflow are lower in the case of the leaching residue. Since the leaching residue is composed of 78.9% of carbon, its grade is decreased in the underflow. It can also be seen that, compared to the model black mass case, the grade is higher in the overflow than is the underflow. The ratio used in the model black mass, 11g of black mass for 14g of feed, corresponds to the 79% of C in the leaching residue. One explanation could be that, since the pH increased from 5 to 7 during the test, the upward velocity of 10cm/min was too high, compared to the 8cm/min at which the test was realised at pH7 and at which good results were obtained.

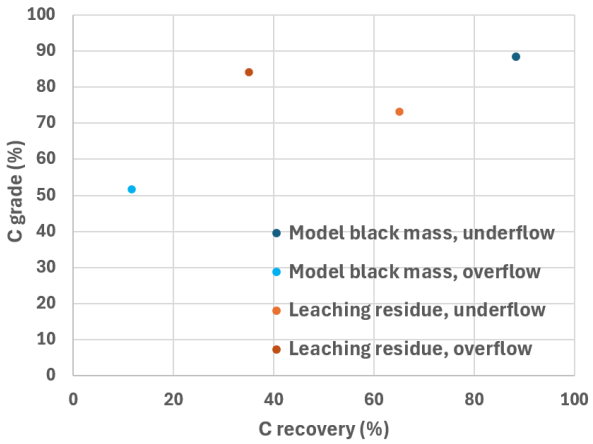

Figure 45: C grade and recovery of the model black mass and leaching residue, continuous sedimentation test with a pulp density of 7.7% for the inlet flow, at pH5, modified using H_2SO_4 and NaOH and a raising speed of 10cm/min.

The grade and recovery of C, in the underflow and overflow, at pH10.5, both for the model black mass and the mechanically pretreated black mass, are shown in Figure 46. Once again, it can be seen that both recovery and grade in the underflow are lower in the case of the mechanically pretreated black mass. Due to a lack of NMC811, the graphite/NMC811 ratio used for the model black mass, does not correspond to the ratio in the mechanically pretreated black mass, where the graphite accounts for 33.1%. Similarly, as in the case of the leaching residue, the C grade in the overflow, 39% in this case, is a little higher than the one in the feed. The grade in the underflow is almost unchanged compared to the one in the feed.

The low efficiency of the continuous tests can be explained partially by the device. Indeed, water and the pulp did not occupy the cross-section homogeneously, a funnel with the large opening directed inside the cell could increase the homogeneity. With a longer cell, the segregation only occurs at the entrances of the pulp and of the water, and both have the distance to homogenise in the rest of the cell. To inject the water by the bottom could help to ensure that the water has the desired effect since its velocity will be parallel to the tube and will not touch the tube and then go upwards as it was the case in this work.

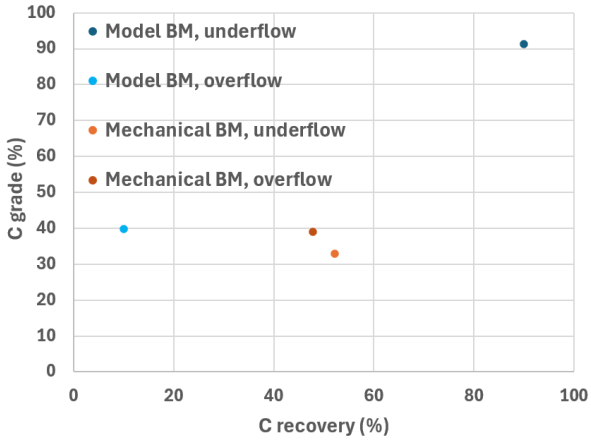

Figure 46: C grade and recovery of the model black mass and the mechanically pretreated black mass, continuous sedimentation test with a pulp density of 7.7% , at pH10.5, modified using NaOH, and a raising speed of 6.7cm/min

Moreover, it has been shown in the previous sections that the presence of ions can influence the settling behaviours of graphite and NMC811. It can be seen in Table 19 that the concentration of aluminum in the continuous sedimentation speed water at pH5 is higher than the one at which aluminum precipitates, which equals $3.5 \cdot 10^{-7}$ M, as shown in Figure 27. Similarly, the quantity of nickel in the continuous sedimentation speed water at pH10.5 is maybe higher than the one at which nickel precipitates, which equals $1.9 \cdot 10^{-8}$M. Since the precision of ICP analysis does not allow the analysis to give a quantitative concentration below 10^{-6} M, it is complicated to evaluate the impact of nickel ions. Therefore, zeta potential and batch sedimentation tests should be realised at the limit concentration detected by the ICP analysis to evaluate the impact of ions at that concentration. If it is negligible, the limit of the ICP

analysis will not be a problem.

	Al	**Co**	**Cu**	**Fe**	**Li**	**Mn**	**Ni**	**P**
Samples	(mol/l)	(mol/l)	(mol/l)	(mol/l)	(mol/l)	(mol/l)	(mol/l)	(mol/l)
BM pretreated mechanically pH10,5	2E-04	N/D	N/D	<3,6E-05	5,7E-03	N/D	<3,6E-05	1,3E-05
Leaching residue pH5	2.3E-05	N/D	N/D	<3.6E-05	3.2E-04	<3.6E-05	<3.4E-05	1.1E-06

Table 19: ICP analyses of the continuous sedimentation speed water, respectively for the test at pH10.5 with the black mass pretreated mechanically and for the test at pH5 with the leaching residue

4.4.4 Continuous sedimentation tests summary

For better understanding, the operational First, continuous sedimentation tests have been realised in deionised water and the upward speed was set to the lowest settling speed obtained during the batch sedimentation test to take into account the significant reduction of the pulp density in the cell. It has been shown that if the upward velocity is too high, the particles will be entrained unselectively, which will significantly reduce the recovery in the underflow. On the contrary, if the upward velocity is too low, the particles will fall unselectively and therefore the recovery will be high, but the grade will be low.

By adjusting the upward velocity, interesting results were obtained at pH5 and 10.5 in deionised water and at pH 10.5 in the presence of nickel ions. In deionised water, at pH5 a grade of 88.44% and a recovery of 88.42% were reached, at pH10.5, a grade of 91.24% and a recovery of 90.02% were reached and at pH10.5 in the presence of nickel ions, a grade of 94.37% and a recovery of 54.30% were reached.

Once the optimal parameters were settled, continuous sedimentation tests in deionised water using industrial black mass, such as leaching residue and mechanical black mass were performed. In both cases, the recovery was not significant and the grade in the underflow unchanged or lower than the one of the feed. Several factors can explain this, the particle size may not be the same as the one of the synthetic black mass. Due to the presence of ions and precipitates, the system was more complicated than the one of synthetic black mass.

5 Conclusion and perspectives

Due to the increasing demand in LIBs, their recycling is important both from an economic and environmental point of view. Since the presence of graphite during the lixiviation step reduce the overall efficiency of the recycling process and that graphite is in the CRM list, its recycling is important.

First of all, the zeta potential of graphite and NMC811 in deionised water and in presence of the ions which emanate from the black mass when it is placed in water or leached was determined to evaluate the optimal conditions at which the zeta potential was different enough to separate graphite and NMC811 by settling. It was shown that, at pH between 3 and 5 the zeta potential of graphite was sufficiently close to 0 and the one of NMC811 sufficiently more negative to assume a significant difference in agglomeration behaviour.
In the presence of nickel and aluminum ions, the zeta potential difference was significant at pH around 11 with a concentration of ion 0.0025M for the nickel and 0.005M for the aluminum. In the presence of cobalt, the zeta potential difference was the highest at pH5 with a concentration of 0.02M, and in the case of lithium ions at pH6 and 9 with a concentration of 0.05M. Since the zeta potential difference in the presence of manganese ions was not significant, settling tests were not realised in the presence of those ions.

Based on the zeta potential difference, flotation tests have been realised at several pHs to study the impact of promoter concentration and pH on the flotation of graphite from black mass as well as the influence of ions present in water flotation. It has been shown that the recovery and the grade of graphite decrease when washing is applied as a pre-treatment.
The promotor concentration of 350gpt seems the most appropriate to maximise both grade and recovery.
It can be concluded that the flotation at acidic pH is not successful and the operating costs will be higher. Therefore, it is advised to float at natural pH, in order to consume less acid and to obtain better results.
It must be kept in mind that the floated black mass was only mechanically treated. Therefore, the organic binder was still present which explain the lower selectivity compared to pyrolysed black mass. Removing the PVDF binder before flotation is advised. It can be done using pyrolysis [19] [36] [37] or using a solvent, such as a Fenton reagent (a combination of Fe^{2+} and H_2O_2) [18].

The evolution of the settling speeds of graphite and NMC811 in deionised water was determined as a function of pH. It was shown that the settling speed of graphite was constant from 3 to 5 and increased linearly from pH5 to 11. It varies from -9cm/min at pH5 and -6cm/min at pH11. Concerning NMC811, the settling speed is close to -3 at pH3 and is close to 0 from pH 5 to 11. After that, at the optimal conditions determined during the zeta potential experiments, in the presence of nickel ions at a concentration of 0.0025M at pH11, in the presence of aluminum ions at a concentration of 0.005M at pH11, in the presence of cobalt ions at a concentration of 0.02M at pH5, and in the presence of lithium ions at pH6 and 9 at a concentration of 0.05M, static settling tests were realised to measure the settling speeds of graphite and NMC811 and determined the conditions at which the settling speed difference was significant. Due to the significant settling speed difference in deionised water,

the settling speed in the presence of nickel ions at a concentration of 0.02M and in the presence of aluminum at a concentration of 0.04M at pH5 were evaluated.
In the presence of ions, it was shown that the precipitation of ions significantly decreases the settling speed of both NMC811 and graphite. It is assumed that, since the charge is the same for all particles, they will repel each other and settle slower. Therefore, in order to benefit from the ions, the ion solutions were filtered before the settling tests.
It was shown that the graphite settling velocity remained almost unchanged in the presence of ions. In the contrary, the cathode settling speed was greatly increased. In the presence of aluminum ions at pH 11 with filtration, it reached -22.8cm/min and the graphite settling speed was around -7.3cm/min. In the presence of nickel ions at pH10.5 with filtration the settling speed of graphite was around -5cm/min and the one of NMC811 around -13.2 cm/min. In the presence of cobalt ions, the graphite settling speed was around -8.6 cm/min and the one of NMC811 around -3.7 cm/min. In the presence of lithium ions at pH6, the settling speed of graphite was around -10.4 and NMC811 around -9.3.
Since the settling speed difference was lower in the presence of ions at pH5, the continuous sedimentation test at pH5 was only realised in deionised water.
Thirdly, continuous sedimentation tests were realised using the slowest settling speed determined as the raising speed. The test in deionised water at pH5 was performed with a raising speed of 10cm/min, the grade reached 88.44% and the recovery 88.42 %. The one as pH10.5 was performed with a raising speed of 6.7 cm/min, the grade reached 90.02% and the recovery 91.24%. In the presence of nickel ions filtrated at pH11, the raising speed was set to 13.6cm/min, the grade reached 94.37% and the recovery 54.30%.
Due to a lack of NMC811 material, the feed of the synthetic black mass was 80%graphite and 20% NMC811.

Finally, the continuous sedimentation tests in deionised water at optimal conditions were performed on lixiviation residue at pH5, the recovery equalled 65.01% and the grade equalled 73.29%, and on mechanically treated black mass at pH10.5, the grade equalled 32.88% and the recovery 52.51%. The analyses of the water used during those tests shown that at pH5, aluminum ions precipitate. Taking also into account the complexity of the black mass, it could explain why the grade and recovery are not as high as the one obtained using synthetic black mass.

Several options should be considered to improve the efficiency and better understand the mechanisms involved in the continuous sedimentation test with industrial black mass.

First, improvements to the experimental device should be considered. The continuous sedimentation cell could be replaced by a longer microflotation cell or a long tube to provide sufficient residence time for the particles to settle without being unintentionally entrained by the upward water flow. In the present configuration, the water and pulp did not occupy the cross-section homogeneously. This issue could potentially be addressed by introducing a funnel with its wider opening facing the inside of the cell, thereby promoting a more homogeneous distribution of the flows. A longer cell would also allow the disturbances and segregation occurring at the pulp and water inlets to dissipate, giving both flows sufficient distance to homogenise in the cell.

The water injection system could also be improved. Injecting the water directly from the

bottom of the cell could ensure that the flow remains parallel to the tube axis and produces the intended upward velocity profile. This could prevent the water from initially impinging on the tube walls before flowing upward, as observed in the present work.

Once the experimental setup has been improved, the operating conditions should be optimised. In particular, the upward water velocity could be further adjusted to maximise the separation efficiency. Since the duration of the experiments was relatively long considering the small amount of sample processed, reducing the residence time would also be necessary for potential scale-up. This could be achieved by increasing the pulp density and/or adjusting the upward velocity to increase the rate at which the pulp enters and passes through the cell.

Further characterisation should then be performed to improve the understanding of the separation mechanisms. Measuring the size of the agglomerates formed during the process could provide valuable information on the agglomeration mechanism and its influence on sedimentation behaviour. In addition, SEM analysis could contribute to a better understanding of the structure and morphology of the black mass particles. Zeta potential and settling velocity measurements could also be performed to evaluate the influence of the ion concentration in the water used for the continuous sedimentation tests at pH 5 and 10.5. These measurements could further be extended to investigate whether the combination of several ions could improve the separation efficiency. For example, the simultaneous use of nickel and aluminium ions at pH 11 could be evaluated.

The influence of aluminium should also be investigated more specifically. Static and continuous sedimentation tests could be performed in the presence of aluminium at concentrations below the precipitation threshold. This would make it possible to determine whether the difference in settling velocities could be exploited without the formation of precipitates on the particle surfaces. Conversely, if aluminium precipitates are found to significantly reduce the efficiency of the separation, a sieving step could be introduced to reduce the aluminium content of the feed. In this case, determining the elemental distribution of the black mass across several particle-size fractions could help identify the optimal cut size.

Finally, the economic and industrial relevance of the process should be assessed. The most suitable point in the overall flowsheet for implementing continuous sedimentation could be evaluated by comparing three possible configurations:

- the mechanically pretreated black mass at pH 10.5, before the leaching step;
- the leaching residue at pH 5;
- both streams, before and after the leaching step.

An economic assessment could then be conducted to identify the most profitable flowsheet. In addition, since flotation generally requires higher energy consumption and a greater amount of reagents, a comparative economic study between continuous sedimentation and flotation would be valuable for determining the most economically attractive separation process.

A Appendix

A.1 Values of the logarithm of the concentration for the solubility of ionic species

pH	$[Ni^{2+}]$	$[Ni(OH)^{+}]$	$[Ni(OH)_2])$	$[Ni(OH)_3^{-}]$	$[Ni(OH)_4^{2-}]$	$[Ni_{tot.disolved}]$
0	12.74	2.84	-6.26	-16.46	-31.26	12.74
1	10.74	1.84	-6.26	-15.46	-29.26	10.74
2	8.74	0.84	-6.26	-14.46	-27.26	8.74
3	6.74	-0.16	-6.26	-13.46	-25.26	6.74
4	4.74	-1.16	-6.26	-12.46	-23.26	4.74
5	2.74	-2.16	-6.26	-11.46	-21.26	2.74
6	0.74	-3.16	-6.26	-10.46	-19.26	0.74
7	-1.26	-4.16	-6.26	-9.46	-17.26	-1.26
8	-3.26	-5.16	-6.26	-8.46	-15.26	-3.26
9	-5.26	-6.16	-6.26	-7.46	-13.26	-5.17
10	-7.26	-7.16	-6.26	-6.46	-11.26	-5.99
11	-9.26	-8.16	-6.26	-5.46	-9.26	-5.40
12	-11.26	-9.16	-6.26	-4.46	-7.26	-4.45
13	-13.26	-10.16	-6.26	-3.46	-5.26	-3.45
14	-15.26	-11.16	-6.26	-2.46	-3.26	-2.40

Table 20: Logarithm of concentration of nickel species at different pH, equilibrium constant for hydrolysis used from [62] and solubility constant used from [69]

pH	$[Co^{2+}]$	$[Co(OH)^{+}]$	$[Co(OH)_2]$	$[Co(OH)_3^{-}]$	$[Co(OH)_4^{2-}]$	$[Co_{tot.disolved}]$
0	14.77	5.16	-5.00	-17.24	-31.53	14.77
1	12.77	4.16	-5.00	-16.24	-29.53	12.77
2	10.77	3.16	-5.00	-15.24	-27.53	10.77
3	8.77	2.16	-5.00	-14.24	-25.53	8.77
4	6.77	1.16	-5.00	-13.24	-23.53	6.77
5	4.77	0.16	-5.00	-12.24	-21.53	4.77
6	2.77	-0.84	-5.00	-11.24	-19.53	2.77
7	0.77	-1.84	-5.00	-10.24	-17.53	0.77
8	-1.23	-2.84	-5.00	-9.24	-15.53	-1.22
9	-3.23	-3.84	-5.00	-8.24	-13.53	-3.13
10	-5.23	-4.84	-5.00	-7.24	-11.53	-4.51
11	-7.23	-5.84	-5.00	-6.24	-9.53	-4.92
12	-9.23	-6.84	-5.00	-5.24	-7.53	-4.80
13	-11.23	-7.84	-5.00	-4.24	-5.53	-4.15
14	-13.23	-8.84	-5.00	-3.24	-3.53	-3.05

Table 21: Logarithm of concentration of manganese species at different pH. equilibrium constant for hydrolysis used from [63] and solubility constant used from [69]

pH	$[Mn^{2+}]$	$[Mn(OH)^{+}]$	$[Mn(OH)_2]$	$[Mn(OH)_3^{-}]$	$[Mn(OH)_4^{2-}]$	$[Mn_{tot.disolved}]$
0	15.30	4.72	-6.88	-19.04	-32.98	15.30
1	13.30	3.72	-6.88	-18.04	-30.98	13.30
2	11.30	2.72	-6.88	-17.04	-28.98	11.30
3	9.30	1.72	-6.88	-16.04	-26.98	9.30
4	7.30	0.72	-6.88	-15.04	-24.98	7.30
5	5.30	-0.28	-6.88	-14.04	-22.98	5.30
6	3.30	-1.28	-6.88	-13.04	-20.98	3.30
7	1.30	-2.28	-6.88	-12.04	-18.98	1.30
8	-0.70	-3.28	-6.88	-11.04	-16.98	-0.70
9	-2.70	-4.28	-6.88	-10.04	-14.98	-2.69
10	-4.70	-5.28	-6.88	-9.04	-12.98	-4.60
11	-6.70	-6.28	-6.88	-8.04	-10.98	-6.06
12	-8.70	-7.28	-6.88	-7.04	-8.98	-6.55
13	-10.70	-8.28	-6.88	-6.04	-6.98	-5.94
14	-12.70	-9.28	-6.88	-5.04	-4.98	-4.70

Table 22: Logarithm of concentration of manganese species at different pH. equilibrium constant for hydrolysis used from [64] and solubility constant used from [69]

pH	$[Al^{3+}]$	$[Al(OH)^{2+}]$	$[Al(OH)_2^+]$	$[Al(OH)_3]$	$[Al(OH)_4^-]$	$[Al_{tot.disolved}]$
0	8.48	3.50	-2.15	-7.18	-14.43	8.48
1	5.48	1.50	-3.15	-7.18	-13.43	5.48
2	2.48	-0.50	-4.15	-7.18	-12.43	2.48
3	-0.52	-2.50	-5.15	-7.18	-11.43	-0.52
4	-3.52	-4.50	-6.15	-7.18	-10.43	-3.48
5	-6.52	-6.50	-7.15	-7.18	-9.43	-6.12
6	-9.52	-8.50	-8.15	-7.18	-8.43	-7.10
7	-12.52	-10.50	-9.15	-7.18	-7.43	-6.99
8	-15.52	-12.50	-10.15	-7.18	-6.43	-6.36
9	-18.52	-14.50	-11.15	-7.18	-5.43	-5.43
10	-21.52	-16.50	-12.15	-7.18	-4.43	-4.43
11	-24.52	-18.50	-13.15	-7.18	-3.43	-3.43
12	-27.52	-20.50	-14.15	-7.18	-2.43	-2.43
13	-30.52	-22.50	-15.15	-7.18	-1.43	-1.43
14	-33.52	-24.50	-16.15	-7.18	-0.43	-0.43

Table 23: Logarithm of concentration of aluminum species at different pH. equilibrium constant for hydrolysis used from [65] and solubility constant used from [69]

A.2 Characterization of the different flotation products

No washing			**Grade**				**Recovery**			
PRODUCT	**Mass**	**Mass**	**C**	**Ni**	**Co**	**Mn**	**C**	**Ni**	**Co**	**Mn**
	(g)	(%)	(%)	(%)	(%)	(%)	(%)	(%)	(%)	(%)
Rougher	44	48%	47.7%	23.7%	3.0%	1.6%	66.6%	37.5%	37.7%	37.7%
Scavenger	12	13%	34.5%	30.9%	3.9%	2.0%	13.2%	13.4%	13.1%	13.0%
Tailing	35	38%	18.2%	38.9%	5.0%	2.6%	20.2%	49.1%	49.2%	49.3%
Total	91	100%	34.6%	30.5%	3.9%	2.0%	100.0%	100.0%	100.0%	100.0%
Washing, 150 gpt escaid			**Grade**				**Recovery**			
PRODUCT	**Mass**	**Mass**	**C**	**Ni**	**Co**	**Mn**	**C**	**Ni**	**Co**	**Mn**
	(g)	(%)	(%)	(%)	(%)	(%)	(%)	(%)	(%)	(%)
Rougher	32.3	35%	39.5%	30.3%	3.8%	1.9%	40.7%	32.2%	31.2%	30.6%
Scavenger	12.5	13%	44.3%	27.8%	3.6%	1.8%	17.7%	11.5%	11.5%	11.4%
Tailing	48.1	52%	27.1%	35.6%	4.6%	2.4%	41.6%	56.3%	57.3%	58.0%
Total	92.9	100%	33.7%	32.7%	4.2%	2.2%	100.0%	100.0%	100.0%	100.0%
Washing, 350 gpt escaid			**Grade**				**Recovery**			
PRODUCT	**Mass**	**Mass**	**C**	**Ni**	**Co**	**Mn**	**C**	**Ni**	**Co**	**Mn**
	(g)	**(%)**	**(%)**	**(%)**	**(%)**	**(%)**	(%)	(%)	(%)	(%)
Rougher	32.8	33%	45%	27.1%	3.3%	1.7%	43.4%	30.4%	29.5%	29.3%
Scavenger	15.1	15%	44.8%	26.2%	3.2%	1.7%	19.9%	11.4%	11.2%	11.2%
Tailing	50.1	51%	24.9%	34.7%	4.4%	2.4%	36.6%	58.2%	59.3%	59.5%
Total	98	100%	34.7%	29.3%	3.7%	1.9%	100%	100%	100%	100%
Washing, 500 gpt escaid			**Grade**				**Recovery**			
PRODUCT	**Mass**	**Mass**	**C**	**Ni**	**Co**	**Mn**	**C**	**Ni**	**Co**	**Mn**
	(g)	**(%)**	**(%)**	**(%)**	**(%)**	**(%)**	(%)	(%)	(%)	(%)
Rougher	41	44%	39.0%	28.8%	3.5%	1.8%	49.7%	40.7%	39.6%	39.1%
Scavenger	15	16%	48.9%	22.9%	3.0%	1.5%	22.8%	11.9%	12.1%	12.1%
Tailing	38	40%	23.4%	36.3%	4.7%	2.4%	27.6%	47.5%	48.3%	48.8%
Total	94	100%	34.3%	30.9%	3.9%	2.0%	100%	100%	100%	100%

Table 24: Grades, obtained using ICP-OES and total organic carbon analyses, and recoveries of the concentrates and tailings, in the cases without washing and with washing, with a concentration of escaid of 150, 350 and 500 gpt. The pH is unmodified in all cases

No washing			**Cumulative recovery**				**Cumulative grade**			
PRODUCT	**Mass** (g)	**Mass** (%)	**C** (%)	**Ni** (%)	**Co** (%)	**Mn** (%)	**C** (%)	**Ni** (%)	**Co** (%)	**Mn** (%)
Rougher	44	48%	66.63%	37.54%	37.69%	37.72%	47.67%	23.65%	3.03%	1.57%
Scavenger	12	13%	79.79%	50.90%	50.82%	50.69%	44.85%	25.20%	3.21%	1.66%
Washing, 150 gpt escaid			**Cumulative recovery**				**Cumulative grade**			
PRODUCT	**Mass** (g)	**Mass** (%)	**C** (%)	**Ni** (%)	**Co** (%)	**Mn** (%)	**C** (%)	**Ni** (%)	**Co** (%)	**Mn** (%)
Rougher	32.3	35%	40.74%	32.20%	31.17%	30.64%	39.50%	30.26%	3.75%	1.92%
Scavenger	12.5	13%	58.43%	43.66%	42.69%	42.01%	40.84%	29.58%	3.70%	1.90%
Washing, 350 gpt escaid			**Cumulative recovery**				**Cumulative grade**			
PRODUCT	**Mass (g)**	**Mass (%)**	**C** (%)	**Ni** (%)	**Co** (%)	**Mn** (%)	**C** (%)	**Ni** (%)	**Co** (%)	**Mn** (%)
Rougher	32.8	33%	43.44%	30.43%	29.49%	29.26%	44.99%	27.06%	3.28%	1.72%
Scavenger	15.1	15%	63.35%	41.84%	40.69%	40.46%	44.93%	26.79%	3.26%	1.71%
Washing, 500 gpt escaid			**Cumulative recovery**				**Cumulative grade**			
PRODUCT	**Mass (g)**	**Mass (%)**	**C (%)**	**Ni (%)**	**Co (%)**	**Mn (%)**	**C (%)**	**Ni (%)**	**Co** (%)	**Mn** (%)
Rougher	41	44%	49.68%	40.67%	39.65%	39.12%	39.04%	28.79%	3.54%	1.79%
Scavenger	15	16%	72.44%	52.52%	51.73%	51.19%	41.68%	27.22%	3.38%	1.72%

Table 25: Cumulative grades and recoveries in the cases without washing and with washing, with a concentration of escaid of 150, 350 and 500 gpt. The pH is unmodified in all cases

Washing, unmodified pH			**Grade**				**Recovery**			
PRODUCT	**Mass** (g)	**Mass** (%)	**C** (%)	**Ni** (%)	**Co** (%)	**Mn** (%)	**C** (%)	**Ni** (%)	**Co** (%)	**Mn** (%)
Rougher	32.3	35%	39.5%	30.3%	3.8%	1.9%	40.7%	32.2%	31.2%	30.6%
Scavenger	12.5	13%	44.3%	27.8%	3.6%	1.8%	17.7%	11.5%	11.5%	11.4%
Tailing	48.1	52%	27.1%	35.6%	4.6%	2.4%	41.6%	56.3%	57.3%	58.0%
Total	92.9	100%	33.7%	32.7%	4.2%	2.2%	100.0%	100.0%	100.0%	100.0%
Washing, pH = 7			**Grade**				**Recovery**			
PRODUCT	**Mass** (g)	**Mass** (%)	**C** (%)	**Ni** (%)	**Co** (%)	**Mn** (%)	**C** (%)	**Ni** (%)	**Co** (%)	**Mn** (%)
Rougher	33	35%	36.0%	31.8%	4.0%	2.0%	37.8%	35.1%	34.1%	33.2%
Scavenger	9.8	11%	38.6%	31.1%	4.0%	2.0%	12.0%	10.2%	10.0%	9.9%
Tailing	50.4	54%	31.3%	32.4%	4.3%	2.3%	50.1%	54.6%	55.9%	56.9%
Total	93.2	100%	33.7%	32.0%	4.1%	2.2%	100%	100%	100%	100%
Washing, pH = 5			**Grade**				**Recovery**			
PRODUCT	**Mass** (g)	**Mass** (%)	**C** (%)	**Ni** (%)	**Co** (%)	**Mn** (%)	**C** (%)	**Ni** (%)	**Co** (%)	**Mn** (%)
Concentrate	27.2	29%	34.2%	32.7%	3.9%	2.0%	29.9%	29.6%	28.7%	28.2%
Tailing	65.6	71%	33.2%	32.2%	4.1%	2.2%	70.1%	70.4%	71.3%	71.8%
Total	92.8	100%	33.5%	32.3%	4.0%	2.1%	100%	100%	100%	100%
Washing, pH = 3			**Grade**				**Recovery**			
PRODUCT	**Mass** (g)	**Mass** (%)	**C** (%)	**Ni** (%)	**Co** (%)	**Mn** (%)	**C** (%)	**Ni** (%)	**Co** (%)	**Mn** (%)
Concentrate	14.1	16%	27.7%	37.4%	4.3%	2.2%	12.5%	18.5%	17.1%	16.7%
Tailing	76.1	84%	35.7%	30.5%	3.9%	2.1%	87.5%	81.5%	82.9%	83.3%
Total	90.2	100%	34.5%	32%	4%	2%	100%	100%	100%	100%

Table 26: Grades, obtained using ICP-OES and total organic carbon analyses, and recoveries of the concentrates and tailings, in the cases with washing and with and without pH modification, with a ph of 7, 5 and 3, in all cases the escaid concentration equals 150 gpt

Washing, 150 gpt escaid			**Cumulative recovery**				**Cumulative grade**			
PRODUCT	**Mass** (g)	**Mass** (%)	**C** (%)	**Ni** (%)	**Co** (%)	**Mn** (%)	**C** (%)	**Ni** (%)	**Co** (%)	**Mn** (%)
Rougher	32.3	35%	40.74%	32.20%	31.17%	30.64%	39.50%	30.26%	3.75%	1.92%
Scavenger	12.5	13%	58.43%	43.66%	42.69%	42.01%	40.84%	29.58%	3.70%	1.90%
Washing, pH = 7			**Cumulative recovery**				**Cumulative grade**			
PRODUCT	**Mass** (g)	**Mass** (%)	**C** (%)	**Ni** (%)	**Co** (%)	**Mn** (%)	**C** (%)	**Ni** (%)	**Co** (%)	**Mn** (%)
Rougher	33	35%	37.82%	35.15%	34.06%	33.20%	36.02%	31.80%	3.99%	2.03%
Scavenger	9.8	11%	49.86%	45.36%	44.07%	43.06%	36.62%	31.64%	3.98%	2.03%
Washing, pH = 5			**Cumulative recovery**				**Cumulative grade**			
PRODUCT	**Mass** (g)	**Mass** (%)	**C** (%)	**Ni** (%)	**Co** (%)	**Mn** (%)	**C** (%)	**Ni** (%)	**Co** (%)	**Mn** (%)
Rougher	27.2	29%	29.92%	29.63%	28.69%	28.23%	34.17%	32.65%	3.93%	2.04%
Washing, pH = 3			**Cumulative recovery**				**Cumulative grade**			
PRODUCT	**Mass** (g)	**Mass** (%)	**C** (%)	**Ni** (%)	**Co** (%)	**Mn** (%)	**C** (%)	**Ni** (%)	**Co** (%)	**Mn** (%)
Rougher	14.1	16%	12.54%	18.52%	17.11%	16.71%	27.66%	37.37%	4.29%	2.22%

Table 27: Cumulative grades and recoveries in the cases with washing and with and without pH modification, with a ph of 7, 5 and 3, in all cases the escaid concentration equals 150 gpt

A.3 Characterization of the continuous sedimentation products

Operational Conditions		**Carbon in overflow**		**Carbon in underflow**		**Nickel in underflow**	
Ions	pH (-)	Grade OF (%)	Recovery OF (%)	Grade UF (%)	Recovery UF (%)	Grade UF (%)	Recovery UF (%)
7.8	5	41.47	7.66	85.07	92.34	7.78	62.48
10	5	51.61	11.58	88.44	88.42	6.83	36.70
16.2	5	68.60	40.76	89.19	59.24	6.34	23.03
8	7	44.94	9.28	85.44	90.72	7.67	61.52
6.65	10.5	39.69	9.98	91.24	90.02	5.31	13.64
6.65	10.5	44.58	9.67	87.16	90.33	7.47	42.31

Table 28: Grade, recoveries and operating conditions of the continuous sedimentation tests realised in deionised water with synthetic black mass, composed of 80% of graphite and 20% of NMC (part I)

Operational Conditions		**Manganese in UnderFlow**		**Cobalt in underflow**	
Ions	pH (-)	Grade UF (%)	Recovery UF (%)	Grade UF (%)	Recovery UF (%)
7.8	5	0.90	46.42	0.65	31.21
10	5	0.77	35.44	0.57	24.33
16.2	5	0.73	22.77	0.54	15.55
8	7	0.88	45.02	0.63	30.41
6.65	10.5	0.60	13.08	0.44	9.10
6.65	10.5	0.85	41.23	0.60	27.28

Table 29: Grade, recoveries and operating conditions of the continuous sedimentation tests realised in deionised water with synthetic black mass, composed of 80% of graphite and 20% of NMC (part II)

References

[1] Qi Huang - Shunli Wang - Zonghai Chen - Ran Xiong - Carlos Fernandez - Daniel-I. Stroe. *Long-Term Health State Estimation of Energy Storage Lithium-Ion Battery Packs*. Springer, 2023, pp. 1–2 (page 1).

[2] Younghun KIM - Mitsuaki MATSUDA - Atsushi SHIBAYAMA - Toyohisa FUJITA. "Recovery of LiCoO2 from Wasted Lithium Ion Batteries by using Mineral Processing Technology". In: *Resurces processing* (2003), p. 3 (page 1).

[3] Liang An, ed. *Recycling of Spent Lithium-Ion Batteries Processing Methods and Environmental Impacts*. Springer, 2019, pp. v, 1–7 (pages 1, 4–6).

[4] Nicola Armaroli and Vincenzo Balzani. "Towards an electricity-powered world". In: *Energy Environmental Science 4* (2011) (page 1).

[5] European Comission. *Proposal for a REGULATION OF THE EUROPEAN PARLIAMENT AND OF THE COUNCIL establishing a framework for ensuring a secure and sustainable supply of critical raw materials and amending Regulations (EU) 168/2013, (EU) 2018/858, 2018/1724 and (EU) 2019/1020*. (consultated the 2025-10-30). URL: `https://eur-lex.europa.eu/legalcontent/EN/TXT/HTML/uri=CELEX:52023PC0160` (page 1).

[6] European Parliament. *New EU regulatory framework for batteries Setting sustainability requirements*. (consultated the 10-29-25). URL: `https://www.europarl.europa.eu/RegData/etudes/BRIE/2021/689337/EPRS_BRI(2021)689337_EN.pdf` (page 1).

[7] Johannes Rieger - Stephan Stuhr - Bettina Rutrecht - Stefan Morgenbesser - Thomas Nigl - Astrid Arnberger - Hartwig Kunanz - and Stefanie Lesiak. "Graphite Separation from Lithium-Ion Battery Black Mass Using Froth Flotation and Quality Evaluation for Reuse as a Secondary RawMaterial Including Non-Battery Applications". In: *Recycling 2025-10-75* (2025), pp. 1–4 (page 1).

[8] GCMRI. *Graphite Anode Bottleneck*. (consultated the 05-15-26). URL: `https://raremetal.org/graphite.html` (page 1).

[9] Anna Vanderbruggen. "Lithium-ion batteries recycling with froth flotation - A study on characterization and liberation stages". In: *School of Chemical engineering, Department of chemical and metallurgical engineering, Aalto University publication series DOCTORAL THESES 166/2022* (2022) (pages 1, 4, 6, 10).

[10] Juan Wu - Li Xiao - Li Shen - Jian-Jun Ran - Hui Zhong - Yi-Rong Zhu - Han Chen. "Recent advancements in hydrometallurgical recycling technologies of spent lithium-ion battery cathode materials". In: *Rare Metals* (2004) (pages 1, 2, 4–6).

[11] Omar Velázquez-Martínez - Johanna Valio - Annukka Santasalo-Aarnio - Markus Reuter - Rodrigo Serna-Guerrero 1. "A Critical Review of Lithium-Ion Battery Recycling Processes from a Circular Economy Perspective". In: *Batteries* (2019) (pages 1, 4–6).

[12] Urs Alexander Peuker Denis Werner and Thomas Mütze. "Recycling Chain for Spent Lithium-Ion Batteries". In: *Metals 10* (2020) (pages 2, 6).

[13] Arno Kwade - Jan Diekmann, ed. *Recycling of Lithium-Ion Batteries The LithoRec Way*. Springer International Publishing AG, 2018 (pages 2, 6).

[14] Christian Ekberg and Martina Petranikova. "Chapter 7 - Lithium Batteries Recycling". In: *Lithium Process Chemistry*. Ed. by Alexandre Chagnes and Jolanta Świątowska.

Amsterdam: Elsevier, 2015, pp. 233–267. ISBN: 978-0-12-801417-2. DOI: https://doi.org/10.1016/B978-0-12-801417-2.00007-4. URL: https://www.sciencedirect.com/science/article/pii/B9780128014172000074 (pages 2, 6, 7).

[15] Esra kilavuz. "Sustainable Lithium-Ion Battery Recycling:Challenges, Innovations, and Pathways to a Circular Economy". In: *ACS sustanable resource management* (2025), pp. 1847–1848 (pages 2, 7).

[16] Jonas Neumann - Martina Petranikova - Marcel Meeus - Jorge D. Gamarra - Reza Younesi - Martin Winter - and Sascha Nowak. "Recycling of Lithium-Ion Batteries—Current State of the Art, Circular Economy, and Next Generation Recycling". In: *Advanced energy materials* (2022) (pages 2, 7).

[17] Jiadong Yua - Yaqun Heb - Zhenzhou Gea - Hong Lia - Weining Xiec - Shuai Wang. "A promising physical method for recovery of LiCoO2 and graphite from spent lithium-ion batteries: Grinding flotation". In: *Separation and Purification Technology 190* (2018) (pages 2, 8–10).

[18] Yaqun He - Tao Zhang - Fangfang Wang - Guangwen Zhang - Weigang Zhang - Jie Wang. "Recovery of LiCoO2 and graphite from spent lithium-ion batteries by Fenton reagent-assisted flotation". In: *Journal of Cleaner Production 143* (2017) (pages 2, 8–10, 48, 65).

[19] Guangwen Zhang - Yaqun He - Haifeng Wang - Yi Feng - Weining Xie -and Xiangnan Zhu. "Removal of Organics by Pyrolysis for Enhancing Liberation and Flotation Behavior of Electrode Materials Derived from Spent Lithium-Ion Batteries". In: *ACS Stustainable Chemistry and Engineering 8* (2020) (pages 2, 8–10, 48, 65).

[20] Anna Vanderbruggen - Johanna Sygusch - Martin Rudolph - Rodrigo Serna-Guerrero. "A contribution to understanding the flotation behavior of lithium metal oxides and spheroidized graphite for lithium-ion battery recycling". In: *Colloids and Surfaces A: Physicochemical and Engineering Aspects 626* (2021) (pages 2, 8, 9).

[21] Tommi Rinne - Natalia Araya-Gómez and Rodrigo Serna-Guerrero. "A Study on the Effect of Particle Size on Li-Ion Battery Recycling via Flotation and Perspectives on Selective Flocculation". In: *Batteries 9* (2023) (pages 2, 9, 27).

[22] Lubing Wanga - Sha Yina - Zhexun Yuc - Yonggang Wang - T.X.Yu - Jing Zhao - Zhengchao Xie - Yangxing Li - Jun Xu. "Unlocking the significant role of shell material for lithium-ion battery safety". In: *Materials and Design 160* (2018) (page 4).

[23] Dominic Bresser - Daniel Buchholz - Arianna Moretti - Alberto Varzi and Stefano Passerini. "Alternative binders for sustainable electrochemical energy storage– the transition to aqueous electrode processing and bio-derived polymers". In: *Energy Environmental Science 11* (2018) (page 5).

[24] John T. Warner. *Lithium-ion battery chemistries : a primer*. Amsterdam Elsevier, 2019, pp. 9–10 (page 5).

[25] Alexandre Chagnes. "Chapter 2 - Fundamentals in Electrochemistry and Hydrometallurgy". In: *Lithium Process Chemistry*. Ed. by Alexandre Chagnes and Jolanta Świątowska. Amsterdam: Elsevier, 2015, pp. 41–42. ISBN: 978-0-12-801417-2. DOI: https://doi.org/10.1016/B978-0-12-801417-2.00002-5. URL: https://www.sciencedirect.com/science/article/pii/B9780128014172000025 (page 5).

[26] Haocheng Ji - Junxiong Wang - Jun Ma - Hui-Ming Cheng - Guangmin Zhou. "Fundamentals, status and challenges of direct recycling technologies for lithium ion batteries". In: *Royal Society of Chemistry, 52* (2023) (pages 5, 7).

[27] Heiner Heimes - Achim Kamper - Christian Offermans - Domenic Klohs - Natalia Solvan Kattali - Timon Elliger - Arno Kwade - Marco Ahuis - Sarah Michaelis - Karl Rottnick. "Recycling of Lithium-Ion Batteries". In: *Rwth Aachen Publications* (2023) (page 7).

[28] Nathália Vieceli- Piamcheewa Benjamasutin - Raksina Promphan - Pia Hellström - Magnus Paulsson and Martina Petranikova. "Recycling of Lithium-Ion Batteries : Effect of Hydrogen Peroxide and a Dosing Method on the Leaching of LCO,NMC Oxides,and Industrial Black Mass". In: *ACS Sustainable chemistry and engineering* (2023) (page 7).

[29] Tommi Rinne. "Innovations in Li-ion Battery Recycling : Advanced physical separation, characterization and industrial process integration". In: *School of Chemical engineering, Department of chemical and metallurgical engineering, Aalto University publication series DOCTORAL THESES 182/2024* (2024) (pages 7, 11).

[30] Barry A. Wills and Tim Napier-Munn. *Mineral Processing Technology; An Introduction to the Practical Aspects of Ore Treatment and Mineral Recovery*. Butterworth-Heinemann, 7th edition, 2005, pp. 267–277 (pages 8, 9).

[31] A.V.Nguyen. "Reference Module in Chemistry, Molecular Sciences and Chemical Engineering". In: Elsevier, 2013. Chap. Froth flotation, pp. 17–18 (page 9).

[32] Zhen Shang- Wenhao Yu-Jiahui Zhou - Xia Zhou - Zhiyuan Zeng - Rabigul Tursun-Xuegang Liu - Shengming Xu. "Recycling of spent lithium-ion batteries in view of graphite recovery: A review". In: *eTransportation20(2024)100320* (2024) (page 9).

[33] Anna Vanderbruggen - Aliza Salces - Rodrigo Serna-Guerrero. "Improving Separation Efficiency in End-of-Life Lithium-Ion Batteries Flotation Using Attrition Pre-Treatment". In: *Minerals 12* (2022) (pages 9, 10).

[34] Jiangshan Liu - Haifeng Wang - Tingting Hu - Xuejie Bai -Shuai Wang - Weining Xie - Juan Hao - Yaqun He. "Recovery of LiCoO2 and graphite from spent lithium-ion batteries by cryogenic grinding and froth flotation". In: *Minerals Engineering 148* (2020) (page 10).

[35] Aliza Marie Salces - Irina Bremerstein - Martin Rudolph - Anna Vanderbruggen. "Joint recovery of graphite and lithium metal oxides from spent lithium-ion batteries using froth flotation and investigation on process water re-use". In: *Minerals Engineering 184 (2022) 107670* (2022) (page 10).

[36] Younghun Kim - Mitsuaki Matsuda - Atsushi Shibayama - Toyohisa Fujita. "Recovery of $LiCoO_2$ from Wasted Lithium Ion Batteries by using Mineral Processing Technology". In: *Resources Processing 51* (2004) (pages 10, 48, 65).

[37] Guangwen Zhang - Yaqun He - Haifeng Wang - YiFenga - Weining Xie - Xiangnan Zhu. "Application of mechanical crushing combined with pyrolysis enhanced flotation technology to recover graphite and LiCoO2 from spent lithium-ion batteries". In: *Journal of Cleaner Production 231* (2019) (pages 10, 48, 65).

[38] Malvern Panalytical. *Zeta potential - An introduction in 30 minutes*. (consultated the 2025-11-28). URL: `https://www.malvernpanalytical.com/en/learn/knowledge-center/technical-notes/tn101104zetapotentialintroduction` (pages 11, 12, 27, 45).

[39] nanoComposix. *Zeta Potential Measurements*. (consultated the 2025-12-01). URL: https://nanocomposix.com/pages/zeta-potential-measurements (pages 11, 12, 27).
[40] Jakub Matusiak and Elżbieta Grządka. "Stability of colloidal systems – a review of the stability measurements methods". In: *Annales Universitatis Mariae Curie-Sklodowska Vol LXXII, 1 Sectio AA* (2017), pp. 41–43 (page 11).
[41] Andreas Pfennig. "Physical unit operation : mechanical separation". In: 2015, pp. 94–96 (page 12).
[42] ProGraphite shop. *Synthetic graphite anode material*. (consultated the 08-18-26). URL: https://www.graphite-shop.com/en/synthetic-graphite--anodes-coated-270.html (pages 13, 49).
[43] Gelon. *NMC 811/111 Lithium Ion Battery Materials*. (consultated the 08-18-26). URL: https://www.gelon-lib.com/quality-33446064-nmc-811-111-lithium-ion-battery-materials (pages 13, 49).
[44] *VWRchemicals. Sulphuric acid 95-97%, GPR RECTAPUR®*. (consultated the 08-17-26). URL: https://www.vwr.com/ni/en/product/24216874/nickel-ii-sulphate-hexahydrate-98-gpr-rectapur (page 15).
[45] *VWRchemicals. Iron(II) sulphate heptahydrate 98%*. (consultated the 08-17-26). URL: https://www.vwr.com/export/en/product/2348588/ironii-sulphate-heptahydrate-98 (page 15).
[46] Maria Farcas. "Technical Report on (Reductive) Leaching of Li-ion Batteries Active Material – BM11: « mechanical » black mass (unpublished)". In: (2026) (page 15).
[47] Thermo Fisher Scientific. *Lithium sulfate monohydrate, 99%*. (consultated the 08-12-26). URL: https://www.thermofisher.com/order/catalog/product/A10410.36l (page 16).
[48] Thermo Fisher Scientific. *Cobalt(II) sulfate heptahydrate, 98%*. (consultated the 08-12-26). URL: https://www.thermofisher.com/order/catalog/product/A16201.36 (page 16).
[49] *VWRChemicals. Aluminium sulphate tetradecahydrate, GPR RECTAPUR®*. (consultated the 08-12-26). URL: https://www.vwr.com/uk/en/product/3004302/aluminium-sulphate-tetradecahydrate-gpr-rectapur (page 16).
[50] *GTK Laboratory Flotation Machine MANUAL* (page 17).
[51] ExxonMobil. *ExxonMobil Sales specification Escaid^{TM}110HydrocarbonFluid*. (consultated the 2026-08-05). URL: https://www.exxonmobilchemical.com/en/chemicals/webapi/dps/v1/datasheets/130000000209/1/en (page 17).
[52] ExxonMobil. *Solvent extraction of metals from Ore*. (consultated the 2026-08-05). URL: https://www.exxonmobilchemical.com/en/industries/industrial-applications/metal-solvent-extraction#:~:text=Escaid%E2%84%A2%20diluents%20are%20used%20in%20metal%20extraction.%20They,Main%20metals%20extracted%20include%20copper%2C%20nickel%20and%20uranium. (page 17).
[53] Thermo Fisher Scientific. (consultated the 2026-08-05). URL: https://www.thermofisher.com/order/catalog/product/A13435.AP?SID=srch-srp-A13435.AP (page 17).
[54] Grosseron. (consultated the 2026-08-05). URL: https://www.grosseron.com/acide-sulfurique-95-analar-normapur-tr-25-l-art_20704.320.html (page 17).
[55] Agilent. *ICP-OES Overview*. (consultated the 2026-08-02). URL: https://www.agilent.com/en/support/atomic-spectroscopy/inductively-coupled-plasma-optical-

emission-spectroscopy-icp-oes/icp-oes-faq?crm_campaign=701QO00001GZnRuYAL&Campaign_Source=PAN_PSM_AtomicSpec_B&crm_source=marketing%20campaign&gclid=0a85f9337b371c56bdf9935c1a88edaa&gclsrc=3p.ds&msclkid=0a85f9337b371c56bdf9935utm_source=bing&utm_medium=cpc&utm_campaign=B_PS_NBr_Atomic%20Spec%20General_EMEA_E_P&utm_term=optical%20emission%20spectroscopy%20oes&utm_content=Info_ICP%20OES_ICP%20OES%20Overview_P (page 25).

[56] Thermo Fisher Scientific. *Inductively Coupled Plasma Optical Emission Spectroscopy (ICP-OES) Information*. (consultated the 2026-08-02). URL: https://www.thermofisher.com/be/en/home/industrial/spectroscopy-elemental-isotope-analysis/spectroscopy-elemental-isotope-analysis-learning-center/trace-elemental-analysis-tea-information/icp-oes-information.html (page 25).

[57] Thermo Fisher Scientific. *ICP-OES Sample Preparation*. (consultated the 2026-08-02). URL: https://www.thermofisher.com/be/en/home/industrial/spectroscopy-elemental-isotope-analysis/spectroscopy-elemental-isotope-analysis-learning-center/trace-elemental-analysis-tea-information/icp-oes-information/icp-oes-sample-preparation.html (page 25).

[58] Cristian Cojocariu Daniel Kutscher Jianfeng Cui. *Key Steps to Create a Sample Preparation Strategy for Inductively Coupled Plasma (ICP) or ICP–Mass Spectrometry (ICP-MS) Analysis*. (consultated the 2026-08-02). URL: https://www.spectroscopyonline.com/view/key-steps-to-create-a-sample-preparation-strategy-for-inductively-coupled-plasma-icp-or-icp-mass-spectrometry-icp-ms-analysis (page 25).

[59] Horiba scientif and analytical instruments. *What is X-ray Fluorescence (XRF) and how does XRF work?* (consultated the 2026-08-03). URL: https://www.horiba.com/int/scientific/technologies/energy-dispersive-x-ray-fluorescence-ed-xrf/what-is-x-ray-fluorescence-xrf/ (page 25).

[60] Science insight. *How Does an Ion-Selective Electrode (ISE) Work?* (consultated the 2026-08-03). URL: https://scienceinsights.org/how-does-an-ion-selective-electrode-ise-work/ (page 26).

[61] Pharma digests. *Total Organic Carbon (TOC) | Principle, Working and Applications*. (consultated the 2026-08-03). URL: https://pharmadigests.com/total-organic-carbon-toc-principle-working-and-applications/#google_vignette (page 26).

[62] montserrat.filella@unige.ch. *Equilibrium constants for hydrolysis and associated equilibria in critical compilations : Nickel*. (consultated the 08-05-26). URL: https://equilibriumdata.github.io/docs/COST/Ni.pdf (pages 31, 68).

[63] montserrat.filella@unige.ch. *Equilibrium constants for hydrolysis and associated equilibria in critical compilations : Cobalt*. (consultated the 08-05-26). URL: https://equilibriumdata.github.io/docs/COST/Co.pdf (pages 33, 69).

[64] montserrat.filella@unige.ch. *Equilibrium constants for hydrolysis and associated equilibria in critical compilations : Manganese(II)*. (consultated the 08-05-26). URL: https://equilibriumdata.github.io/docs/COST/Mn.pdf (pages 36, 69).

[65] montserrat.filella@unige.ch. *Equilibrium constants for hydrolysis and associated equilibria in critical compilations : Aluminium*. (consultated the 08-05-26). URL: https://equilibriumdata.github.io/docs/COST/Al.pdf (pages 38, 70).

[66] Luis Verdugo - Lian Zhang - Barbara Etschmann - Warren Bruckard - Jorge Menacho - Andrew Hoadley. "Effect of lithium ion on the separation of electrode materials in spent lithium ion batteries using froth flotation". In: *Separation and Purification Technology 311 (2023) 123241* (2023) (page 41).

[67] François Larouche - Farouk Tedjar - Kamyab Amouzegar - Georges Houlachi - Patrick Bouchard - George P. Demopoulos - and Karim Zaghib. "Progress and Status of Hydrometallurgical and Direct Recycling of Li-Ion Batteries and Beyond". In: *Material 13* (2020) (page 44).

[68] Mengdi Hao - Suting Weng - Cong Zhong - Yejing Li - Xuefeng Wang. "Structure and evolution of solid electrolyte interphase (SEI) at the electrode-electrolyte interface". In: *Materials Today Energy 53* (2025) (page 44).

[69] Eni Generalic. *Constantes du produit de solubilité*. (consultated the 08-05-26). URL: `https://www.periodni.com/fr/constantes_du_produit_de_solubilite.html` (pages 68–70).